Application of modified clays in nutrient removal from wastewater

Ph.D. Dissertation

Tanya Chauhan

Supervisor	Head of the Doctoral School
Dr. Zoltán Németh	Prof. Dr. Valéria Mertinger

Antal Kerpely Doctoral School of Materials Science and Technology

Faculty of Materials and Chemical Engineering

University of Miskolc

Miskolc

2024

This thesis is dedicated to my parents (Advocate Purushottam Chauhan & Mrs Rukmani Chauhan), my dear younger brother (Lakshya Chauhan) and my partner in crime (Prajjawal Chauhan) for their endless love, support and encouragement.

Table of Contents

LIST OF FIGURES

LIST OF TABLES

LIST OF ABBREVIATIONS

CEC	Cation exchange capacity	CPHEEO	Central Public Health and Environmental Engineering Organization
CM	Naturally occurring raw montmorillonite	DTG	Derivative thermogravimetric
EDX	Energy-dispersive X- ray spectroscopy	SDS	sodium dodecyl sulphate
FFT	Fast Fourier Transform	CFU	Colony forming unit
FTIR	Fourier transform infrared spectroscopy	Mt	Montmorillonite
HAADF	High-angle annular dark-field imaging	STP	Sewage treatment plant
HRTEM	High-resolution transmission electron microscopy	BOD	Biological oxygen demand
ICP-OES	Inductively coupled plasma optical emission spectrometer	PZC	Point of zero charge
IPCC	Intergovernmental Panel on Climate Change	CTEPs	Common effluent treatment plants
MMT	Montmorillonite	CTAB	Cetyltrimethylammonium bromide
Na-CM	Sodium exchanged montmorillonite	CTAC	Cetyltrimethylammonium chloride
PILCs	Pillared interlayered clays	OD	Optical density
SEM	Scanning electron microscopy	IPCC	Intergovernmental Panel on Climate Change
SSA	Specific surface area	MOEFCC	Ministry of Environment,Forest and Climate Change
STEM	Scanning transmission electron microscopy	CPCB	Central Pollution Control Board
TEM	Transmission electron microscopy	EEA	European Environment Agency
TGA	Thermogravimetric analysis	EPA	Environmental Protection Agency
XPS	X-ray photoelectron spectroscopy	p.e.	Population equivalent
XRD	X-ray powder diffraction	GOI	Government of India
LB	Luria-Bertani	NGT	National Green Tribunal
COD	Chemical oxygen demand	TSS	Total suspended solids

1. INTRODUCTION

According to the Intergovernmental Panel on Climate Change (IPCC) Report on Climate Change 2022, nearly half of the world's population faces severe water scarcity for at least some part of the year. Water pollution is a serious threat to the existence of living beings on Earth. Population explosion, urbanization, and industrialization over the decades have changed the pattern of land use and the hydrological cycle of the world. Increased frequency of floods, rainfall, droughts and other natural disasters in past years have proved that we are failing to maintain the ecological balance. Mobilization of bioavailable nutrients such as nitrogen and phosphorus into the water bodies is also one of the factors responsible for the degradation of water quality around the globe. A significant fraction of these elements enter the surface water via human or natural activities and are transported to coastal ecosystems through rivers. The major anthropogenic sources of nutrient water pollution are agricultural runoff, sewage, industrial and urban effluent [1] (**Fig. 1**).

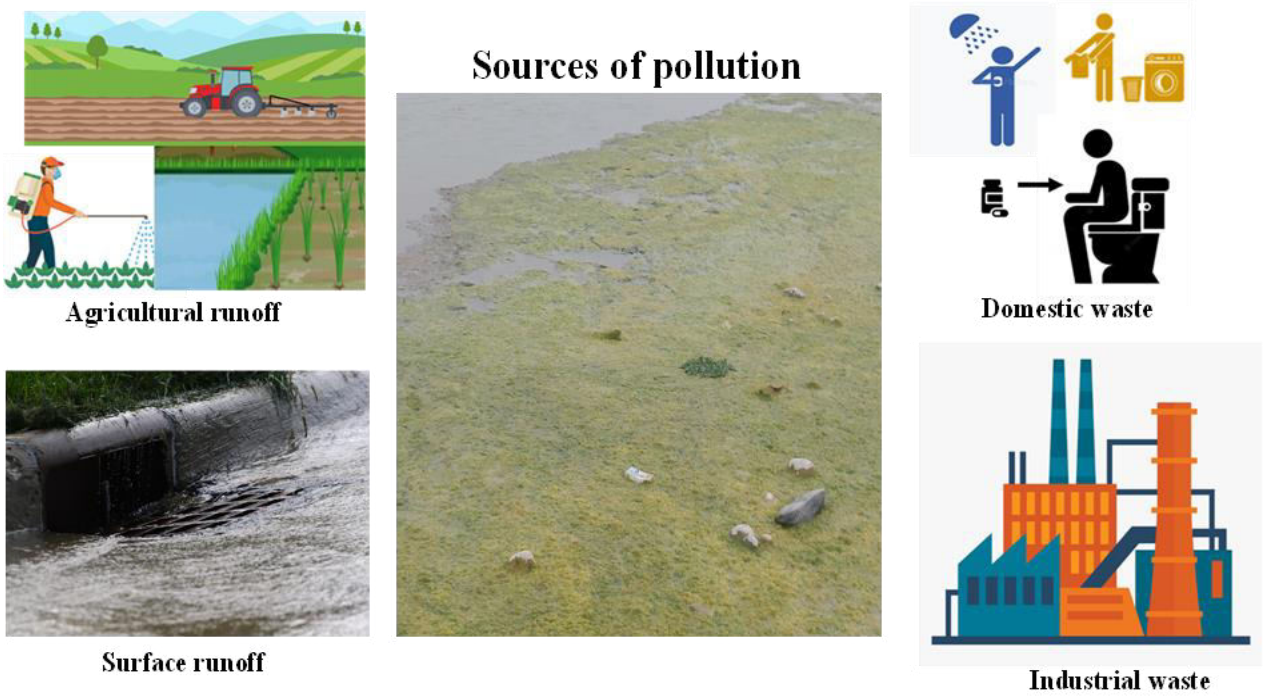

Figure 1: Sources of nutrient pollution.

Aquatic ecosystems are very sensitive with respect to the concentration of phosphorus. Although it is an important element for the growth of phytoplankton, but it can be a nuisance if the concentration increases up to a certain limit. Nutrient enrichment by nitrogen and

phosphorus in a water body can lead to an undesirable and unavoidable situation called eutrophication (**Fig. 2**).

Figure 2: Eutrophication of waterbody in Rishikesh, Uttarakhand, India [own source].

In this, the surface of the water is covered by uncontrolled growth of weeds, algae and cyanobacteria (blue-green algae) which further prevents the penetration of sunlight in the water column, thus affecting other aquatic species which are living in depth. A series of events are

initiated under the influence of eutrophication starting with abundant growth of algae and plants and when these plants die a lot of oxygen is used for the decomposition of their organic matter. As a result, carbon dioxide is produced which reduces the pH of the water and makes it acidic. The BOD (biological oxygen demand) of the water body decreases and creates hypoxic conditions for aquatic plants and animals [2] [3]. Eventually either they die or move to other places and like this healthy habitat are destroyed and converted into dead zones [4]. The process of eutrophication is shown in **Fig. 3.**

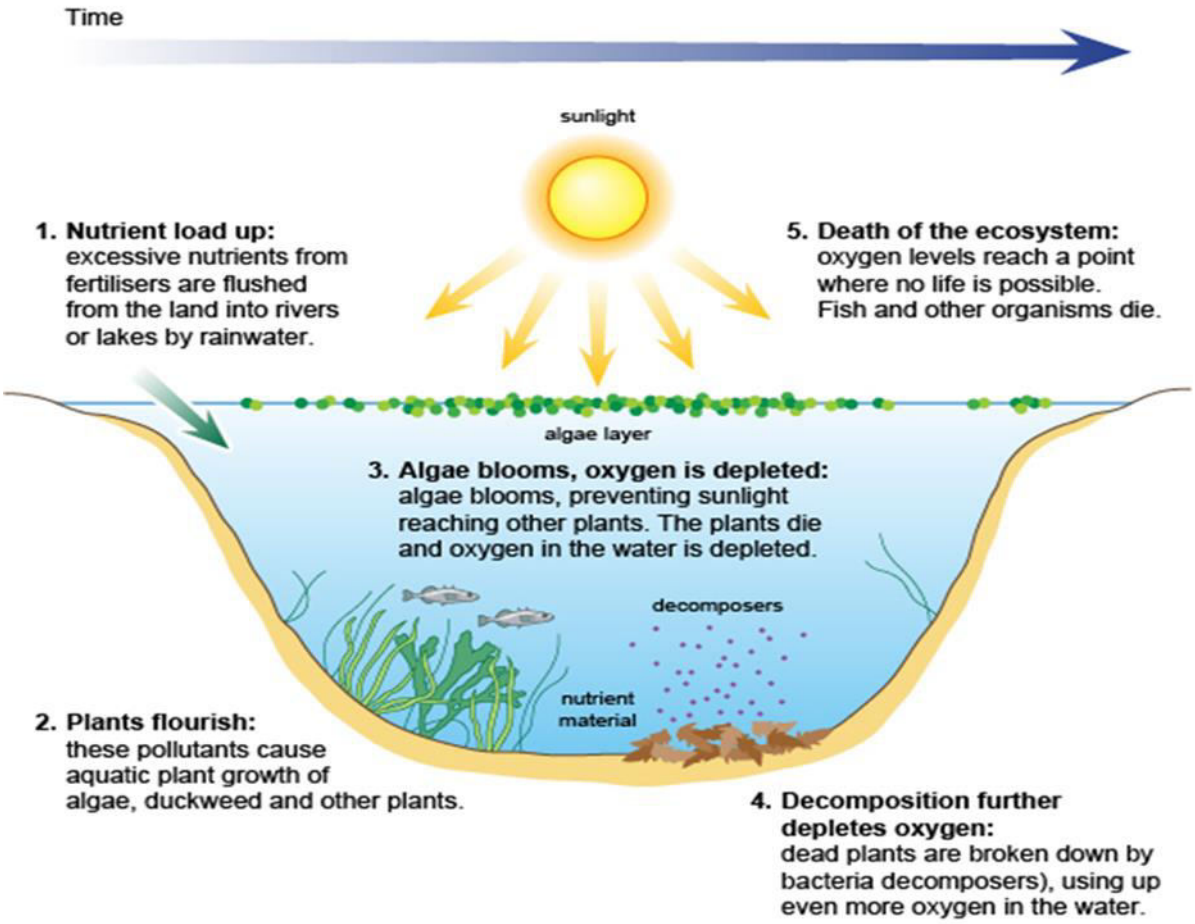

Figure 3: Events occurring during the process of eutrophication [5].

Previous studies have demonstrated that phosphorus concentration above 0.02 mg/L can initiate the process of eutrophication [5]. Rivers, lakes, ponds, wetlands even seas are being damaged by the imbalance of nutrient levels. Europe's seas are no longer safe according to one study presented by the European Environment Agency in 2019 (EEA report, 2019). According to the report assessment, 23 % of the Baltic Sea, North-East Atlantic, Black Sea, and Mediterranean Sea are already facing the problem of eutrophication. The spatial mapping of the seas was also

done to show the extent of harm caused by nutrient pollution (**Fig. 4**). Therefore, in many countries, there are strict standards for the discharge limit of phosphorus originating from wastewater treatment plants. According to the European Commission, the concentration of total phosphorus which is acceptable to get discharged into the sensitive areas is 2 mg/1 P (10 000 - 100 000 p. e.) and 1 mg/1 P (more than 100 000 p. e.) or at least there should be a reduction of 80% with respect to the load of influent. In India, the pollutant discharge standards from STPs are dictated by the Central Pollution Control Board (CPCB) which is governed by the Ministry of Environment, Forests and Climate Change (MOEFCC). The general standards which were given by CPCB for effluent discharge did not pay much attention to important pollutants like phosphates till 2015 only BOD (Biological oxygen demand), nitrates COD (Chemical oxygen demand), pH, TSS (Total suspended solids) and ammonical nitrogen were taken into consideration. Later on, this matter was taken to the National Green Tribunal (NGT) responsible for India's environmental litigation for making these standards more strict. The effluent discharge limit of dissolved phosphates in inland surface water was 5 mg/L till 2015 but in 2019 new regulations came into effect with the help of NGT and the Supreme Court of India to improve the quality of STP effluent. Now the discharge limit of total phosphorus is 1 mg/L. Since the discharge standards became stricter, now STPs will be encouraged to reuse and recycle the wastewater. For small and medium-sized industries the effluent is collected at a common place and treated collectively in CTEPs (Common effluent treatment plants). For CTEP, the discharge standards are given by the Central Public Health and Environmental Engineering Organization (CPHEEO) governed by the Ministry of Urban Development, New Delhi. According to CPHEEO, the discharge limit of phosphates is 5 mg/L in inland surface water. These standards are mandatory to be followed and a regular check is kept on STPs and CETPs by state governments pollution control board.

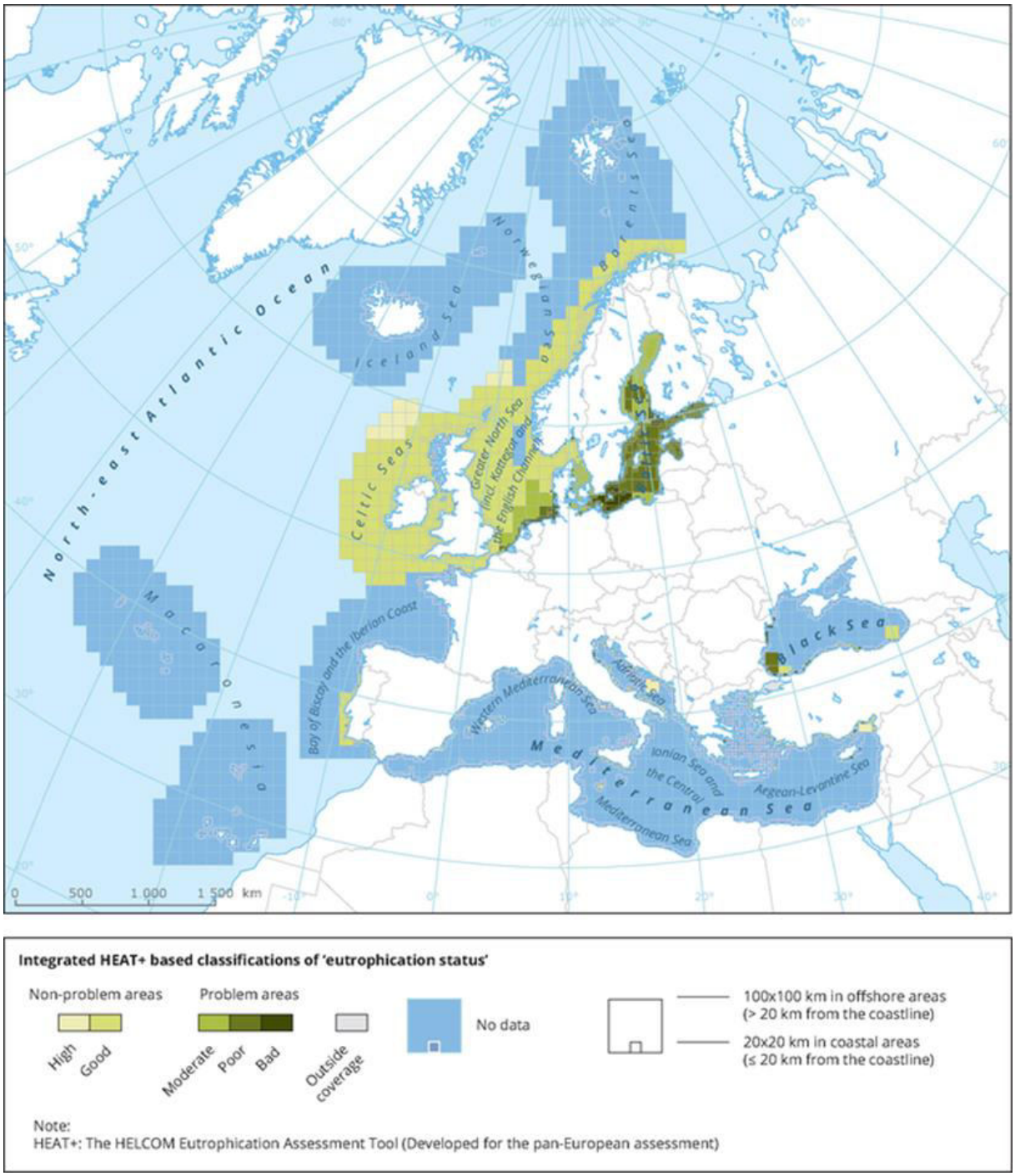

Figure 4: Nutrient pollution in seas (EEA report 2019; ISSN1977-8449).

Not only Europe but other parts of the world are also struggling to maintain proper nutrient levels in their water bodies. According to the United States Environmental Protection Agency (EPA) assessment, 58 % of their rivers and streams, and 45% of lakes have elevated amounts of phosphorus. In India also, the rivers, ports and many wetlands are under the effect of eutrophication. Recently, a study conducted by R.V Rodrigues and colleagues reported that the

major ports (Cochin, Mangalore and Kandla) situated on the west coast of India have shown a significant amount of eutrophication [7]. In another study conducted by Biswajit et al., the status of wetlands situated in the eastern part of India (Calcutta) was studied and it was found that 40 % of the East Kolkata Wetlands region is under the eutrophic stage [8]. This region is also one of the important parts of the Ramsar site. Wetlands are a very crucial part of our ecosystem, and they are also known as the 'kidneys of Earth'' because they help in the natural purification of water, recycling of nutrients, prevention of floods and support many migratory birds. India's wetlands are under the threat of eutrophication. Many of them have already been converted to lands due to ecological succession.

Another emerging pollutant detrimental to aquatic ecosystems and human health is *Escherichia coli (E. coli)* bacteria which is an indicator of faecal contamination. These are found in the intestines of human beings and animals. It is a sign of contaminated water bodies not suitable for drinking or recreational activities. Today, many Indian rivers and beaches are highly polluted by faecal coliform due to the direct dumping of untreated sewage water into the rivers or ocean without any guidelines and the insufficiency of STPs (Sewage treatment plants) to deal with heavy loads of inlet water. In one very recent study conducted by Abhay and colleagues, it was reported that three major beaches (Marve, Erangal and Danapani Beach) of Mumbai City (the capital of Maharashtra, India) have shown a significant amount of faecal bacteria and the concentrations were above the standard limits set by CPCB (Central Pollution Control Board) [9]. The results were alarming and required the immediate attention of the concerned authority to prevent further consequences. In another study presented by Bhagwana Ram and Manish Kumar, the water quality of the Sabarmati River was investigated, and they also sampled *E. coli* to check antibiotic resistance. The concentration of *E. coli* in the river was found to be 19,467 and 76,600 CFU mL^{-1} which is extremely high and according to the CPCB standards, the river water is neither suitable for drinking even after the treatment nor for recreational activities [10]. According to CPCB standards, the amount of Total coliform organisms should be present in drinking water source after conventional treatment and disinfection shall be 5000 MPN/100 mL or less and for outdoor bathing it shall be 500 MPN/100 mL or less (NITI Ayog report 2022, GOI). The conventional methods which are used for the elimination of these microorganisms from water are chlorination, ozonation, and filtration [11]. However, these disinfection techniques have limitations for e.g. the end products which are produced during chlorination are very harmful and toxic carcinogenic chemicals. Filtration methods are better, but they are not very cost-efficient and have fouling problems. Ozonation is a very efficient method but it could also produce harmful substances and reactive free radicals

[12]. Therefore, there is a need to develop cheap and alternative methods which can be applied to wastewater purification.

Around the globe, researchers and scientists are working on finding a solution for the purification of water using suitable methods. Clays have been known as natural water pollutant scavengers for a long time. Interaction and migration of a pollutant with the clay depend upon its charge, cation exchange capacity and surface area [13]. They are physically and chemically active in nature. It can combine with water to make slurries and suspensions. Also, it attracts many ions onto its surface or into their internal structure thus restricting the mobility of the ions.

Clays are naturally occurring minerals found in soil or sediments which has a particle size of less than 2 μm. They are also called as phyllosilicate minerals due to the presence of layered silicate sheets [14]. Their basic structural foundation consists of silica tetrahedral and alumina octahedral (central ion can consist of Al^{+3}, Fe^{+2}, Mg^{+2}) sheets. Tetrahedral sheets consist of corner-linked tetrahedra with oxygens in the corner and Si^{+4} is the dominant central atom. Octahedral sheets consist of edge-linked octahedra with OH in the corners and cations at present at the centre. Based on the arrangement of these sheets, clays can be divided into two types namely 1:1 type (kaolinite, halloysite) and 2:1 type (smectite, vermiculite, illite) (**Fig. 5**). The 1:1 type consists of one tetrahedral and one octahedral sheet arranged alternately with no interlayer spacing. In the 2:1 type, one octahedral sheet is present in between two silica tetrahedral sheets with interlayer space where exchangeable cations (Na^{+}, Ca^{+2}, K^{+}) are present [15]. When these tetrahedral and octahedral sheets are arranged in layers, the layers may be electrically neutral or negatively charged. Generally, in 2:1 type clay mineral isomorphic substitution is observed in which Si^{+4} gets substituted by Al^{+3} in the tetrahedral layer and Al^{+3} gets substituted with Mg^{+2} in the octahedral layer this imparts a negative layer charge to the clay minerals. The charge is balanced by the cations present in the interlayer region.

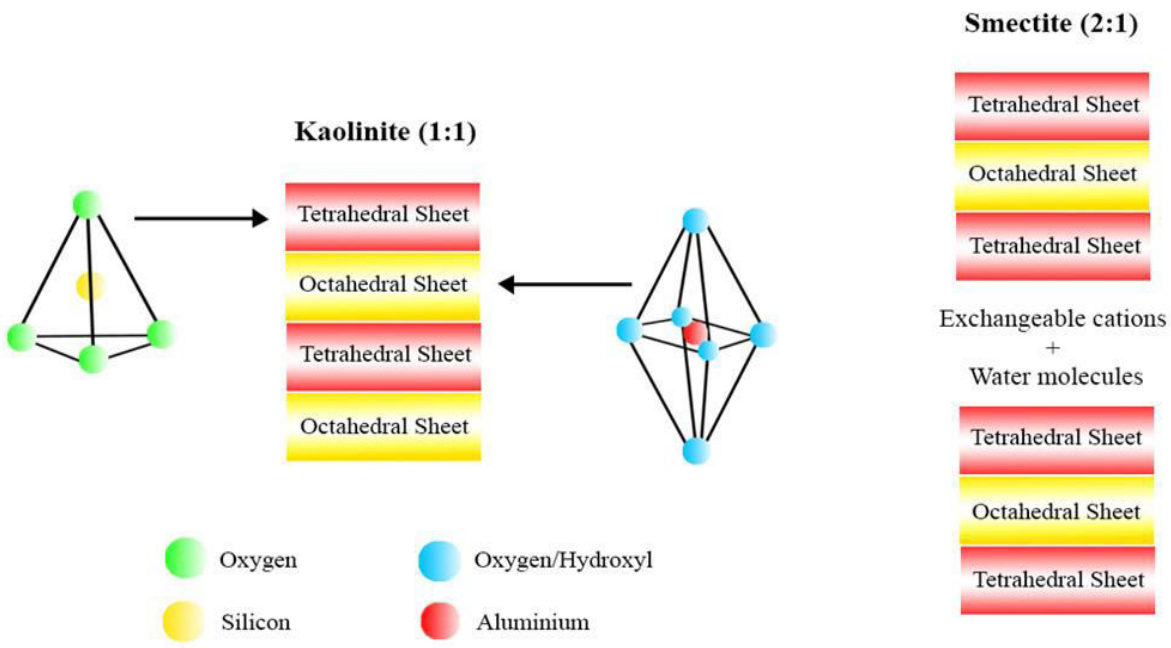

Figure 5: Schematic representation of crystal structure of Kaolinite and Smectite clay.

In this study, montmorillonite clay is used as raw material which belongs to the smectite group. It is a porous clay mineral with a 2:1 layered structure. One of the characteristic properties of montmorillonite is that it is hydrophilic in nature and shows expansion when exposed to water. The interlayer ions have a strong tendency to hydrate under humid conditions. The water molecule penetrates the interlayer region and can shift the clay sheets apart which imparts swelling property to the clay structure [16]. Another distinctive feature of montmorillonite is adsorption [17]. The use of natural and modified clays in the adsorption of different water pollutants such as toxic heavy metals coming out from industrial waste, antibiotics and personal care products originating from pharma and cosmetic industries and nutrients have been reported in the literature [18][19][20].

2. LITERATURE REVIEW

Clay minerals are very promising tools for the development of novel materials that are flexible and can be applied in different applications such as adsorbents, catalysts, photocatalysts, drug delivery systems and nanocomposites [21]. An extensive study has been done in the field of clay science for the development of multifunctional clay materials which can be used to eliminate a wide range of contaminants ranging from gaseous (CO_2) to different types of emerging water pollutants such as synthetic hormones, dyes, pesticides and drugs [22] [23][24]. Based on the requirement of the target pollutant, the physical and chemical properties of the clay can be tuned accordingly. Therefore, clay-based adsorbents have been gaining attention a lot these days. Also, they are economically and more environment friendly as compared to other materials. Although clay has many advantages in the field of adsorption, catalysis and ion exchange but it has one drawback that restricts its use in the field of water treatment which is the lack of permanent porosity. The layered structure of montmorillonite clay starts to expand in the presence of water but during dehydration or heating it starts to disintegrate and they are no longer accessible to the chemical processes. To overcome this weakness and to improve the performance of clay adsorbents, researchers have tried to modify the structural and surface properties of clay minerals using different strategies. Different techniques are used for the modification of clay such as activation with acids [25], alcohols, surfactants [26] or doping with metals [27]. But among all, clay pillaring or intercalation is the most promising process which can improve the porosity, create more active sites for the reaction and increase the specific surface area as well. In this method, the interlayer cations of clay minerals are exchanged with bulky polyhydroxy metal cations. Upon further heat treatment, these hydroxy metal cations are converted into metal oxide pillars (**Fig. 6**). These oxide pillars keep the clay structure intact and provide stability and rigidity. These newly formed microporous structures are referred as pillared interlayered clays (PILCs).

The concept of pillaring was first proposed by Barrer and Macleod in the 1950s and they used aluminium tetra alkyl ions as pillaring material [28]. The problem with using organic species for intercalation was their low thermal stability at higher temperatures. Later in the 1970s, Brindley and Sempels used a hydrolysis product of $AlCl_3$ for intercalation in sodium-saturated beidellite [29]. This was the first time when an inorganic pillared clay was produced using aluminium ions. After that, Yamanaka and Brindley used zirconium polyhydroxy cations for pillaring in 1979 [30]; later the same group produced iron pillared clay as well. In 1973 during

the time of the oil crisis, the application of these materials as catalysts was explored in the field of oil cracking [31].

In literature, other elements are also used as pillaring agents such as Ti, Ga, Cr, Cu, and La and sometimes more than one metal ion is also used such as Al-Fe, Al-Zr but among all Al ion is the most extensively studied cation because its hydrolysis properties are very well explored and understood [32]. Zirconium ions started to gain attention in 1988 when Bartley threw light on the solution chemistry of zirconium ions and the factors responsible for the successful pillaring of zirconium into the clay structure [33]. Later work of Cool and Vasant also emphasized the parameters that can influence the preparation of zirconium pillaring solution. According to them, zirconyl ion is present as a tetramer in solid zirconium chloride with the formula of $[Zr_4(OH)_8(H2O)_{16}]^{8+}$. In water, rapid polymerization of tetramer takes place and the solution becomes acidic due to hydrolysis of the tetramer [31].

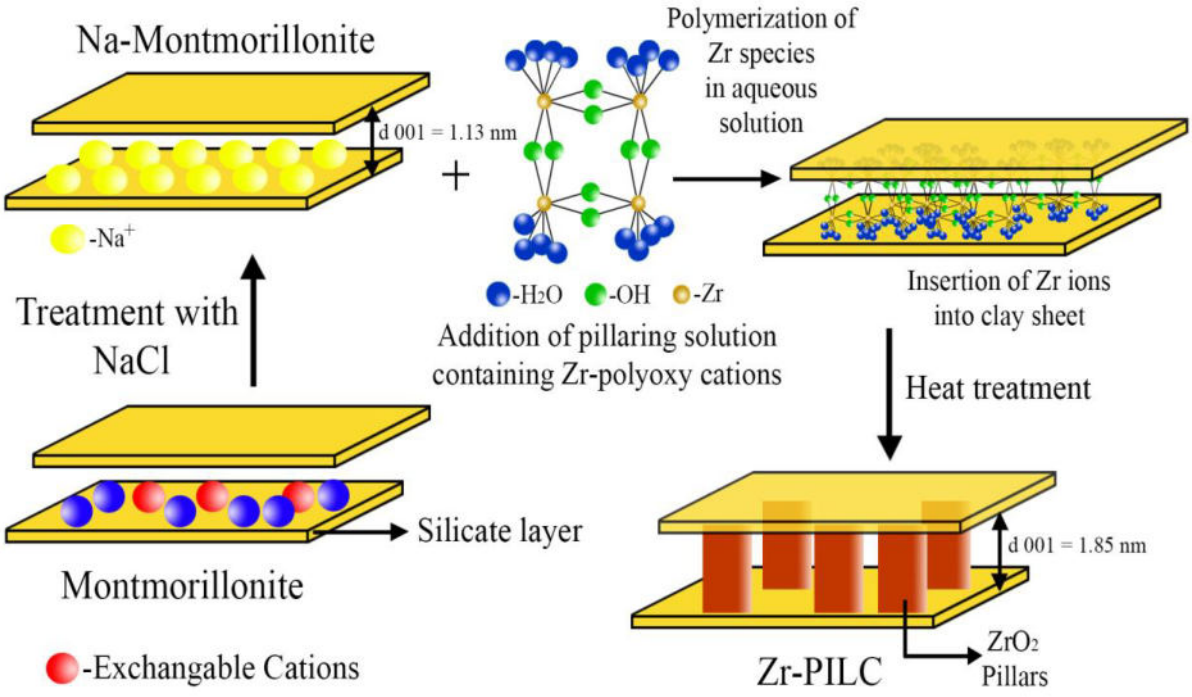

Figure 6: Schematic representation of pillaring of montmorillonite clay with zirconium ions [35].

2.1 Methods for preparation of Pillared Clays

The conventional method of preparation of pillared clays usually involves four main steps:

1. *Preparation of the pillaring solution:*

   As mentioned above, there have been different types of pillaring species used for the preparation of pillared clays based on their sizes and chemical structure. The nature and flexibility in the structure of the pillared clays depend upon the type of chemical agent used for clay pillaring. Usually, these types of pillaring agents are used for intercalation: organic cations, organometallic cations, metal clusters, polyoxycations and oxide sols [34][35]. Literature shows that polyoxycations and oxide sols are more promising pillaring agents that are produced by hydrolysis of metal salts in acidic or alkaline conditions. Precursors including Al, Zr, Fe, and Ti could be considered the most significant and extensively used. Based on the desirable properties of pillars obtained from polyoxycations and oxide sols and their usefulness, different initial materials and methods could be used for the preparation of the pillaring solution.

2. *Ion exchange reaction between the interlayer cations and pillaring ions*

   After the preparation, the next step is to react these pillaring agents with clay. Before these precursors make contact with clay, another important step is required which is purification of clay or pre-treatment with exchangeable cations. As we have mentioned earlier, montmorillonite which is the most common type of clay used for the pillaring process consists of two-dimensional aluminosilicate layers. The substitution of Si^{4+} in tetrahedral units with trivalent metal cations and the replacement of Al^{3+} with lower valence cations such as Fe^{2+} and Mg^{2+} will produce an overall negative charge on the clay sheets. To balance the charge many small hydrated metal cations are located between the silicate layers. These cations are highly exchangeable and facilitate the entry of guest molecules in the interlayer space. The raw clay contains a mixture of ions such as Mg^{2+}, Ca^{2+} and Na^{+}. It is important to saturate the clay with one type of cation. Clay activation can be done by using two methods:

   A) *Activation by acid:* In this method, the interlayer cations are replaced with protons. Usually, HCl and H_2SO_4 are used as sources of protons. As a result of acid activation, the porosity, specific surface area and surface acidity increases [36]. But as compared

to metal cations saturated clays, the proton-saturated clays are more unstable and the layers are attacked by the surface and interlayer hydrated protons [37].

B) *Activation with Na^+:* The clay can be saturated by Na^+ ions by using chemicals such as NaCl and Na_2CO_3 [38][39]. Na^+ ions facilitate the insertion of pillaring species by replacing themselves and they also help in the expansion of the clay sheets.

After the activation of clay, it is applied as powder or suspension to make contact with the pillaring solution. The dilute pillaring solution can be added to the clay suspension in two ways, either add the pillaring solution directly to the clay suspension or add the metal salt along with the hydrolysing material to the dilute solution of clay. The former method is known as *ex situ* and the latter one is the *in situ* method. For the production of pillared clays on a larger scale and to reduce the use of water, there are other methods as well which are: adding the clay powder directly to the pillaring solution to produce a clay slurry of 40%, a concentrated clay mineral dispersion is kept inside a dialysis bag which is placed inside pillaring solution or the clay powder and pillaring agent powder is kept inside a dialysis bag which is placed inside distilled water [40]. The function of a dialysis bag is to facilitate the transport of molecules to and fro across the bag till equilibrium is established.

3. *Washing the clay*

   The next step is to wash the prepared sample thoroughly to remove the excess amount of ions and pillaring agent present in the clay and to create more interlayer space. This can be done in many ways, but the most common one is mixing with water and then using a centrifuge. Generally, washing improves the quality of the pillared clays and helps in the formation of equally distributed pillars.

4. *Heat treatment*

   After washing, the product should be dried and calcined properly. In literature, different temperatures and methods are used for heating the material. Drying can be done in several ways which include slow and rapid drying. Air or oven drying is considered a slow-drying process; microwave and freeze-drying come under rapid drying. The different methods of drying produce different types of products with different morphological characteristics [41]. Air-dried products produce closed structures however microwave-dried pillared clays show sheet-like porous structures. On the other hand, freeze-dried sample usually produces card house structures in pillared clays. In the calcination step, pillared clay is heated for a specific

time at a certain temperature and at a particular rate. During the process, the pillaring precursors are converted into stable metal oxide clusters by dehydration and dihydroxylation. The temperature which is usually used is from 300 up to 700˚C above that the oxide pillars start to collapse [42].

2.2 Methods for modification of pillared clays

Based on the field in which these pillared materials will be used and to improve the selectivity, adsorption capacity, specific surface area, porosity and surface acidity these pillared clays are modified further. Various modification methods are used on these materials to enhance their properties based on the target application. A few of the modification techniques use surfactants such as sodium dodecyl sulphate (SDS) [26], hexadecyltrimethylammonium bromide (CTAB) [43] and cetyltrimethylammonium chloride (CTAC) [44] are the most widely used surfactants used to modify the structure of pillared clays and to induce organophilic property as well [45]. After modification, the specific surface area tends to decrease because of the incorporation of surfactant molecules in between the empty spaces of clay sheets. The organic-inorganic modification of these adsorbents makes them suitable for the elimination of both organic and inorganic pollutants from water due to their structural diversity. Amine pre-adsorption is another promising method used to increase the micropore volume, porosity, pillar distribution and density of the pillared clays. In this method, the sodium ions which are present in between the silicate layers are exchanged with amines so that they can block the active sites of the clay and prevent the interlayer substitution with polycations. Upon further heat treatment, these amines are destroyed thus leaving many free spaces inside the clay [46]. These amine groups restrict the formation of pillars in all areas. This method is highly demanded when molecular sieve selectivity and uniformly distributed pillars are required in the adsorbent. The only disadvantage of this method is the high cost.

Modifications on pillared clay are usually done to achieve a selective adsorbent. Selectivity is the result of chemical interaction initiated by the modifying material which takes place on the surface of the adsorbent and with the help of carbon modification we can control the size of the pores as well. In this technique, carbon sedimentation takes place inside the structure of pillared clays under the influence of different operating conditions. As a result, narrowing, blocking the openings and filling the volume of the pores take place [47]. This method can be achieved either by mixing a polymer solution (e.g. polyvinyl alcohol) into the pillaring solution and then adding

the solution to the clay suspension or adding the polymer solution to the pillared clay suspension followed by a carbonization step to convert the polymer to carbon. This modification helps in targeting the contaminants with appropriate molecular size but it can decrease the specific surface area by filling the pores [48]. To improve the catalytic performance of pillared clay, metal cation doping is one of the promising techniques. Although, it can reduce the specific surface area and micropore volume of the adsorbent. Also, to load the metal cations inside the pores of the pillared clays and to prevent the precipitation of metal cations on the external surface of pores; metal doping should be carried out under controlled conditions. Adding metal cations into the clay structure can be done in two ways, either before or after the pillaring process. In the first method, the pillared clay is first treated with an alkaline solution after that alkaline-treated pillared clay is allowed to interact with the desired metal cation and cation exchange takes place under controlled pH conditions [49]. In the latter one, the sodium ions which are already present in the clay structure are replaced with desired metal cations before the pillaring process. The resultant material is then allowed to undergo a pillaring process. After pillaring, some metal cations are still there in the porous structure of the clay. The number of metal cations doped is not controllable in this method [49]. Some authors have also tried modification with ligands to produce an adsorbent efficient for the immobilization of heavy metals from contaminated water. Unmodified clays are suitable adsorbents for heavy metals due to their cation exchange capacity, but this is a reversible process, and pollutants cannot be fixed on the surface of pillared clays for a long time. On the other hand, the grafting of chelated complexes on the surface of clay ensures the irreversible immobilization of heavy metals on the adsorbents. In this process, one of the major obstacles is the availability of a small surface area for the incorporation of ligands [50]. Brown *et al.* found that the BET surface area of the N-[3- (trimethoxysilyl)propyl]ethylenediamine triacetic acid trisodium salt modified clay reduced more than twice after modification and micropore volume was also reduced as well but the advantage is the stability of chelate complexes in lower pH [51].

Another type of modification which includes the usage of natural biopolymer ‘chitosan’ is gaining attention due to the presence of abundant amine and hydroxyl chelating functional groups within the chains. It is a linear polysaccharide composed of glucosamine and N-acetyl glucosamine linked in a β(1–4) glycosidic bond produced by deacetylation of chitin [52]. Chitin is an important structural component in the exoskeleton of aquatic organisms, terrestrial organisms and cell walls of some microorganisms. At the industrial scale, chitosan is produced from the biowaste of aquatic organisms like shell waste of prawns, shrimps, lobsters and crabs. Apart from these, insects such as silkworms, houseflies and fungi are also used for the

extraction of chitosan [53]. Because of its biocompatibility, low cost, biodegradability, non-toxicity, and antibacterial properties; it has been used in the food industry, cosmetics, medicine and wastewater treatment [54]. Wie Tan *et al.* prepared chitosan/hydroxy-aluminium pillared montmorillonite nanocomposites and studied the properties of prepared materials by using different characterization techniques. Chitosan solution with different concentrations and Al-pillaring solution were added to the clay suspension. The resulting solution was stirred for 2 days followed by washing with deionized water and then centrifuged. After that, the nanocomposites were air-dried at 50˚C [55]. Chitosan-based Ti-pillared clays were prepared by Xiu Zheng and colleagues to support PdO_x nanoparticle catalyst. Chitosan chains and PdO_x nanoparticles were incorporated in pore channels of titanium pillared clays. First, chitosan solution was prepared to which Pd^{+2} solution was added dropwise. Then this solution was added to the Ti-pillared clay followed by stirring at 60˚C, the mixed suspension was centrifuged and washed [56]. Similar type composites were prepared by Yuli Chen *et al*. but they stabilized the Pd species on chitosan and its derived carbon/pillared montmorillonite clay for catalytic applications [57].

2.3 Application of pillared and modified pillared clays

a) Pillared clays as a catalyst in wastewater treatment

The application of pillared clays was first explored in the field of oil cracking [58]. In the 1930s acid-treated montmorillonite clays were commonly used for cracking reactions. However, due to their low thermal stability, the application of these materials was not appreciated [59]. After that zeolites substituted these materials and began to gain more attention. The only drawback of these materials was their limited pore size. To handle the cracking of heavier crude oil, larger pore-size catalysts were required. Then pillared clays came into the picture because of their ability to achieve desired pore dimensions. Since then, pillared clay catalysts have attracted much attention in the field of wastewater treatment as well. Their high specific surface area, larger micropore volume and more sorption sites make them suitable candidates for the removal of water pollutants [60]. In one study, Ti-pillared bentonite clays modified with Cu, Ag and Fe were used for the removal of BPA (bisphenol A). These materials were designed to work on the principle of adsorption and advanced oxidation processes (AOPs). AOPs work on the generation of highly active free hydroxyl radicals ($OH^{\cdot}$) that help in the breakdown of the organic pollutants in wastewater [61]. Al-Fe pillared clays were used as catalysts in the elimination of phenol and total

organic carbon (TOC) *via* a wet oxidation process in the presence of hydrogen peroxide [62]. Extrudates developed from Al/Fe and Al/Ce/Fe pillared bentonite were used as catalysts for the oxidation of phenol [63].

b) Removal of heavy metals

The use of pillared clays and their modified forms in the removal of toxic heavy metals from aqueous solutions has been studied extensively in the past few years. Al-pillared clays are one of the most widely used adsorbents [64][65][66]. In one of the studies conducted in Gujarat, India; Al-pillared bentonite clays were prepared from natural bentonite collected from Ashapur mines. The prepared materials were applied in the removal of cobalt (II) ions from aqueous solution. The maximum adsorption achieved was 99.8% and 87% from initial concentrations of 10 and 25 mg/L [67]. Chromium pillared clays (Cr-PILCs) were applied in the removal of Pb (II) ions from water. The maximum adsorption capacity achieved was 222 mg/g [68]. Some studies also confirmed the use of Ti-pillared clays in the removal of As (III) and As (V) ions [69][70]. Sodium dodecyl sulfate (SDS) modified Fe-pillared clays were used in the removal of aqueous Cu (II) and Co (II) ions. The maximum adsorption capacities achieved were 20.6 and 20.2 mg/g for Cu (II) and Co (II) respectively [26].

c) *Removal of phosphates from wastewater*

For the elimination of phosphates from water, several techniques have been developed such as chemical precipitation, ion exchange, crystallization, and biological treatment [71]. The application of these conventional methods is limited because of high cost, large sludge production and complex operational parameters [72]. In India, the most common technology used in STPs for the removal of phosphates is chemical precipitation and enhanced biological phosphorus removal (EBPR). Metal salts such as aluminium sulphate and ferric chloride salt are added to the sewage water to precipitate out insoluble metal phosphates from water. During the process, a large amount of chemical salts are used which further produces a high quantity of sludge. In EBPR technology, bacteria which are known as polyphosphate-accumulating organisms (PAOs) are used. PAOs have a tendency to accumulate polyphosphates in their cells and they derive energy from these polyphosphates **(Fig**.**7**). However, using these microorganisms is a tedious task because they need both aerobic and anaerobic conditions for the uptake and release of phosphates and their performance is sensitive to the quality and flow of influent (CPHEEO, 2012).

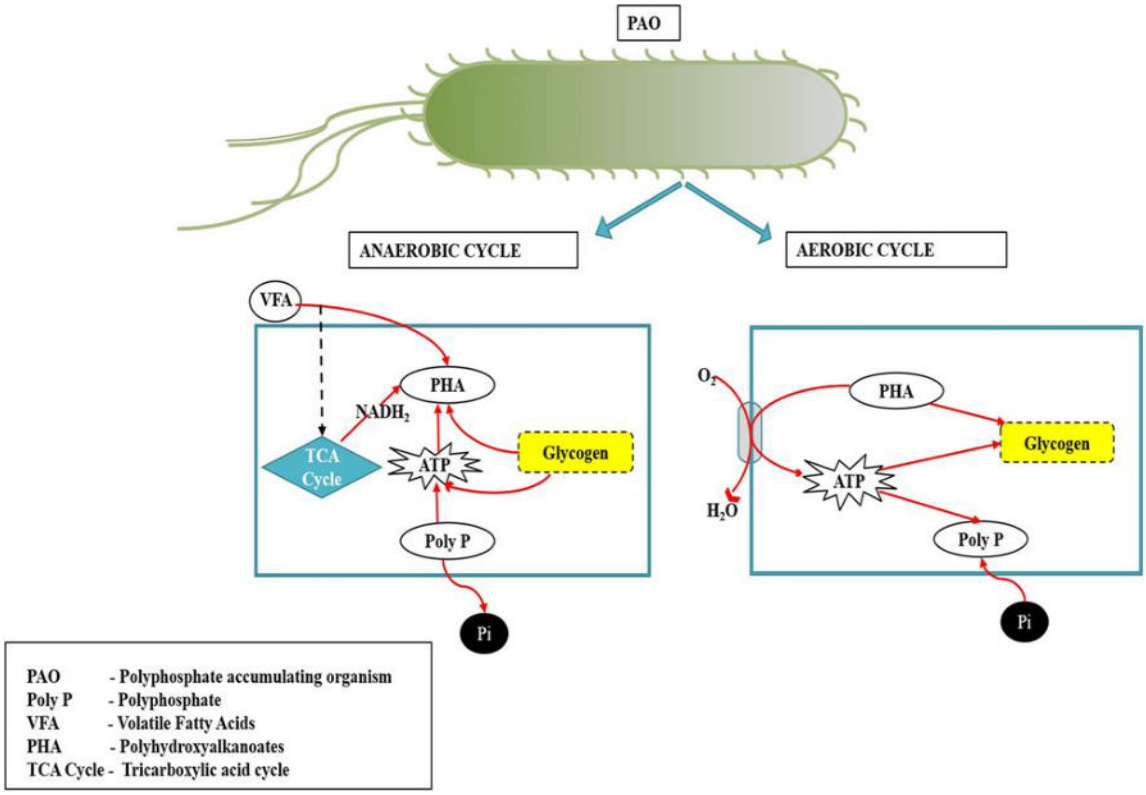

Figure 7: Mechanism of removal of phosphorus by polyphosphate-accumulating organisms (PAOs) [76].

Adsorption is a better alternative due to the availability of low-cost adsorbents with high phosphate removal efficiency and regeneration capacity. A wide range of adsorbents is used for phosphate removal such as metal oxides and hydroxides, zeolites, biochar, steel slag and modified clays [74] [75]. For an adsorbent to be perfect for adsorption, it should have a high surface area and more active sites. Among these materials, clay-based adsorbents are the most promising material for the elimination of phosphorus from water due to their low cost and wide abundance. But their natural form is not very effective therefore modification is required to make them more sustainable and efficient. To improve its phosphate adsorption capacity a series of metal ions such as Fe [76], Al [77], La, or mixed La/Al [78] have been used to modify raw montmorillonite [79]. In the 1990s a novel lanthanum-modified bentonite (Phoslock) was developed by the Commonwealth Scientific and Industrial Research Organisation (CSIRO) of Australia. However, the efficiency of the product was not very high due to its moderate adsorption capacity and there was a risk of leaching out La^{+3} into the water as well [80].

The use of zirconium-based materials has an edge over other materials because of their non-toxicity, better affinity towards phosphates, resistance towards acids/base fluctuations- and

thermal stability [81] [82]. Oxides and hydroxides of zirconium have shown good results in the immobilization of phosphates from the water. Liu et al. in 2008 reported the phosphate adsorption capacity of mesoporous ZrO_2 to be 29.7 mg/g in the pH range of 6.7-6.9 [83]. Liting Zhang and his fellow researchers prepared ZrO_2-coated coal fly ash magnetic spheres with a phosphate adsorption capacity of 16.5 mg P/g in a pH range of 2 [72]. However, the use of pure metal oxides for water purification is not economically feasible and this is one of the biggest limitations of these adsorbents. Therefore, these Zr -pillared clays can be used as a sustainable alternative for water purification. To our knowledge, Huang and co-authors reported the phosphates adsorption study of Zr and Zr/Al mixed pillared clays in 2015 for the first time. The maximum phosphate adsorption capacity of Zr-PILC and Zr/Al-PILC achieved at pH 5 was 13 and 17 mg P/g respectively [19]. Lin et al., 2018 prepared zirconium-modified raw (ZrRBT), Na^+ -pretreated (ZrNaBT), Ca^{+2}-pretreated (ZrCaBT) bentonites with phosphate adsorption capacities of 9.1, 7.3, and 13.4 mg/g at pH 7 [84]. Yinhong and colleagues investigated the phosphate adsorption capacity of zirconium-loaded Ca-montmorillonite. The calculated maximum phosphate adsorption capacity observed was 22.37 mg/g [5]. Recently, a comparative study was carried out by Jingwan Huo et al., in which Zr-modified clays were prepared by using different types of clays based on their structure (kaolinite, vermiculite, and montmorillonite). The phosphate adsorption capacity of Zr-modified montmorillonite was found to be the highest among all i.e., 15 mg P/g [85]. These days chitosan is also gaining attention in the field of adsorption due to its favourable chemical structure. Because of the presence of amino ($–NH_2$) and hydroxy (–OH) groups, it can add more active sites for reaction in adsorbent. The chelating ability of chitosan is mainly governed by the acidity of $-NH_3^+$ groups [55]. In one of the studies conducted by Rajeshwaari and colleagues, the removal of phosphate ions using polyethylene glycol/chitosan and polyvinyl alcohol/ chitosan composites was investigated. The phosphate adsorption capacity of PVA/chitosan and PEG/ chitosan was found to be 45.18 and 74.85 mg/g respectively [54]. Banu and Meenakshi developed Zr^{+4} ions embedded chitosan- soya bean husk activated biochar composite beads for recovery of phosphates from aqueous solution. The adsorption capacity achieved was 90 mg/g at pH 7 [86]. Aswin Kumar and Viswanathan prepared chitosan-supported bentonite composites by adding bentonite clay suspension to the chitosan solution, the resultant suspension was stirred for 24 h at 60˚C. After that 3 % $ZrOCl_2 \cdot 8H2O$ solution (w/v) was added to the chitosan-bentonite colloidal solution (Zr@CSBent); similarly, synthesis of Fe@CSBent and Ca@CSBent were obtained. The phosphate adsorption capacity of the prepared materials was found to be ~40, 22 and 13 mg/g at pH 3 respectively [87]. Qian Liu et al. prepared Zr-loaded cross-linked chitosan

particles by membrane forming technique. The maximum phosphate adsorption capacity achieved was ~71.68 at pH 3 [88]. **Table 1** shows the comparison between the phosphate adsorption capabilities of different adsorbents documented in the literature. Most of the adsorbents were found to work at very low pH.

Table 1: Comparison between the adsorption capacities of other adsorbents reported in literature towards phosphate ions.

Sample	Adsorption capacity (mg/g)	pH	Reference
Lanthanum-modified bentonite	14	6	[89]
Aluminium-pillared acid-activated bentonite powder (Al-ABn)	12.87	5	[90]
Alginate immobilized aluminium-pillared acid-activated bentonite beads (Al-ABn-AB)	11.11	5	[90]
Al-Bent	12.7	3	[91]
Fe-Bent	11.2	3	[91]
Fe-Al Bent	10.5	3	[91]
Phoslock	10.5	5	[80]
Fe-Bent	20.9	3	[92]
Ni-Bent	29.1	3	[92]
Lanthanum encapsulated biopolymer chitosan-kaolin clay hybrid composite	40	6.4	[93]
Fe_3O_4/ZrO_2/Chitosan	26.5	3	[94]

d) Biological pathogen removal

Clay minerals are known as naturally occurring antimicrobials which are capable of the elimination of biological pathogens from water. Key factors which are responsible for the adsorption of bacteria and viruses on the surface of clay structure are surface charge, surface functional groups, specific surface area and hydrophobicity [95]. Different types of clays and modifications have been reported in the literature for the removal of bacteria from water. Pyrophyllite is a 2:1 type, hydrous aluminosilicate clay mineral with a chemical structure of $Al_2Si_4O_{10}(OH)_2$. This clay was effective in 94% removal of *Escherichia coli* bacteria from an aqueous solution at pH 7. The negatively charged bacteria were removed due to their adhesion to positively charged surfaces of pyrophyllite [96]. In one of the

studies, kaolinite and montmorillonite were used for the adsorption of *Pseudomonas putida*. Better adsorption of *P. putida* was observed on kaolinite than on montmorillonite. Adsorption of bacteria on clay minerals resulted in the shift of absorption bands of water molecules suggesting the involvement of hydrogen bonding during the process of adsorption [97]. Cu^{+2}-exchanged montmorillonite clays (Cu-MMT) have been prepared by Hang Xu and Sheng Xia for the elimination of *E. coli* K_{88} bacteria responsible for diarrheal disease from water. Copper compounds are known for their antibacterial properties but in water it is difficult for Cu^{+2} ions to make contact with bacteria therefore a large amount of copper salt is used to increase the efficiency. To decrease the Cu^{+2} supplementation, clay minerals are used as supporting material. Among Cu^{+2}-exchanged acid-activated montmorillonite (Cu-AAM), Cu-Na-MMT and Cu-Ca-MMT; Cu-AAM has shown the highest antibacterial activity. The possible mechanism suggested was the surface charge of Cu-MMT helped in bringing the bacteria closer to the clay surface where Cu^{+2} ions exert antibacterial activity [98]. Ting Wu and colleagues studied the antimicrobial properties of quaternary phosphonium salt (tetradecyl tributyl phosphonium bromide, TDTB) intercalated clays against *E. coli* and *Staphylococci aureus (S. aureus)*. They concluded that the antibacterial activity of the prepared organ-clay minerals depends upon three factors; the releasing amount of phosphonium salt, surface charge and particle size of organ-clay minerals [99]. Clay-polymer composites were synthesized by adsorption of cationic polymers onto negatively charged clay mineral platelets (Bentonite). The polymer used is cationic starches which are generally used as additives in paper-making, textile and cosmetic industries. The composites were used in the filtration system for disinfection of *E. coli* from water. The antimicrobial effect was created by the cationic polymers adsorbed on the clay surface which helped in the lysis of the bacterial cell by creating a positive surface potential on the clay complex which facilitates the adherence of bacteria as a result of strong electrostatic interaction that would cause segregation of negatively charged phospholipids from the cell membrane [100]. Montmorillonite clay was exchanged with cationic surfactant cetyl pyridinium to produce CP-AAM (acid-activated montmorillonite), CP-Na-MMT and CP-Ca-MMT for adsorption of *Salmonella enteritidis.*CP-AAM was observed to have the highest antibacterial activity. The charge of these modified clays was responsible for attracting the bacteria towards their surface via electrostatic interactions. There might be the possibility of having a hydrophobic attraction between the hydrophobic alkyl chains of cetylpyridinium and lipophilic components of the bacterial cell walls, such as lipoproteins, liposaccharides and phospholipids [101]. A new class of metal-doped hybrid clay

composites has been designed by Emmaneul et al., by using kaolinite clay, Carica *papaya* seeds and $ZnCl_2$.The materials were found to have bacteriostatic properties against *Vibrio cholera* and *Salmonella typhyi*. The bacteria removal efficiency of these materials was a result of the interaction between the phosphate units of bacterial cell walls and metal species on the surface of composites. It is proposed that the phosphate units from bacterial cell wall form the bonds with metal oxide surface. In these composites as well, it was suggested that ZnO is responsible for capturing the bacteria [102]. Clay minerals (mica and montmorillonite) were exfoliated for the production of nanoscale silicate platelets exhibiting strong surface interaction with bacteria and inhibiting their normal microbial growth. These nanoscale silicate platelets were allowed to associate with magnetic iron-oxide nanoparticles [103].

There are few studies which suggest that zirconia also has antibacterial properties [104][105]. But to our knowledge, there is not a single article in literature which has used zirconium pillared clays against *E. coli* adsorption. Despite having so many outstanding properties, the application of clay minerals in the field of water purification has not yet been fully explored. Clay-based adsorbent materials might have the potential to substitute conventional methods used for the disinfection of wastewater.

3. KNOWLEDGE GAP

- In literature, the synthesis method of pillared clays has been reported but the effect of sodium pre-treatment and ratio of Zr^{4+}/clay on the process of pillaring is still not very clear. From the literature, it is difficult to optimize the Zr^{4+}/clay ratio at which the best pillaring can be achieved also there is very little information about the size of zirconium pillars which are created in between the silicate layers. A detailed comparative analysis of the prepared materials was done for a better understanding of the nature of zirconium pillars created inside the clay structure. In this work, a novel analysis about the dimensions and distribution of microstructures produced by the pillaring process was made with the help of HRTEM, STEM-EDX and HAADF imaging techniques.

- In literature, the usage of Zr-pillared clays in the removal of phosphates from water and the mechanism of phosphate adsorption on clay surface is not widely explored. The modified clays which are reported in the literature have shown better adsorption capacity at acidic pH but we tried to improve the adsorption capacity of Zr-pillared clays by applying modification with a natural biopolymer chitosan. After modification, the pillared clays were working effectively even at neutral pH. To the best of our knowledge, no study has reported the application of chitosan-based zirconium pillared clays in the sequestration of phosphates at acidic and neutral pH.

- There is very limited research on the applicability of clay-based composites in the elimination of biological pathogens from water. The physical and chemical properties of montmorillonite clay are suitable for converting them into a sustainable, environment and budget-friendly option for water remediation. We took a novel approach to explore the ability of Zr-pillared clays for the removal of *E. coli* bacteria from an aqueous solution. There has been no study reported in the literature on the adsorption of *E. coli* bacteria using zirconium pillared clays.

4. AIM OF THESIS

The primary objective of this study is to create sustainable and environment-friendly clay-based adsorbent materials suitable for the elimination of water contaminants such as phosphates and bacteria. To achieve this goal, naturally occurring montmorillonite clay is used and modified using zirconium oxychloride octahydrate and chitosan. The present study focuses on the synthesis methods of Zr-pillared clays and chitosan-modified zirconium pillared clay and their application in wastewater treatment. The aim of the thesis is divided into three parts:

i. The first part is the development and optimization of the synthesis method of zirconium pillared clays and chitosan-modified clay using a suitable precursor material (CM and Na-CM) at different Zr^{4+}/clay ratios (2.5, 5 and 10 mmol/g). CM is the naturally occurring raw montmorillonite and Na-CM is the sodium pre-treated montmorillonite. A detailed investigation will be performed to determine the influence of Na^{+} pre-treatment on the process of Zr^{4+} cations intercalation in between the silicate layers. A thorough comparative analysis of the prepared materials will be done for a better understanding of the nature of zirconium oxide pillars created inside the clay structure using different techniques like XRD, STEM-HAADF, EDX, FT-IR spectroscopy, TGA and CO_2 adsorption for specific surface area analysis.

ii. The second part focuses on the potential use of prepared materials in the sequestration of phosphates from water. Comprehensive sets of experiments will be conducted in batch mode at different pH (4 and 7) and in a wide range of phosphate concentrations (1-20 mg/L) to determine the phosphate adsorption capacities of the prepared adsorbent materials. The experimental data will also be modelled with different adsorption isotherm models such as Langmuir, Freundlich and Toth models. The mechanism of phosphate adsorption on clay adsorbent will also be explored with the help of different techniques such as XPS and DLS.

iii. In the third part, the application of prepared materials will be explored in the adsorption of *E. coli* bacterial cells from an aqueous solution. *E. coli* cells are indicators of contaminated water bodies not suitable for drinking or recreational activities. In this study, a novel approach is taken for the removal of bacterial cells using zirconium pillared clays.

5. EXPERIMENTAL SECTION

5.1 Materials

For the synthesis of Zr-pillared clays:

- Naturally occurring raw montmorillonite (CM) from VWR
- Zirconium oxychloride octahydrate ($ZrOCl_2.8H_2O$ of purity 98%)
- Potassium chloride (KCl)
- Ethanol
- Sodium chloride (NaCl)
- Silver nitrate ($AgNO_3$)
- Hydrochloric acid (HCl)
- Copper sulphate ($CuSO_4$)
- Tris (hydroxymethyl) aminomethane
- Ethylenediamine ($C_2H_8N_2$ of purity 99%)

For the synthesis of chitosan-modified zirconium pillared clays

- Chitosan with a degree of deacetylation of ≥75 %
- Acetic acid
- Sodium pre-treated montmorillonite (Na-CM)
- Zr-pillared clay (Na-Zr-50-2.5)

For the phosphate adsorption test

- Potassium dihydrogen phosphate (KH_2PO_4)
- Distilled water
- Nylon membrane filters (0.45µm)

For adsorption of *E. coli*

- Tryptone
- Bacteriological agar
- Yeast extract
- NaCl
- *Escherichia coli* DH5α (SZMC 21399) (Gram-negative) strain obtained from the Department of Microbiology, Faculty of Science and Informatics, University of Szeged
- For the adsorption test, Na-CM and Na-Zr-50-2.5 clay samples were used.

5.2 Synthesis

i. Preparation of Zr-pillared clays

The zirconium-pillared clays were prepared from two precursor clay materials named raw montmorillonite (CM) and sodium pre-treated montmorillonite (Na-CM). For preparing Na-CM, raw clay was saturated with 1M NaCl for 24 h. The next day, clay was recovered from the salt solution using a centrifuge followed by washing and drying at 60 ˚C. $ZrOCl_2.8H_2O$ pillaring solution (0.1 M) was prepared and aged for 24 h at room temperature. The Zr-pillared clays were synthesized using three Zr^{4+}/clay ratios (2.5, 5, 10 mmol/g). The precursor clay materials were dispersed in distilled water to make a clay suspension. The clay suspension was stirred for 2h at room temperature then the pillaring solution was added to the clay dropwise and kept at 50 ˚C under vigorous stirring. The suspension was left for stirring for 2h, followed by an ageing of 12 h at 50 ˚C. After this, the intercalated clay was centrifuged, washed thoroughly and dried at 120 ˚C. The Cation exchange capacity (CEC) of CM (56 $cmol^+/kg$) and Na-CM (52 $cmol^+/kg$) was also determined using the adsorption of copper ethylenediamine complex, $[Cu(en)_2]^{+2}$ [106]. The total number of samples prepared is shown in Table 2.

Table 2: Number of samples prepared with precursor and Zr^{4+}/clay ratios.

No.	Zr-modified samples	Precursor material	Zr^{4+}/Clay (mmol/g)
1	Zr-50-2.5	CM	2.5
2	Zr-50-5	CM	5
3	Zr-50-10	CM	10
4	Na-Zr-50-2.5	Na-CM	2.5
5	Na-Zr-50-5	Na-CM	5
6	Na-Zr-50-10	Na-CM	10

ii. Preparation of chitosan-modified zirconium pillared clays

For the preparation of chitosan-based zirconium pillared clays, 1g of chitosan powder was added to 2% (v/v) acetic acid aqueous solution and mixed until it dissolved completely. After this, 2g of Na-Zr-50-2.5 was added to 100 ml of distilled water and stirred for 1 h at room temperature. To this pillared clay suspension, the chitosan solution was added dropwise at room temperature under slow stirring. The solution was left for overnight ageing. The next day it is washed thoroughly, centrifuged and dried at 80˚C for 4h. The synthesized material is named as Ch-NaZr2.5 **(Fig. 8)**. Sodium pre-treated montmorillonite is also treated with chitosan solution and the material is named as Ch-NaCM.

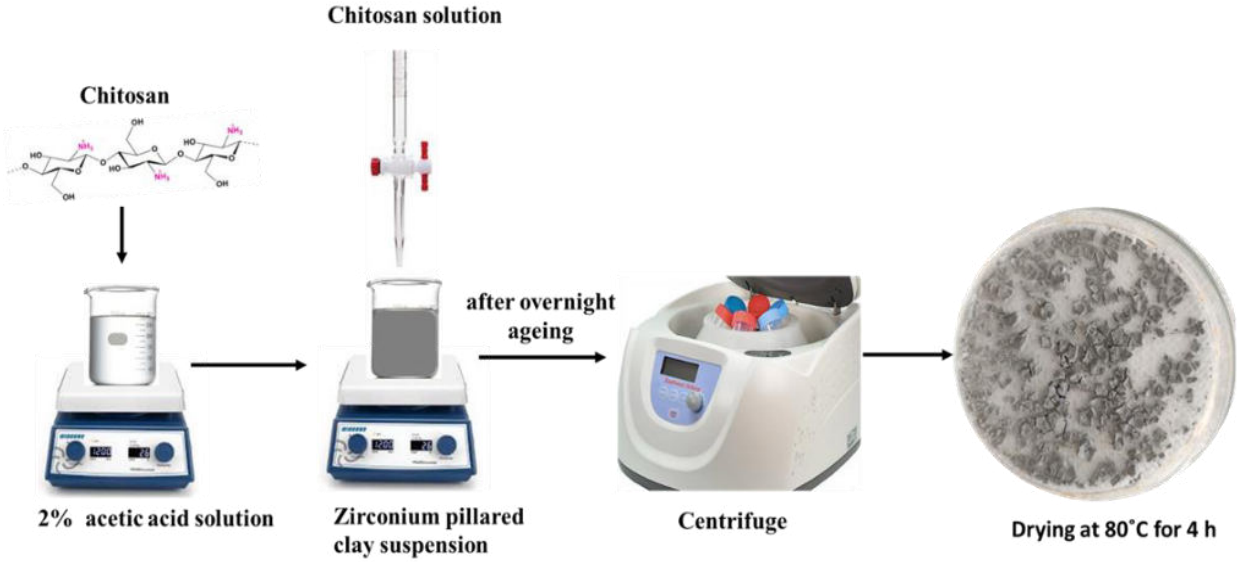

Figure 8: Schematic diagram of the synthesis of chitosan-based zirconium pillared clay.

iii. Preparation of LB-media, LB-agar plate, and Physiological saline solution

Luria-Bertani (LB) liquid broth is the most widely used medium for growing *E. coli* bacteria. For preparing 1 L of LB medium, 10 g of tryptone, 5 g of yeast extract and 10 g of NaCl were dissolved in ultrapure water with the help of a magnetic stirrer. After that, 35 mL of LB solution was transferred into the Erlenmeyer flask. The mouth of the flask was sealed with a cotton plug to avoid any contamination and was put into an autoclave for sterilization at 121

°C for 15 min, (103 to 117 kPa) [107]. This sterile media was used for culturing the *E. coli* and making starter bacterial suspensions. To attain this, a single colony of *E. coli* DH5α was taken from the LB agar plate with the help of an inoculation loop and put into the sterile LB liquid. Afterwards, the LB suspensions plugged with cotton were placed in an incubator overnight under continuous shaking at 160 rpm and 37 °C. The next day, the optical density of the bacterial starter solution was measured using a sterile LB medium as a blank solution. The optical density was measured at 600 nm (OD_{600}). This value helps in determining the growth stage of bacteria and the cell concentration of the starter culture. The OD measurement was crucial to check and ensure a uniform initial cell concentration for all the adsorption tests. During the experiments, the cell count of the used starter cultures was $1.00 \pm 0.05 \times 10^9$ CFU/mL.

The LB agar plates provide a nutrient-rich surface for the growth of bacteria. To prepare this, 15 g of bacteriological agar was added to 1000 mL of the LB medium. For proper mixing of agar in LB medium, the solution was autoclaved and sterilized properly. The prepared transparent LB agar solution was cooled to ~50 °C with the help of a water bath and then it was spread evenly on sterile plastic Petri dishes having a diameter of 90 mm. The prepared plates were left to solidify in a biological safety cabinet under aseptic conditions. These plates were later used in the colony counting method.

The *E. coli* adsorption experiments were carried out in a physiological saline solution. In this solution, the bacterial cells could survive with minimal cell division thus ensuring a constant cell density throughout the study. It was prepared by dissolving 8.5 g NaCl in ultrapure water (1L) followed by sterilization in an autoclave at 121°C.

5.3 Characterization techniques

5.3.1 X-ray powder diffraction (XRD)

XRD measurements were performed with Bruker D8 Advance instrument (Cu-Kα source, 40 kV and 40 mA generator settings) in parallel beam geometry obtained with Göbel mirror and Vantec1 position sensitive detector (1° opening). Measurements were recorded in the 2-70˚ (2θ) range with 0.007˚ (2θ)/24 counting time.

5.3.2 Surface area measurement

The specific surface area was determined by CO_2 adsorption at 273 K using the ASAP 2020 instrument (Micromeritics Instrument Corp. USA). Dubinin Asthakov model was applied for

the CO_2 adsorption isotherms. Before making the measurements, the samples were degassed at 90 ˚C for 24 h.

5.3.3 Thermogravimetric analysis (TGA)

TGA was done using the MOM Derivatograph C/PC instrument. Approximately, 100 mg of sample was heated from 25 to 1000 ˚C at a rate of 5 ˚C/min under air.

5.3.4 Fourier transform infrared spectroscopy (FTIR)

FTIR, Bruker Vortex 70 was used to investigate the structure, bonding, and chemical properties of clay samples. Measurements were taken in the wavenumber range of 400 to 4000 cm^{-1} with an average of 50 scans and a resolution of 4 cm^{-1}.

For modified clays before and after phosphate adsorption, the measurements were taken by Bruker Tensor 27 spectrometer with Pike Technologies GladiATR magnifying Diamond ATR sampler in a wavenumber range of 400 to 4000 cm^{-1} with an average of 128 scans and a resolution of 4 cm^{-1}.

5.3.5 High-Resolution Transmission Electron Microscopy (HRTEM)

HRTEM micrographs were obtained using a Hitachi HF3300S environmental transmission electron microscope. Digital micrographs of the clay samples were further analyzed using Fast Fourier Transforms (FFT). An in-house developed, open-source image analysis code was used to measure basal spacing in HRTEM images [108]. The thickness and spatial distribution of the Zr-rich domains were further studied in Scanning TEM (STEM) mode using High Angle Annular Dark Field (HAADF) imaging and Energy Dispersive X-ray Spectroscopy (EDX, Oxford Instruments SDD X-Max^N 80T). Non-negative matrix factorization (NMF), which was implemented via the HyperSpy library for Python, was used to aid the localization of Zr-rich regions in the EDX spectrum images.

5.3.6 Dynamic light scattering (DLS)

Zeta potential (ζ) measurements were performed by microelectrophoresis (Zetasizer Nano ZS, Malvern Instruments, UK). Clear disposable capillary cells (DTS 1070, Malvern Instruments, UK) were used for the electrophoretic measurements. NaOH and HCl solutions of 0.1 and 0.01 M were used as titrants to adjust the pH values and distilled water was used as dispersant. Measurements were taken in the pH range of 3 to 11.

5.3.7 X-ray photoelectron spectroscopy (XPS)

X-ray photoelectron spectroscopy (XPS) examined the samples' chemical states and composition using the Supra plus instrument (Kratos, Manchester, UK). Measurements were controlled by ESCApe 1.5 software (Kratos). The instrument was equipped with an Al K_α excitation source. The binding energy scale was corrected using the C-C/C-H peak at 284.8 eV in the C 1s spectra. The charge neutralizer was turned on for the XPS analysis. The 300 by 700-micron spot size was used to acquire the spectra at a 90° take-off angle. Survey and high-resolution spectra were recorded at pass energies of 160 eV and 20 eV, respectively. Shirley background subtraction was used for background subtraction.

5.3.8 Scanning electron microscopy (SEM)

The surface morphology of the clay samples was investigated by scanning electron microscope. It was performed by a ThermoFisher Helios G4 PFIB CXe operating in the range of 5-20 keV. Before the measurement, the sample surface was coated with gold.

5.3.9 Energy-dispersive X-ray spectroscopy (EDX)

The EDX measurement of the clay samples was completed with the SEM equipped with an EDAX AMETEK Elect Plus detector. Typical EDX maps and spectra were acquired using an acceleration voltage of 20 keV with a beam current of 13 nA and a dwell time of 500 µs.

6. RESULTS

6.1 Investigation of pillared clays prepared from CM and Na-CM

The properties of the as-prepared Zr-pillared clays were tested using different characterization techniques and their results will be discussed in the sub-sections below:

6.1.1 XRD analysis of precursor and pillared clays

Figure 9A displays the XRD patterns of Zr-pillared montmorillonite (Zr-50-2.5, Zr-50-5, and Zr-50-10) and raw montmorillonite (CM). In CM, a very distinct diffraction peak appeared at 6.97˚ corresponding to a basal spacing of 1.26 nm, and a weak peak appeared at 19.82˚ corresponding to the montmorillonite (Mt) crystal structure. There were two further notable diffraction peaks at 21.95˚ and 26.64˚, which were identified as quartz and cristobalite impurities, respectively. In Zr-50-2.5, the intensity of the Mt peak decreased and shifted toward lower 2θ, i.e., 5.08˚ corresponding to a basal spacing of 1.74 nm. The increase in basal spacing by 0.48 nm implied the intercalation of Zr^{4+} cations into the interlayer space of the clay mineral, however, the decreased peak intensity suggested a degree of aperiodicity in the clay structure. In Zr-50-5, two weak reflections were obtained at 2θ = 5.08˚, 8.8˚ corresponding to d_{001} values of 1.74 and 1 nm, respectively. Weak reflections indicate that the layers of clays were not homogenously spaced. In Zr-50-10, the Mt peak shifted toward 2θ = 8.94˚, corresponding to d_{001} = 0.99 nm. The thickness of the silicate layer in montmorillonite is ~1 nm [45] – this means that at higher concentrations of zirconium, the basal spacing decreased and the crystal structure of the clay started collapsing.

Figure 9B displays the XRD patterns of Na-CM and its Zr-modified forms (Na-Zr-50-2.5, Na-Zr-50-5, and Na-Zr-50-10). In Na-CM, a reflection appeared at 2θ = 7.77˚ with a d_{001} value of 1.13 nm corresponding to the Mt peak. A remarkable shift of the Mt peak toward the lower 2θ value and higher basal plane spacing was observed in the pillared samples. In Na-Zr-50-2.5 and Na-Zr-50-5, well defined Mt peaks were observed at 2θ = 4.84˚, 4.76˚ (d_{001} =1.82, 1.85 nm), respectively. These d_{001} values matched the literature data [109] [5]. The increase in basal spacing by 0.69 and 0.72 nm proves that pillaring was successful in both samples. However, in the case of Na-Zr-50-10, a split in the peak was observed at 2θ = 4.60 ˚, 7.37 ˚ (d_{001} = 1.93, 1.19 nm) which suggested the presence of two fractions of clay with different basal spacing.

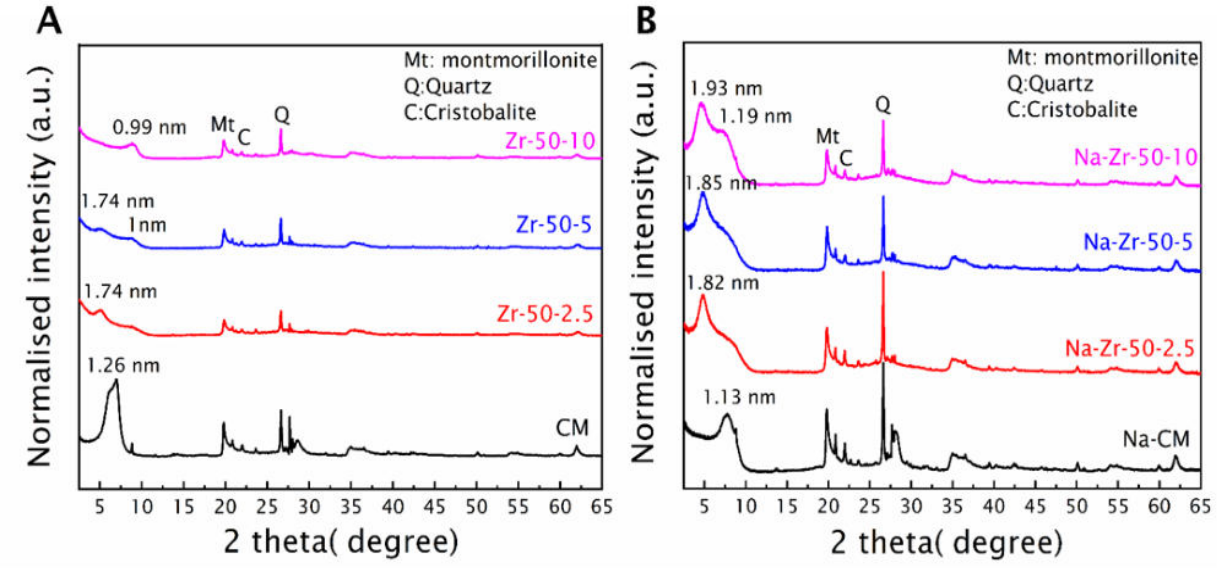

Figure 9: XRD patterns of raw and Zr pillared montmorillonite **(A)**; and sodium saturated montmorillonite clays **(B).**

6.1.2 Measurement of specific surface area (SSA)

The specific surface area of clay samples was analysed using CO_2 at 273 K. The CO_2 adsorption isotherms are shown in **Fig.10**. The Dubinin-Astakhov (DA) model was used for the estimation of specific surface area. The micropore volume and SSA values are summarized in **Table 3.** It was observed that the SSA of pillared clays obtained from CO_2 adsorption were very high as compared to their precursor material. The SSA of CM was 40.5 m^2/g and increased significantly after the intercalation of Zr^{4+} ions; Zr-50-2.5 achieved the maximum SSA followed by Zr-50-10 and Zr-50-5. The SSA of precursor material (Na-CM) was 28.3 m^2/g but after the intercalation of Zr^{4+} cations in between clay sheets it increased to 216 and 240 m^2/g in Na-Zr-50-2.5 and Na- Zr-50-5 respectively. The micropore volume also increased from 0.012 cm^3/g (Na-CM) to 0.099 and 0.122 cm^3/g in Na-Zr-50-2.5 and Na- Zr-50-5 respectively. The possible explanation for this could be when zirconium oxide pillars are created inside the silicate layer, expansion of the clay layers takes place and vacant sites are created in the interlamellar space of clay particles. Which is responsible for introducing microporosity and a larger specific surface area.

Table 3: Textural properties of precursor and Zr-pillared clays.

Sample	Specific surface area S_{DA} (m^2/g)	Micropore volume (cm^3/g)	Average pore diameter (nm)
CM	40.5	0.021	2.03
Zr-50-2.5	280	0.143	2.04
Zr-50-5	129	0.054	1.7
Zr-50-10	134	0.056	1.67
Na-CM	28.3	0.012	1.75
Na-Zr-50-2.5	216	0.099	1.84
Na- Zr-50-5	240	0.122	2
Na-Zr-50-10	135	0.057	1.7

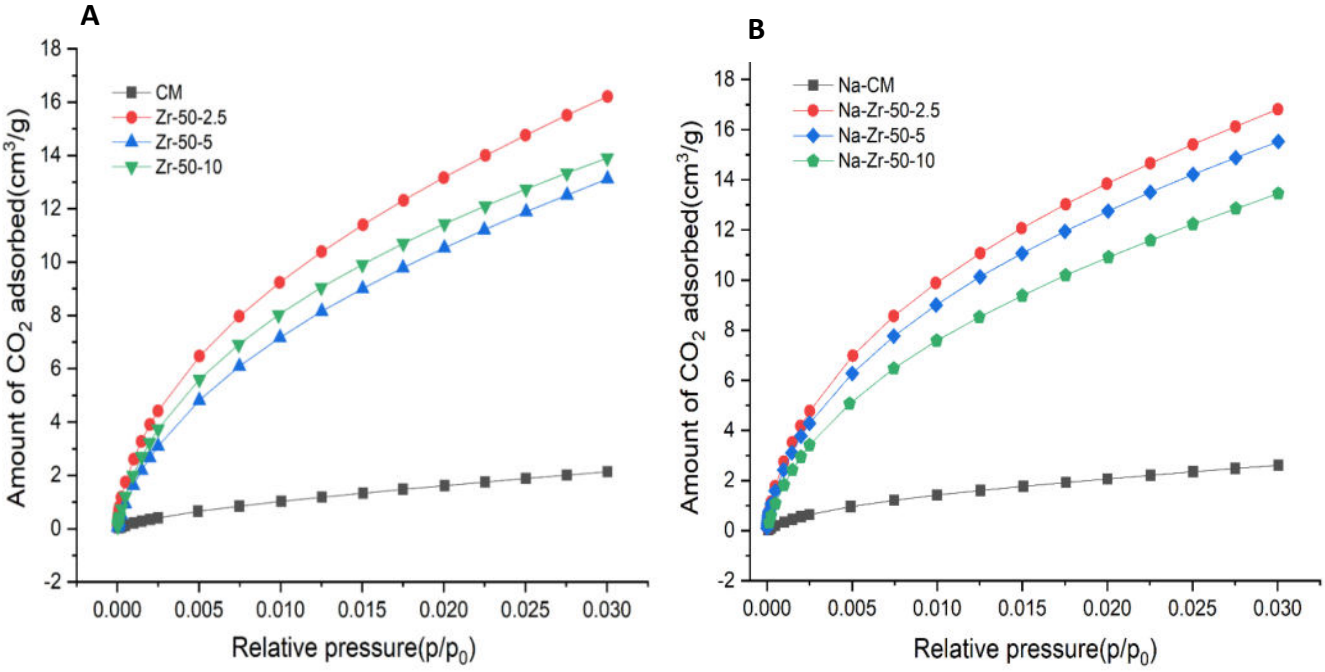

Figure 10: CO_2 adsorption isotherms on CM **(A)** and Na-CM **(B)** and their pillared forms.

6.1.3 FTIR analysis of raw and pillared clays

The FTIR spectra of the raw and the pillared clays are shown in **Figs. 11 & 12**. In **Fig. 11**, CM exhibited a band at 3623 cm^{-1} corresponding to the stretching vibration of the O-H bond coordinated with aluminium atoms of the octahedral layer [110]. In the pillared samples, this band disappeared. Bands near 3422 cm^{-1} and 1635 cm^{-1} were attributed to the H-O-H stretching and bending vibrations of adsorbed water [111] [112]. The former band is related to the presence of interlayer water. As an effect of the modification, these bands disappeared in zirconium-treated samples. The Si-O stretching vibration was represented in the range of 1200-700 cm^{-1} [110] [113]. This band was shifted towards a higher wavenumber in zirconium-treated samples. The bands at 915 cm^{-1} and 846 cm^{-1} originated from the deformation of Al-Al-OH and Al-Mg-OH, respectively [114] [115]. The intensity of bands between 500-1000 cm^{-1} decreased in the Zr-modified samples.

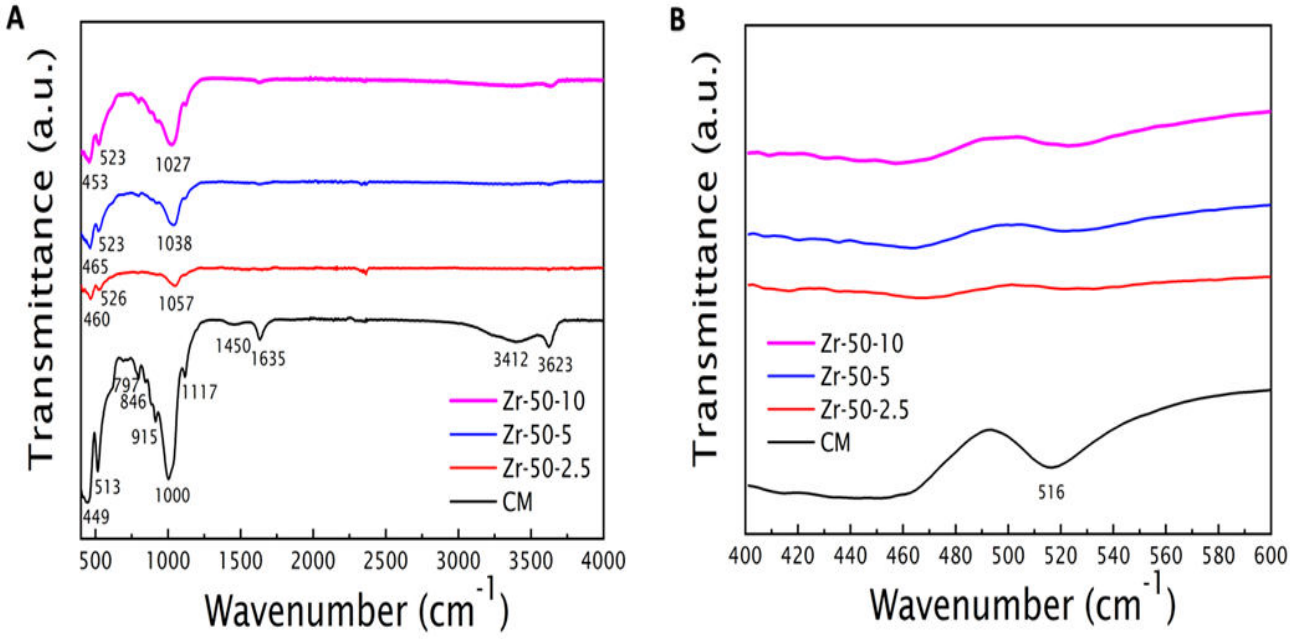

Figure 11: FTIR spectra of CM and Zr-50-2.5, Zr-50-5 and Zr-50-10 **(A, B).**

In pillared forms of Na-CM (Na-Zr-50-2.5, Na-Zr-50-5), new bands were identified in the spectral range of 400-500 cm^{-1} **(Fig. 12B)**. In Na-Zr-50-2.5, two new bands were observed at 404 and 418 cm^{-1}. Three new bands at 410, 420 and 442 cm^{-1} appeared in the case of Na-Zr-50-5 **(Fig. 12B)**. These new vibration bands were attributed to the presence of Zr-O bonds [116] [117] [118]. The FTIR results supported the XRD results which confirm the successful intercalation of Zr^{4+} cations in between the clay sheets.

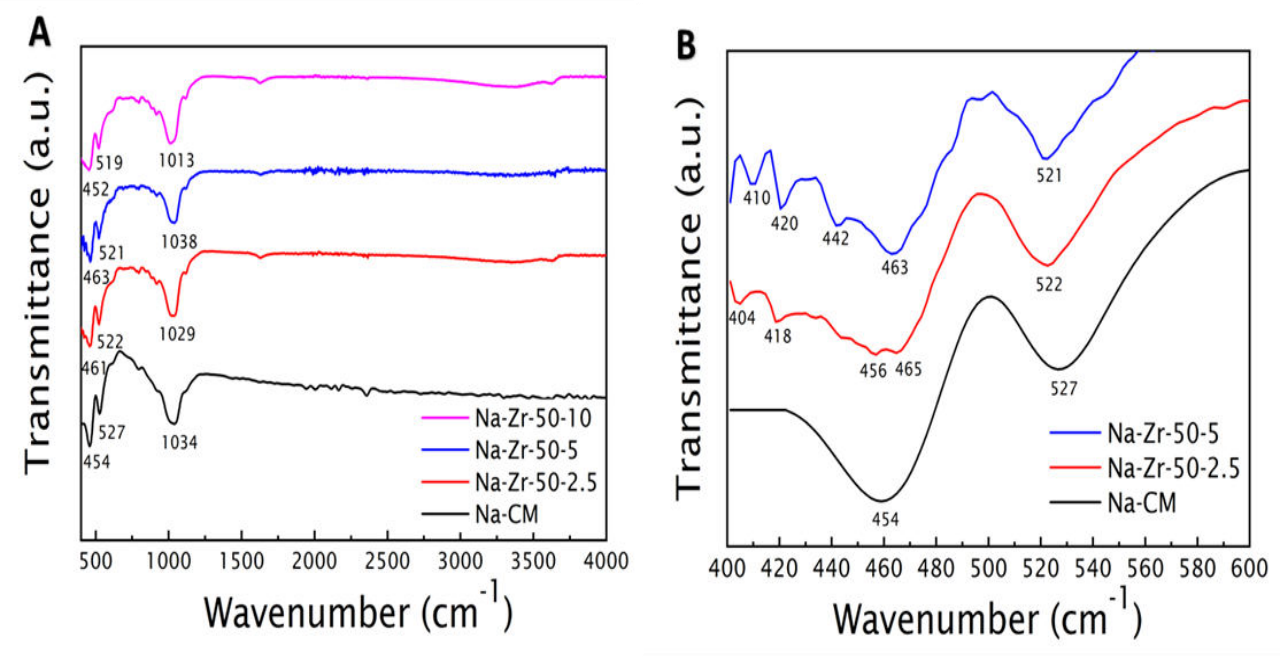

Figure 12: FTIR spectra of Na-CM and Zr pillared Na-CM **(A, B).**

6.1.4 Thermal behaviour of raw and pillared clays

Fig. 13 and 14 show the thermogravimetric and the derivative curves of precursor and pillared clays. TG curve represents the percentage mass loss in the material over a range of temperatures; the derivative of which with respect to temperature (DTG) was used to study the steps of thermal transformation. In **Fig. 13**, the thermogravimetric curves of Na-CM and pillared clay samples show that the stability of the clay structure increased after pillaring. This can be attributed to the fact that during the process of pillaring, stable metal oxide pillars are formed between the silicate sheets that impart rigidity to the clay structure. Previous studies revealed that the thermal decomposition of clay takes place in two steps: in the range of 35-150˚C, physically adsorbed water is lost, and in 450-800˚C, dehydroxylation of silicate structure takes place [119] [120]. In consistence with this, the first step of thermal

decomposition could be seen between 25-110 ˚C, while the second step was observed between 400 and 800˚C. Pillared samples exhibited higher relative mass loss than Na-CM at lower temperatures and lower mass loss at higher temperatures corresponding to the removal of hydroxyl groups from the internal and external surface of the PILCS. In the case of Zr-modified samples, additional mass loss in the first step can be expected due to zirconium ions. In the case of CM and its pillared forms, similar results were obtained except in Zr-50-5 and Zr-50-10 in which the percentage of first weight loss is lesser than CM (**Fig. 14)**.

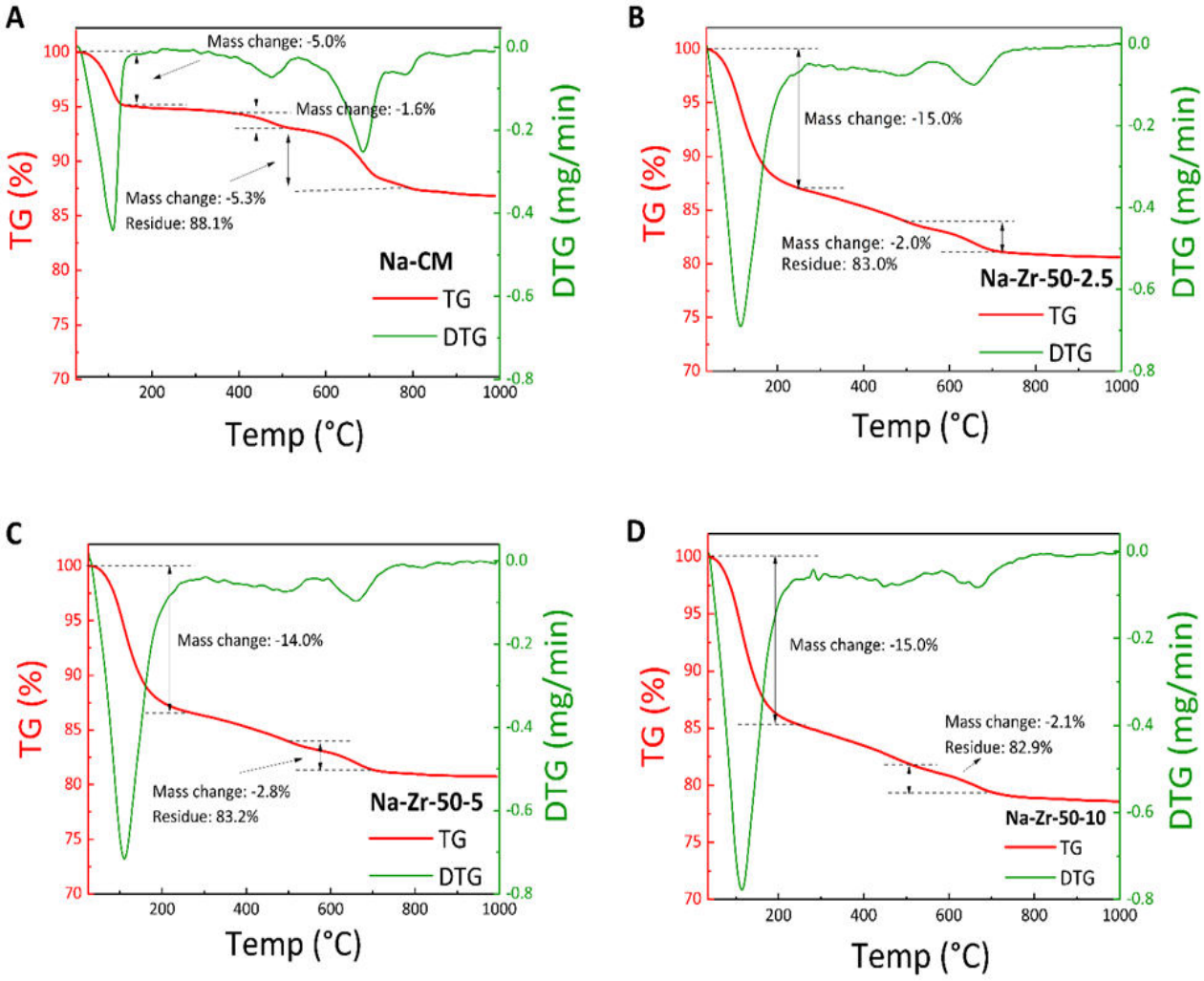

Figure 13: Thermogravimetric curves of Na-CM **(A)**; Na-Zr-50-2.5 **(B);** Na-Zr-50-5 **(C)** and Na-Zr-50-10 **(D).**

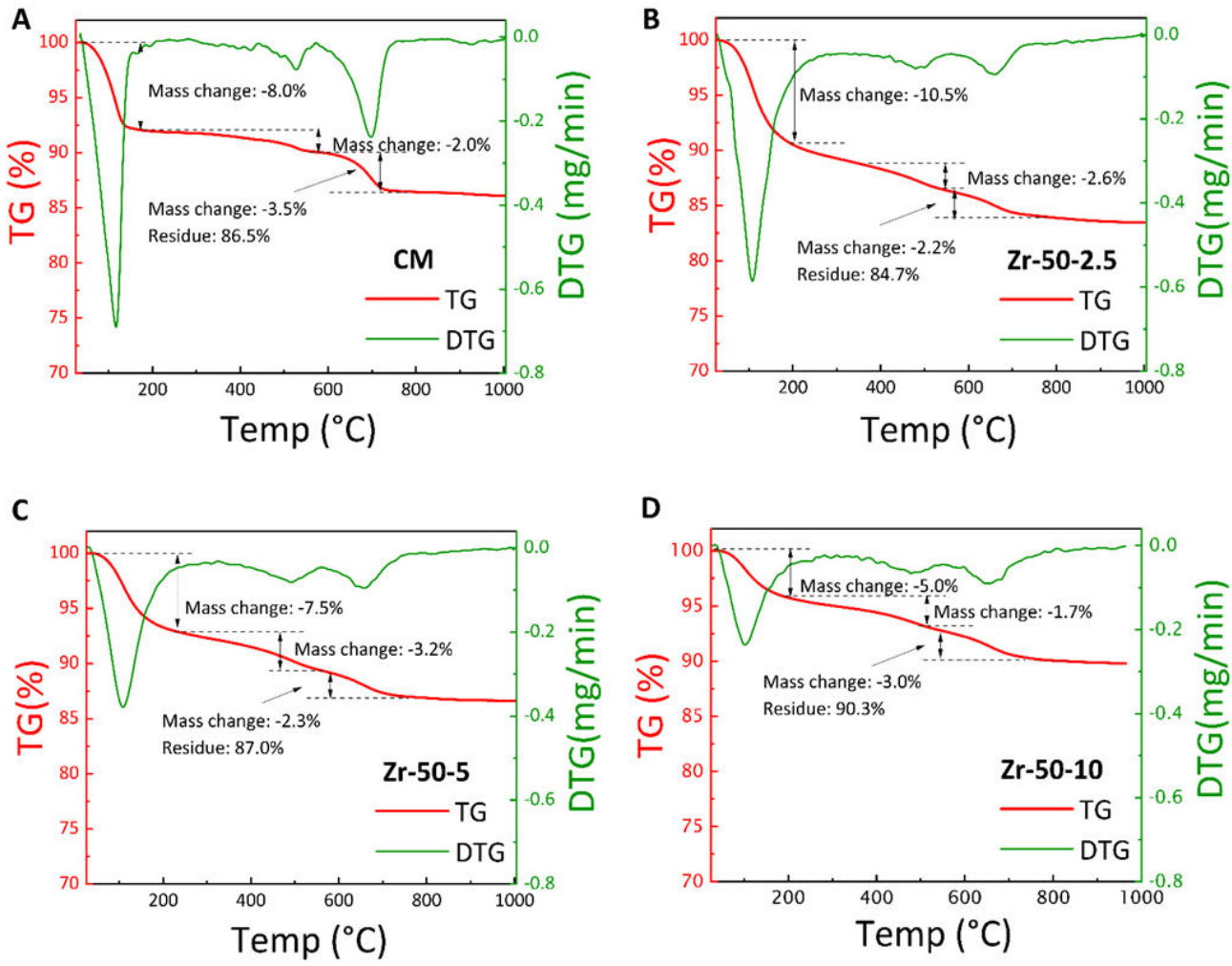

Figure 14: Thermogram of CM **(A);** Zr-50-2.5 **(B);** Zr-50-5 **(C)** and Zr-50-10 **(D).**

6.1.5 High-Resolution Transmission Electron Microscopy (HRTEM) analysis of raw and pillared clays

The nature of the ZrO_2 pillars created in between the silicate layers was further investigated using STEM-HAADF imaging and EDX spectroscopy. A comparison of a HAADF image and the Zr-rich component from the corresponding EDX spectrum image **(Fig. 15C)**, acquired in a viewing direction parallel to the clay basal planes, reveals that the bright areas in the former can be ascribed to intercalated ZrO_2. This interpretation is also supported by the high HAADF-intensity of these areas, which stems from the much larger atomic number of Zr compared to the other elements present in the clay. Higher-resolution HAADF images (**Fig. 15D, E)** display thin Zr-rich layers evenly distributed throughout the material. Due to this very even distribution of ZrO_2 in the Na-treated samples, it was not possible to distinguish individual layers over a

large field of view at higher Zr loading (i.e., in Na-Zr-50-10). For both Na-Zr-50-2.5 and Na-Zr-50-5, the thickness of the bright layers, measured at FWHM, varied between approximately 1-2 nm. The domains were separated from peak to peak by approximately 1.5-3.0 nm. The measured layer thicknesses and separations approximately match the basal distance of the expanded clay (or a multiple of the same), indicating that the intercalation occurs at every or every second layer, which agrees with the XRD results **(Fig. 9)**.

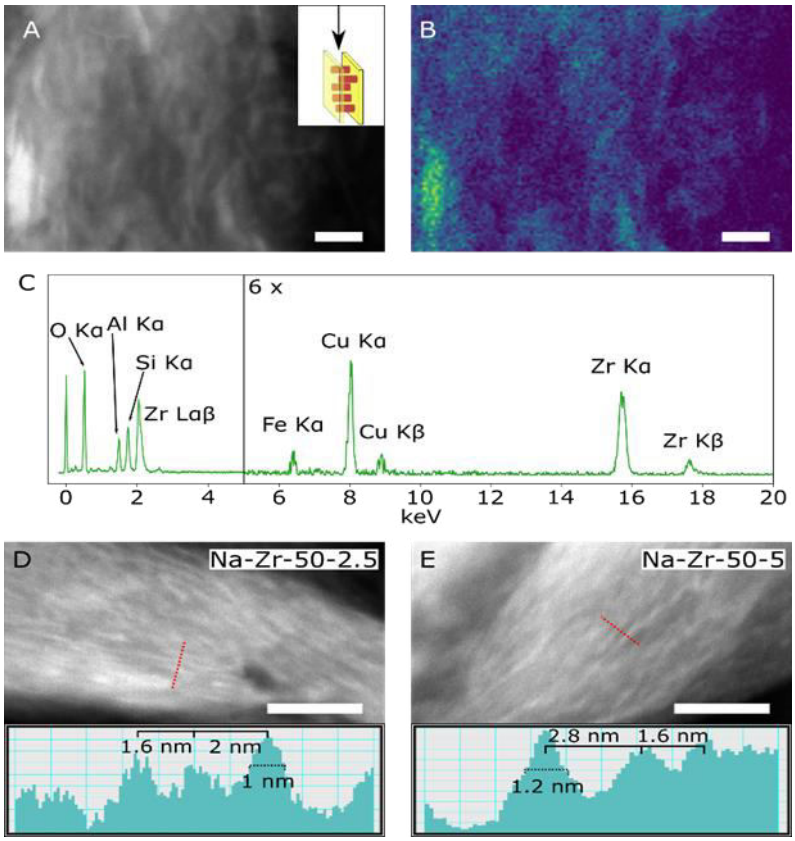

Figure 15: The similarities between the STEM-HAADF (A) and STEM-EDX map of Zr-rich areas **(B)** in Zr-50-10 show that the bright fringes in the HAADF images can be correlated to areas rich in Zr. The inset in **(A)** illustrates the viewing direction, where the intercalated ZrO_2 layers are parallel to the electron beam. **(C)** The NMF-component used to construct B is dominated by Zr, but additionally contains the Al and Si from the surrounding clay. Additionally, higher resolution HAADF images of Na-Zr-50-2.5 **(D)** and Na-Zr-50-5 **(E)** with inset line profiles exemplify the relative size and spacing of the fringes. The scale bars in each image represent 20 nm.

The hybrid, partial nature of intercalation was confirmed by basal spacing measurement using image analysis as shown in **Fig. 16**. As seen, the modification procedure increased the basal spacing in all samples. The left column shows a representative HRTEM image with colour-coded maps of the basal spacing and modulation strength (measurement quality). The right column shows a matrix of basal spacing histograms obtained by manual measurement (orange) and image analysis (blue). Green curves show components of fit bimodal normal distributions to the data obtained by image analysis: the dashed curve indicates the component attributed to the precursor clay and the continuous line is attributed to the component of intercalated layers. Circles and horizontal error bars show the mean of the manual measurements (orange), the mean of the basal spacing obtained by image analysis (blue) and the mode of the component attributed to the intercalated layers (green). The distributions of basal spacing of the precursor clays were unimodal, with a mode at 1.1 nm. The modification process introduced a second mode that corresponded to intercalated layers at a basal spacing of approximately 1.5 nm. The extent of pillaring appeared to have been affected by the concentration of Zr^{4+} ions and the type of precursor: Na-saturated clay exhibited a higher extent of pillaring and slightly longer basal spacing. The optimum concentration of Zr^{4+} appeared to be 5 mmol/g – above this concentration, pillaring appeared weaker since the basal spacing distributions exhibited a weaker second mode, corresponding to intercalated layers.

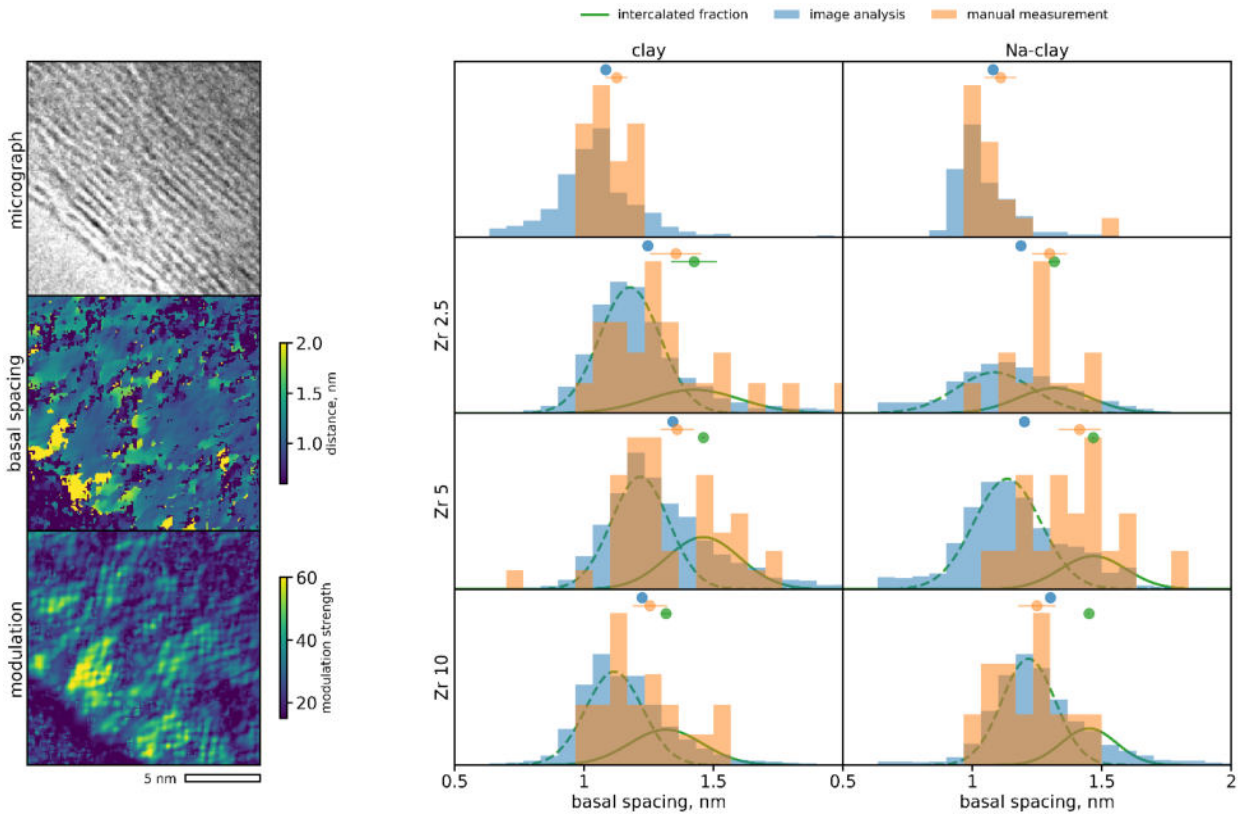

Figure 16: Detailed analysis of basal spacing based on HRTEM imaging.

Since no increased basal spacing was detected by XRD for Zr-50-10, yet some interlayer expansion was detected by HRTEM (**Fig. 16**), further STEM-HAADF and EDX analysis was performed. The HAADF image (**Fig. 17A**) shows sparse Zr-rich domains which are unevenly distributed with large separations. At larger fields-of-view, the Zr-rich domains appear in partially agglomerated structures that have no clear relation to the surrounding layered CM structure, as shown in the HAADF and EDX images (**Fig. 15A, B**). This lack of even, regular intercalation is consistent with the XRD results, which detects only the periodic 1 nm spacing between the CM basal planes.

The very sparse pillaring in Zr-50-10 means, however, that the separation between individual pillars is sufficient for HRTEM imaging. To determine the structure and morphology of the intercalated ZrO_2 pillars, representative HRTEM images of the precursor and Zr-intercalated clays were acquired in a viewing direction perpendicular to the clay basal planes. To better be able to distinguish individual pillars, the images were acquired at the very edges of the clay agglomerates to reduce the number of overlapping layers. **Figs. 17B** and **C** show representative images and their corresponding, radially averaged Fourier transform. The strong peak at 3.9 nm^{-1} seen in pillared samples (Fig. 17C inset) – missing from precursor materials (Fig. 17B inset) – can be attributed to the (110) reflection of tetragonal ZrO_2 or the (200) reflection of monoclinic ZrO_2 [121]. Upon filtering the images at these frequencies, distinct 5-10 nm size domains were observed, corresponding to the pillar diameter and further demonstrating the very sparse pillaring in the Zr-50-10 sample. This supports both the successful formation of crystalline ZrO_2 under the present reaction conditions and demonstrates the crucial role of the Na pre-treatment of the CM for achieving an even intercalation.

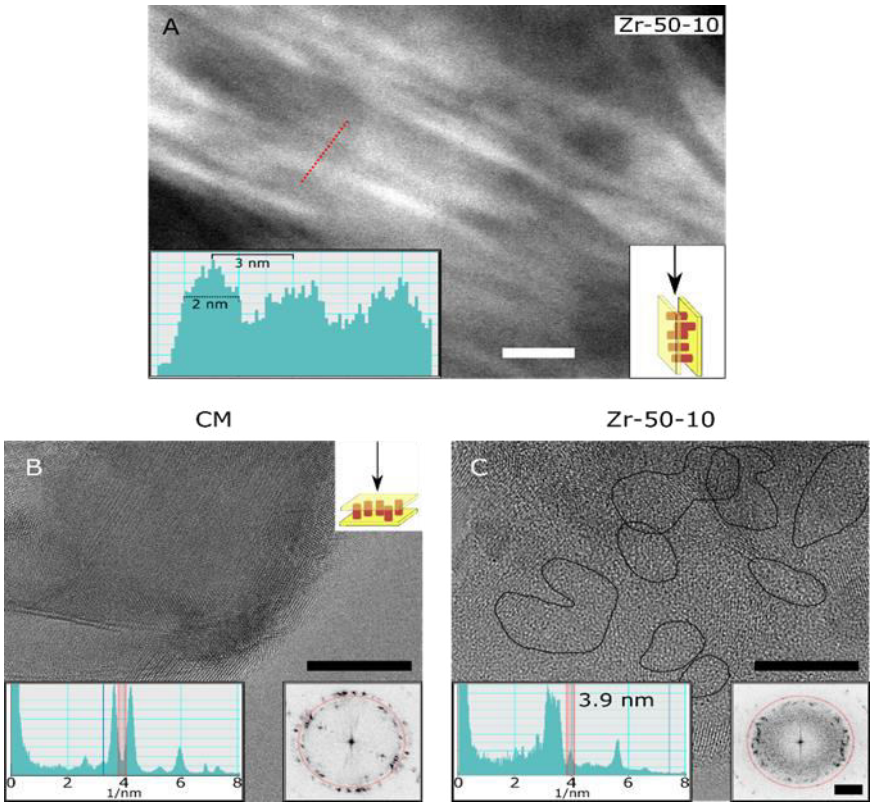

Figure 17: HAADF image of Zr-50-10 **(A)** showing the presence of large ZrO2-domains. Representative HRTEM images of CM **(B)** and Zr-50-10 **(C),** both with their respective Fourier transforms and radially averaged Fourier transforms as insets, the red rectangle and circle indicating the peak at 3.9 1/nm corresponding to the (110) or (200) reflection of ZrO_2. The scale bars in images A-C correspond to 10 nm. The scale bar in the Fourier transforms insets in B-C correspond to 2 nm^{-1}.

6.2 Application of Zr-pillared and chitosan-modified zirconium pillared clays in phosphate removal from water

The application of prepared materials was explored in the adsorption of phosphates from water. In the below sections the experimental conditions, adsorption isotherms used and mechanism of the phosphate adsorption on clay adsorbents is discussed.

6.2.1 Experimental conditions of phosphate adsorption tests

All phosphate adsorption experiments were carried out in a batch mode at pH 4 and 7 at room temperature with an adsorbent loading of 1 g/L. To ensure adequate contact between clay samples and phosphates in the water, the solutions were put in an orbital shaker at 400 rpm for different time intervals (30-240 minutes). The experiments were conducted in a phosphate

concentration range of 1-20 mg P/L. After adsorption, the solutions were filtered with syringe filters, and phosphate concentration in the filtrate was determined using Varian 720-ES axial view inductively coupled plasma-optical emission spectrometer (ICP-OES) and expressed as mg P/L in this study (1 *mg P/L=3.06 mg of phosphate/L*). *The adsorption capacity of the adsorbent in this study is shown in mg P/g (1 mg P/g = 3.06 mg of phosphate/g).*

The phosphate adsorption capacity of Zr-pillared clays was calculated using the following equation:

$$Q_t = \frac{(C_i - C_t) * V}{m}$$

where Q_t (mg P/g) is the phosphate adsorption capacity at different time periods, Ci and C_t were the phosphate concentration in solution at initial and different time periods (mg P/L), m (g) was the weight of adsorbent, V(L) was the volume of solution taken.

The equilibrium adsorption capacity was calculated by,

$$Q_e = \frac{(C_i - C_e) * V}{m}$$

where C_i and C_e were the initial and equilibrium phosphate concentration in solution (mg P/L) respectively, m (g) was the weight of adsorbent, and V(L) was the volume of solution taken.

6.2.2 Phosphates adsorption kinetics

Fig. 18 shows the adsorption capacity of raw clay (Na-CM) was almost zero throughout the 240 minutes. However, in the Na-Zr-50-2.5 sample, the phosphate adsorption was very rapid in the first 90 minutes and then changed gradually until Q_t reached 11.3 ± 0.17 mg P/g after 210 minutes where the adsorption equilibrium was achieved (**Fig. 19A**). At the beginning of the adsorption phase a high standard deviation was also observed because there were many accessible vacant adsorption sites available in the adsorbent and there were many free adsorbates in the solution as well. During the later phase of adsorption, the saturation of available adsorption sites took place and equilibrium was achieved (**Fig. 19A**). However, in the Na-Zr-50-5 sample, in the first 120 minutes the adsorption was very rapid after that a sudden drop was observed at 150 minutes and after that, it started to increase again (**Fig. 19B)**. In this samples equilibrium was not achieved and a high standard deviation was observed throughout the whole adsorption process. The maximum phosphate adsorption capacity achieved at 240 minutes was 11.5±1.34 mg P/g. In literature, it is well documented that Zr-based adsorbents

have shown excellent properties in the sequestration of phosphates from water based on the principle of Lewis-acid base interaction [122]. However, the higher zirconium loading in the clay structure does not confirm more adsorption of phosphate ions. Among both the pillared clays, the sample having less concentration of Zr^{4+} ions i.e. 2.5 mmol/g has shown a better adsorption curve.

To gain more insight into the adsorption mechanism and kinetics, the pseudo-first-order kinetic model (1), pseudo-second-order kinetic model (2) and Elovich models (3) were applied to kinetic data. The following equations were used to study adsorption kinetics [84].

$$Q_t = Q_e (1\text{-}\exp^{-k_1 t}) \quad (1)$$

$$Q_t = k_2 Q_e^2 t / 1 + k_2 Q_e t \quad (2)$$

$$Q_t = \frac{1}{\beta} \ln (1 + \alpha\beta t) \quad (3)$$

Where t was the adsorption time (min); Q_t (mg/g) and Q_e (mg/g) are the phosphate adsorption capacities at time t (min) and at equilibrium, respectively; k_1 (1/min) and k_2 (g/mg min) are rate constants of a pseudo-first-order kinetic model and pseudo-second-order kinetic model, respectively; α is the initial adsorption rate (mg/g min) and β is the desorption constant (g/mg).

The non-linear fitting plots of pseudo-first-order, pseudo-second-order and Elovich models are depicted in **Fig.19A and B.** The kinetic model parameters are shown in **Table 4**. Based on the correlation coefficient (R^2) values, it was found that for Na-Zr-50-2.5 the Elovich model (0.93) gave the best fit to the kinetic data followed by pseudo-second-order (0.87) and pseudo-first-order (0.73). The well-fitting of the Elovich model suggests that the chemisorption took place between phosphates and clay surfaces [84]. However, for Na-Zr-50-5 there was a slight difference between the Elovich kinetic model (0.88) and pseudo-second-order kinetic model (0.89).

Table 4: Kinetics parameters of the pseudo-first-order kinetic model, pseudo-second-order kinetic model and Elovich kinetic model for phosphate adsorption onto Na-Zr-50-2.5 and Na-Zr-50-5.

Sample	pseudo-first-order kinetic model			pseudo-second-order kinetic model			Elovich kinetic model		
	R^2	k_1 (1/min)	Q_e (mg/g)	R^2	k_2 (g/mg min)	Q_e (mg/g)	R^2	α (mg/g min)	β (g/mg)
Na-Zr-50-2.5	0.73	0.0169	11.42	0.87	0.0021	13.02	0.93	1.72	0.46
Na-Zr-50-5	0.83	0.0266	10.73	0.89	0.0027	12.42	0.88	1.26	0.43

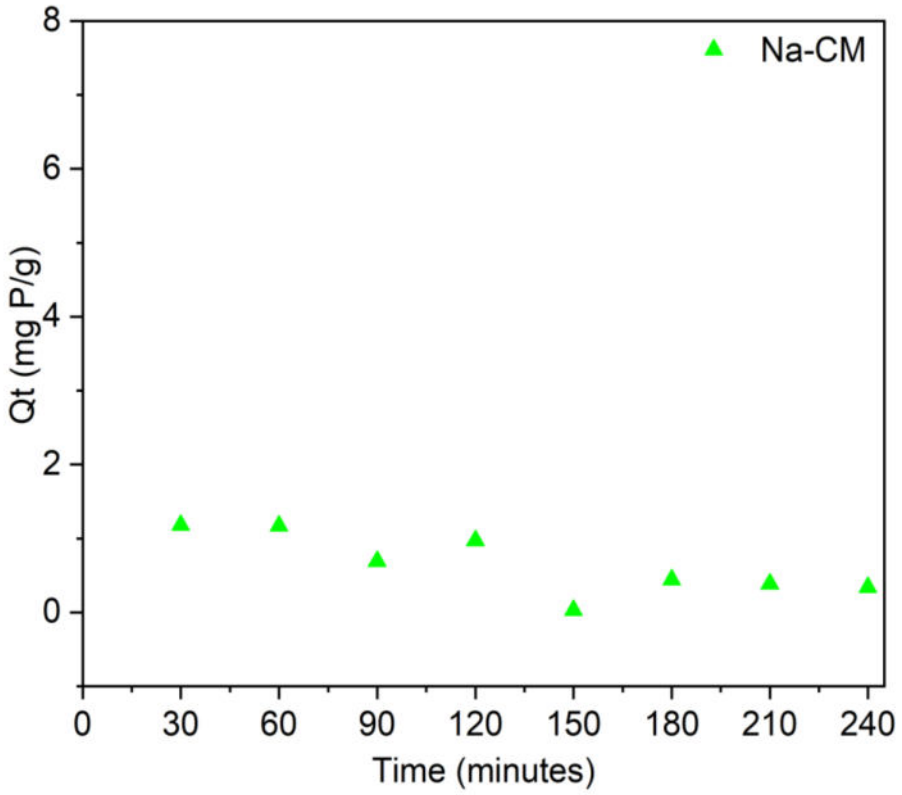

Figure 18: Phosphate adsorption capacity of raw montmorillonite (Na-CM).

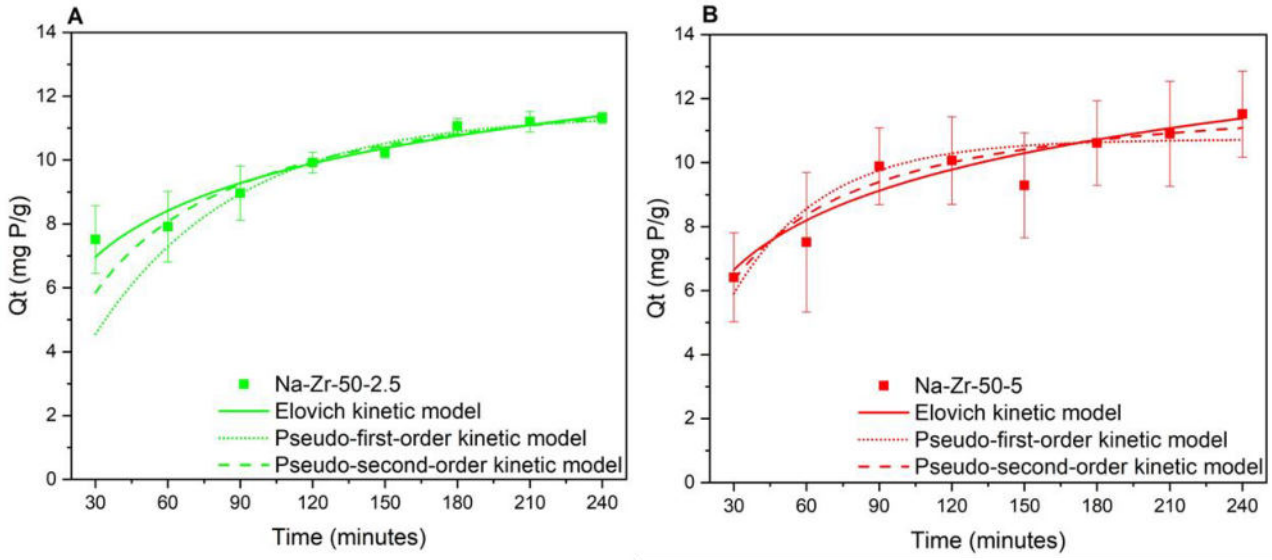

Figure 19: Pseudo-first order, pseudo-second order and Elovich kinetic fitting plots of phosphate adsorption on Na-Zr-50-2.5 **(A)** and Na-Zr-50-5 **(B)** at pH 4.

6.2.3 Adsorption isotherms

The adsorption experimental data were fitted with Langmuir (4), Freundlich (5) and Toth (6) adsorption isotherm models.

$$Q_e = \frac{Q_{max}\, K_L\, C_e}{1+K_L\, C_e} \quad (4)$$

$$Q_e = K_F\, C_e{}^{1/n} \quad (5)$$

$$Q_e = \frac{Q_{max}\, K_T C_e}{[1+(K_T C_e)^t\,)]^{1/t}} \quad (6)$$

Where Q_e (mg P/g) is the phosphate adsorption capacity at equilibrium, C_e (mg P/L) is the equilibrium phosphate concentration in the solution, K_L (L/mg) is the Langmuir constant related to the energy of adsorption, Q_{max} (mg P/g) is the maximum phosphate adsorption capacity, K_F (mg/g·(L/mg)$^{1/n}$) is the Freundlich constant related to adsorption capacity, and 1/n is a dimensionless indicator measuring the adsorbent surface heterogeneity, K_T is the Toth equilibrium isotherm constant (L/mg), t is the dimensionless Toth exponent [123].

Figures 20-22 depict the equilibrium adsorption capacities of phosphates for Na-Zr-50-2.5, Na-Zr-50-5 and Ch-NaZr2.5 as a function of equilibrium concentrations at pH 4 and 7. For all three

samples, phosphate adsorption data were best fitted with the Toth model based on regression coefficient (R^2) values (**Table 5**). Toth model is a three-parameter isotherm used to study the adsorption on heterogeneous surfaces [124][125]. It is an extended modification of the Langmuir model. By comparing the values of Q_{max} (mg P/g) obtained from the Toth model, the values were very deviated from the experimental data, and also the standard deviation was very high. However, values obtained from the Langmuir isotherm were much closer to the experimental data. The Langmuir model is the most widely applied sorption isotherm which fits well with different types of experimental data [126]. It assumes that adsorption is homogenous, in which all active sites are energetically equivalent, and the surface of the adsorbent is covered with a monolayer [123]. If we compare the Q_{max} values obtained from the Langmuir model (**Table 5**), then the chitosan-modified sample has shown the highest phosphate adsorption capacity at both pH.

Table 5: Parameters of isotherm models for phosphate adsorption onto different Zr-PILCs and chitosan-modified zirconium pillared clay (Ch-NaZr2.5).

		Na-Zr-50-2.5		**Na-Zr-50-5**		**Ch-NaZr2.5**	
Model	**Parameter**	**pH 4**	**pH 7**	**pH 4**	**pH7**	**pH 4**	**pH 7**
Langmuir	Q_{max} (mg P/g)	11.5 ± 0.98	8.3 ± 0.64	9.6 ± 0.93	6.19 ± 0.21	14.5 ± 0.42	11.8 ± 0.35
	K_L	3.1 ± 1.16	4.05 ± 1.8	5.6 ± 3.86	3.7 ± 0.88	7.1 ± 0.58	4.05 ± 0.48
	R^2	0.93	0.93	0.93	0.93	0.98	0.97
Freundlich	K_F	8.16 ± 0.61	4.93 ± 0.69	8.04 ± 0.09	4.53 ± 0.18	11.4 ± 0.24	9.25 ± 0.03
	1/n	0.19 ± 0.06	0.26 ± 0.07	0.34 ± 0.10	0.16 ± 0.02	0.15 ± 0.01	0.12 ± 0.01
	R^2	0.81	0.89	0.89	0.93	0.95	0.96
Toth	Q_{max} (mg P/g)	7.9 ± 3.71	5.07 ± 4.97	6.9 ± 8.5	3.5 ± 1.26	11.13 ± 3.82	7.23 ± 2.95
	K_T	7.52 ± 8.97	8.04 ± 13.7	8.27 ± 14.7	13.7 ± 14.4	12.3 ± 9.7	18.12 ± 27
	t	0.93 ± 0.08	0.90 ± 0.16	0.9 ± 0.30	0.89 ± 0.04	0.94 ± 0.05	0.92 ± 0.04
	R^2	0.95	0.94	0.94	0.98	0.98	0.98

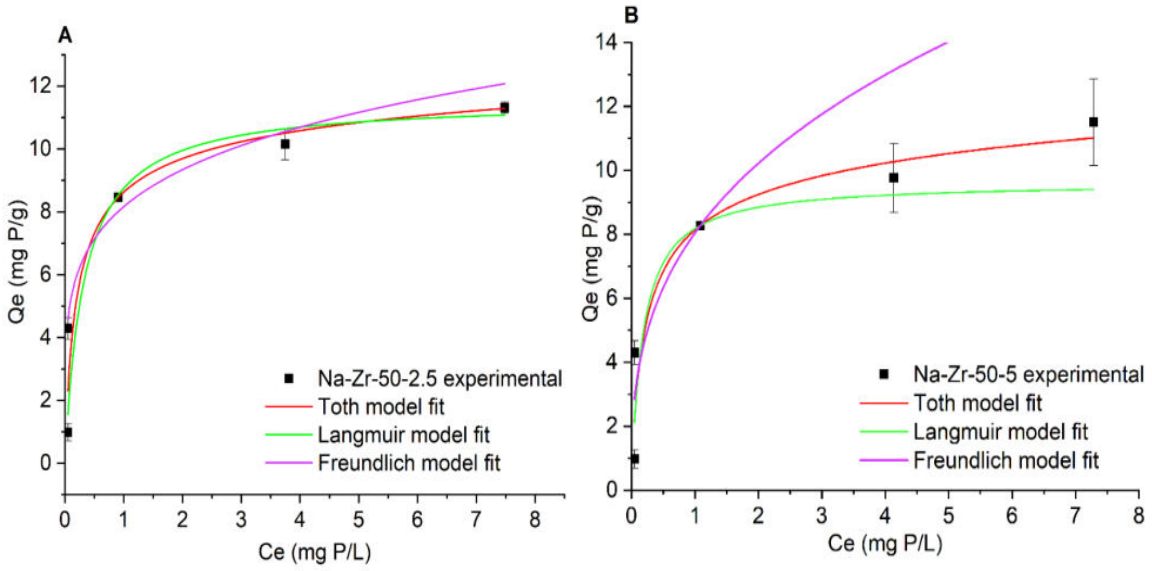

Figure 20: Adsorption isotherms of phosphates on Zr-pillared clays at pH 4.

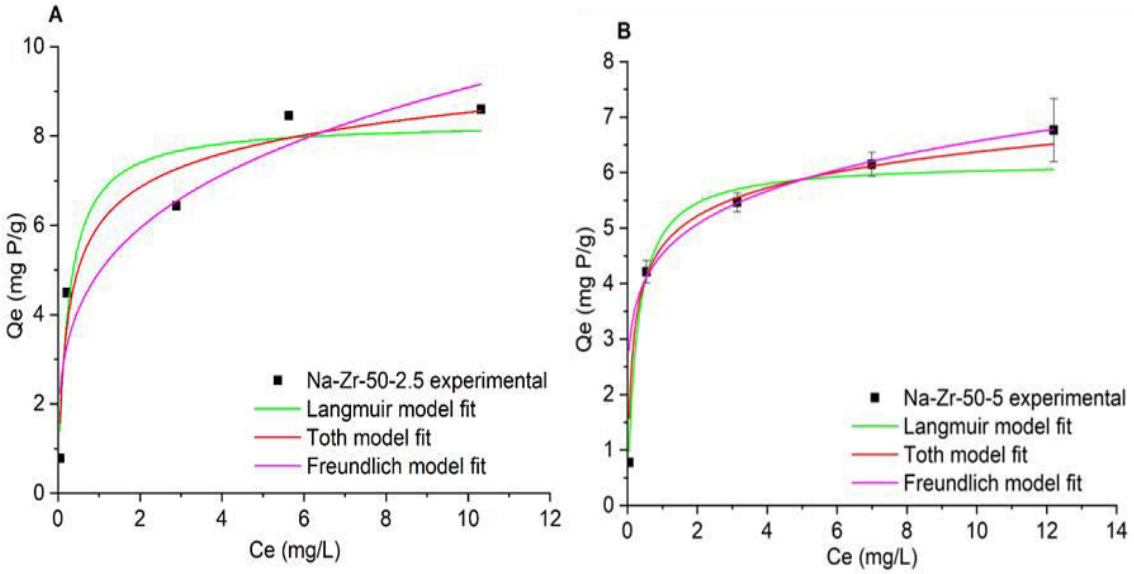

Figure 21: Adsorption isotherms of phosphates on Zr-pillared clays at pH 7.

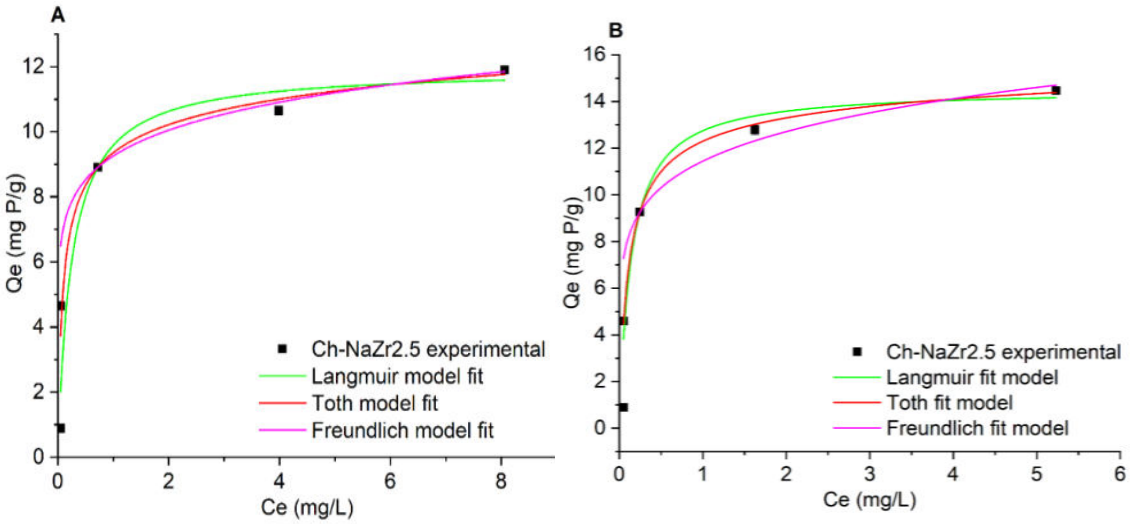

Figure 22: Adsorption isotherms of chitosan-modified zirconium pillared clay (Ch-NaZr2.5) at pH 7 (A) and 4 (B).

6.2.4 Mechanism of phosphate adsorption

The initial pH of the solution is one of the important parameters influencing the adsorption of phosphates on the clay adsorbent. In the crystal lattice of clay, silicon and aluminium ions are present. When these ions are replaced by other less positive valence ions, a pH-independent permanent negative charge is created on the basal surface of clay. This negative charge can be balanced by exchangeable interlayer cations. Along with this, the edges of clay particles contain polarisable Al–OH and Si–OH groups which became positively or negatively charged depending on the pH of the solution [127]. The intercalation of positively charged zirconium ions facilitates the charge neutralization or blocking of negative charge, as a result, the effect of negative charges on the reactivity of edge groups is neutralized [128]**. Fig. 23** shows the effect of pH on the zeta potential of raw clay and modified clays.

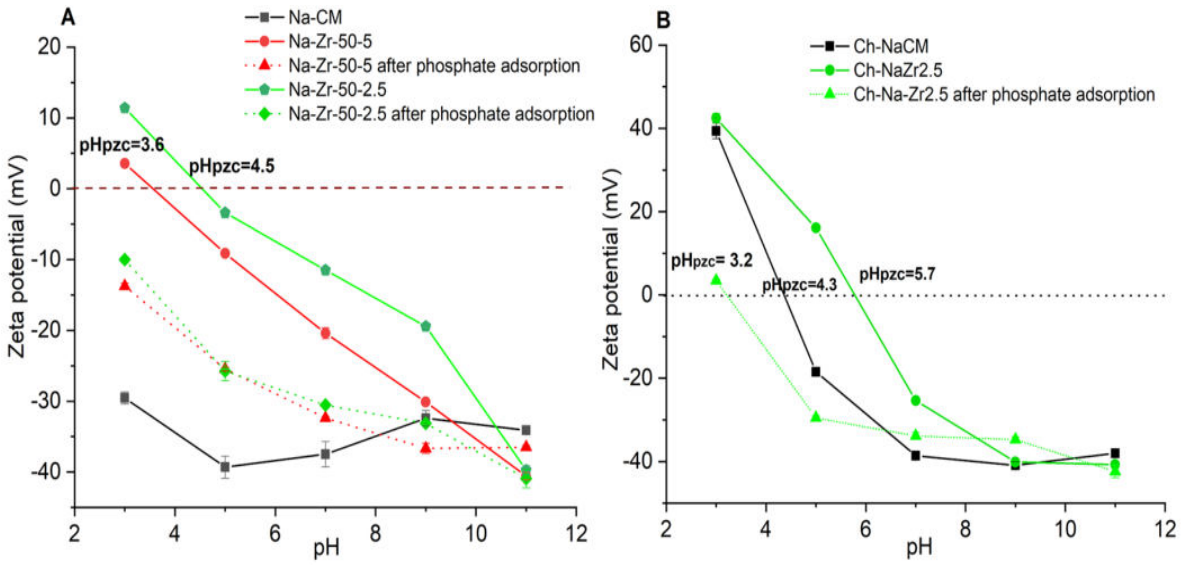

Figure 23: Effect of pH on zeta potential of raw montmorillonite (Na-CM) and Zr-pillared clays **(A)** chitosan-modified Zr-pillared clay **(B)** before after phosphate adsorption.

Fig. 23A depicts that the zeta potential of raw montmorillonite (Na-CM) was negative in the whole pH range and point of zero charge (pH_{PZC}) was not achieved. This confirms the dominance of structural negative charge on the basal surface. However, in the Zr-pillared samples, a significant change in zeta potential values was observed. It has increased to 11 mV and 3 mV in samples Na-Zr-50-2.5 and Na-Zr-50-5 at pH 3, respectively (**Fig. 23A)**. The former sample shifted the zeta potential in a more positive range than the latter, favouring the strong interaction between the clay surface and phosphate species. One of the possible explanations for achieving higher zeta potential in Na-Zr-50-2.5 could be the arrangement and distribution of ZrO_2 pillars in the interlayer region of montmorillonite clay. In STEM-HAADF and EDX analysis (section 6.1.5) of these samples it was found that the ZrO_2 pillars were separated by a distance of 1.6-2 nm and 2.8-1.6 nm in Na-Zr-50-2.5 and Na-Zr-50-5 respectively. Through adsorption experiments, it was revealed that a Zr^{4+}/clay ratio of 2.5 mmol/g is the optimum concentration for preparing adsorbent materials suitable for targeting phosphate ions. Furthermore, the composition of the prepared clay materials can affect not only the adsorption properties but also the orientation of the ZrO_2 pillars. It is assumed that the increased Zr^{4+} amount caused the formation of a less regular clay structure in the Na-Zr-50-5 sample. The ZrO_2 pillars in the Na-Zr-50-5 sample could have negatively affected the adsorption test results.

In the case of the chitosan-modified Zr-pillared sample (Ch-NaZr2.5) it was increased to 42 ± 1.2 mV (**Fig. 23B**). The zeta potential of Zr-pillared clay shifted to a much higher positive value after the treatment of chitosan. This confirms the introduction of more positive reactive sites in the clay structure. This can favour the electrostatic attraction between modified clays and negatively charged phosphate species. After phosphate adsorption, the zeta potential of all three samples (Na-Zr-50-2.5, Na-Zr-50-5 and Ch-NaZr2.5) became negative in the whole pH range. The pH_{PZC} of Ch-NaZr2.5 was 5.7 before adsorption, after being loaded with phosphates, it shifted to a lower value (3.2) (**Fig. 23B**). The adsorption mode of ions on a mineral surface is mainly divided into inner and outer complex formation. The chemical interaction in the former is stronger than in the latter, and generally, the value of pH_{PZC} does not change by the formation of outer sphere complexes because of insufficient sorbate-sorbent interaction [85]. The result thus indicates that phosphates were adsorbed on modified clays by forming inner-sphere surface complexes.

Another possible mechanism for adsorption could be ligand exchange. During the process, the hydroxyls (-OH) groups of the adsorbent are exchanged by phosphates. This results in an increase of aqueous solution pH due to the release of -OH ions [77]. However, we checked the pH of the solutions before and after phosphate adsorption (**Fig. 24**). After adsorption, the pH of the solutions was found to be increased slightly. Because there is very little pH increase during the phosphate adsorption process, it is possible that ligand exchange is not the primary driving force.

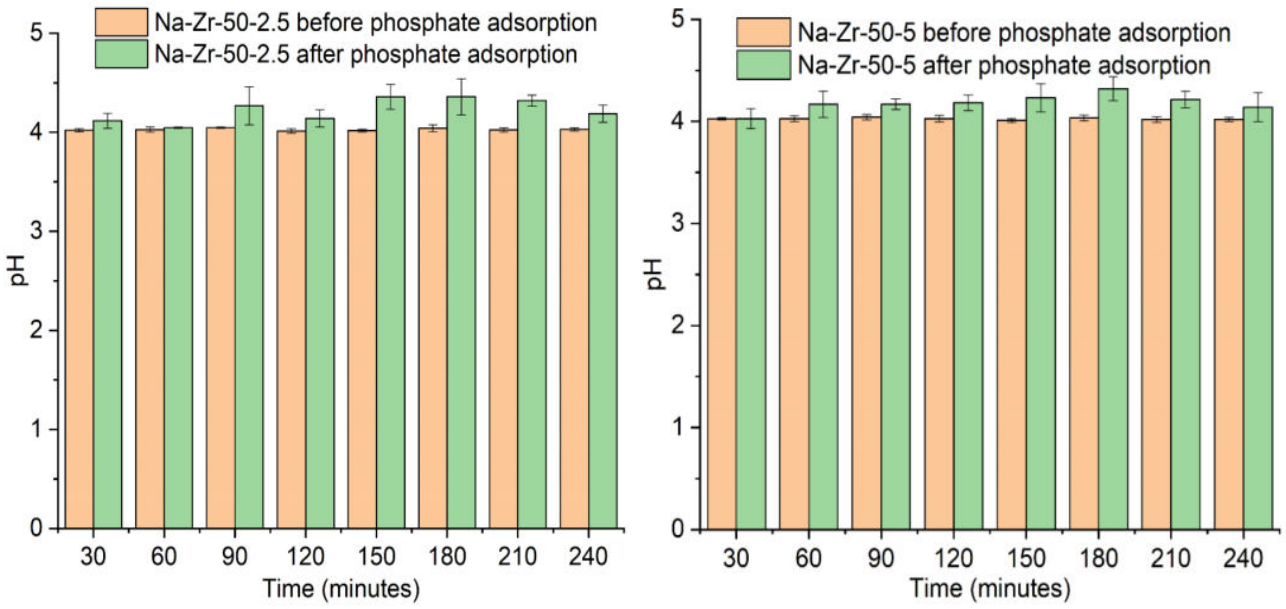

Figure 24: pH of the Zr-pillared clays before and after the adsorption tests.

In order to learn more about the sorption mechanism and ascertain the elemental makeup of the modified adsorbents, XPS measurements were also carried out. The survey spectra of all the modified clay samples before and after the adsorption of phosphates are shown in **Fig. 25A**. Clay samples obtained after the phosphate adsorption show the presence of P 2p signals associated with a binding energy of 134 eV (**Fig. 25C**). It was also observed that after phosphate adsorption, the binding energy of Zr 3d shifted to more positive binding energies. After phosphate adsorption, there was a Zr $3d_{5/2}$ peak shift of 0.3 eV for Na-Zr-50-2.5, 0.1 eV for Na-Zr-50-5 (**Fig. 25B**), and 0.3 eV, for Ch-NaZr2.5 compared to the Zr $3d_{5/2}$ peak measured for the samples before phosphate adsorption. The adsorption of phosphate ions is supported by the peaks that developed in P 2p spectra for clay samples after adsorption. This shift in the binding energy of the Zr $3d_{5/2}$ peak might indicate the interaction between Zr-PILC and phosphate ions [129]. In the chitosan-modified sample (Ch-NaZr2.5), an N 1s signal appeared at a binding energy of 400.1 eV attributed to the amino group in chitosan. The surface mass concentration of elements present on adsorbent before and after phosphate adsorption is shown in **Table 6**. The Ch-NaZr2.5 contained a higher surface mass concentration of carbon, oxygen, and nitrogen compared to other samples, confirming the successful loading of chitosan on the pillared clay sample. Also, adsorbents loaded with phosphates after adsorption showed a higher surface mass concentration of phosphorus, further proving the occurrence of phosphates on adsorbents.

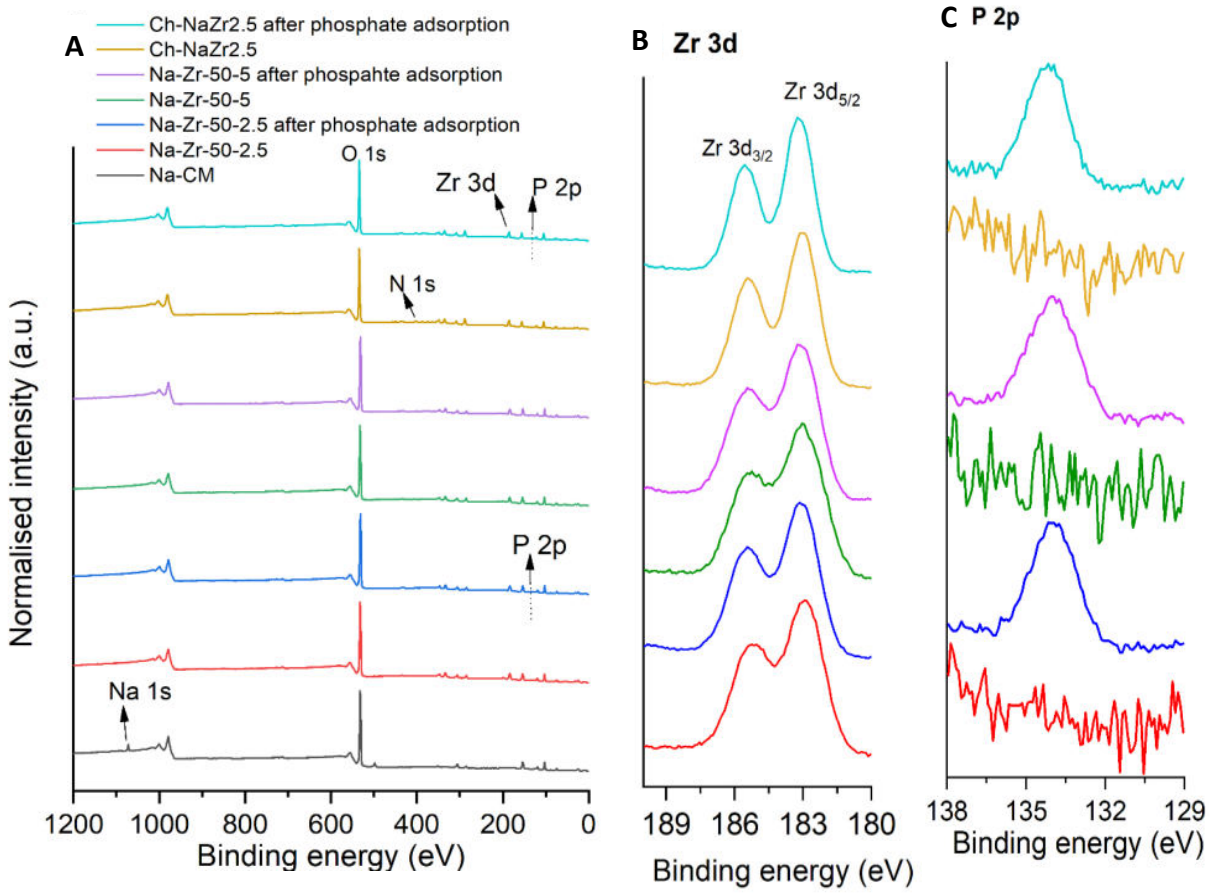

Figure 25: XPS survey spectra of raw and modified clays before and after phosphate adsorption **(A)**, high-resolution Zr 3d spectra of Zr-pillared clays before and after phosphate adsorption **(B),** and P 2p spectra of modified clay samples before and after phosphate adsorption **(B),** and P 2p spectra of modified clay samples before and after phosphate adsorption **(C)**.

Table 6: Surface mass concentrations of modified clays before and after phosphate adsorption determined by XPS analysis.

	Mass conc. %					
	Ch-NaZr2.5	Ch-NaZr2.5 after phosphate adsorption	Na-Zr-50-2.5	Na-Zr-50-2.5 after phosphate adsorption	Na-Zr-50-5	Na-Zr-50-5 after phosphate adsorption
O	50.4	51.5	49.5	49.2	47.6	49.2
Si	18.6	17.4	22.6	21.8	22.3	22.2
Al	5.6	5.8	9.9	9.3	9.6	8.9
Zr	9.7	9.7	10	8.5	9.0	9.4
P	-	1.0	-	1.2	-	1.1

Fe	2.1	2.0	2.1	2.5	2.7	2.2
K	-	0.6	-	0.3	-	0.3
Ca	1.7	1.5	-	1.8	1.6	1.6
Mg	-	-	-	0.9	0.8	0.6
C	9.8	8.8	5.6	4.2	6.1	4.2
Na	0.2	0.2	0.3	0.3	0.3	0.3
N	1.9	1.5	-	-	-	-

To further understand the phosphate adsorption mechanism an ATR-FTIR investigation was also conducted. FTIR spectra of clay samples before and after phosphate adsorption are shown in **Fig. 26**. The vibrations at 3620 cm^{-1} corresponded to the stretching vibration of the O-H bond [130]. The band observed at 1635 cm^{-1} is due to the bending vibration of water [131]. In sample Ch-NaCM, the vibrations at 1414 and 1548 cm^{-1} corresponded to C-O-H in-plane bending and N-H bending of the amide II group of chitosan respectively [132][130]. These bands were shifted to 1455 cm^{-1} and 1542 cm^{-1} in the Ch-NaZr2.5 sample respectively, indicating that zirconium ions interacted with these groups. In sample Ch-NaZr2.5 after phosphate adsorption, these vibrations disappeared which indicates that these were the active sites where adsorption took place [88]. Some changes in the intensities or positions of the peaks between 521 and 1013 cm^{-1} are attributed to the bending vibration of Si-O-Al, and the stretching vibration of the Si-O bond was also observed in samples loaded with phosphate groups.

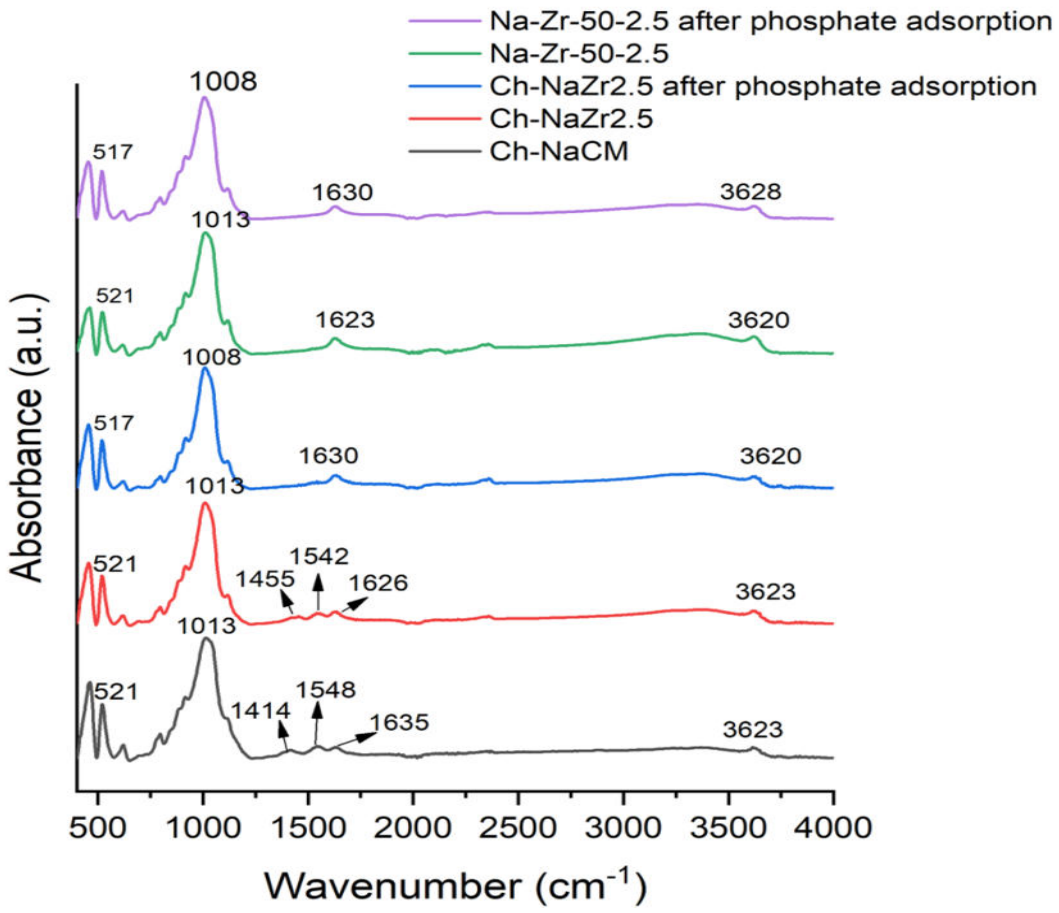

Figure 26: ATR-FTIR spectra of modified clays before and after phosphate adsorption.

The surface morphology (SEM images) along with EDX elemental mapping of Na-Zr-2.5, Na-Zr-50-5 and Ch-NaZr2.5 clay samples before and after phosphate adsorption are shown in **Fig. 27-29**. The surface of Na-Zr-50-2.5 and Na-Zr-50-5 is more compact and has a block-like appearance before adsorption (**Fig.** 27A, 28A and 29A) and after adsorption, it becomes more flaky and has lamellar morphology as can be seen in Fig. 27B, 28B, 29B). The EDX-elemental mapping of Zr (**Fig**. 27C, 28C and 29C) and P (Fig. 27D, 28D and 29D) confirms the adsorption of phosphates on zirconium-modified clays.

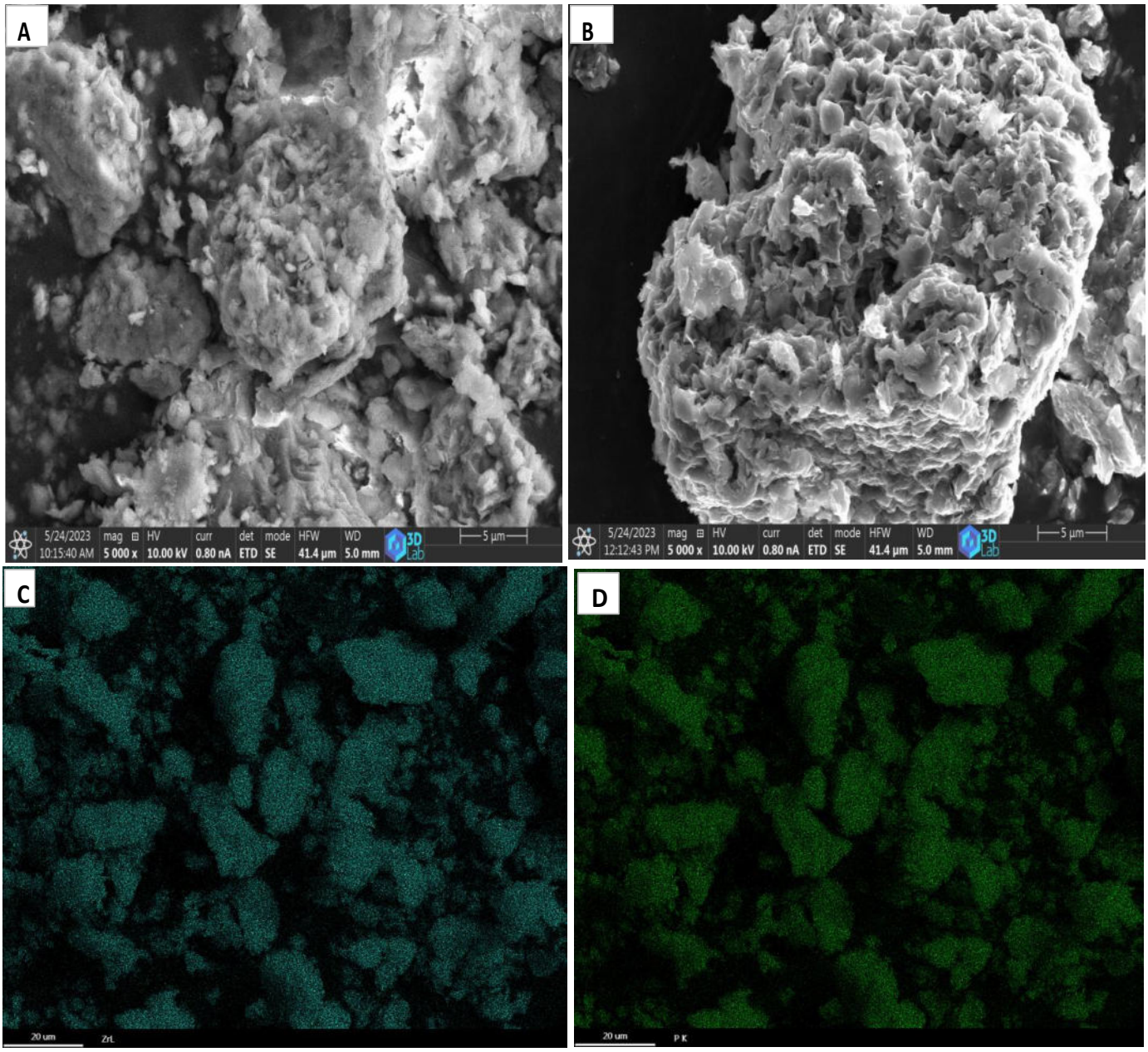

Figure 27: SEM micrographs of Na-Zr-50-2.5 before **(A)** and after phosphate adsorption **(B)** with EDX elemental mapping of Zr **(C)** and P **(D).**

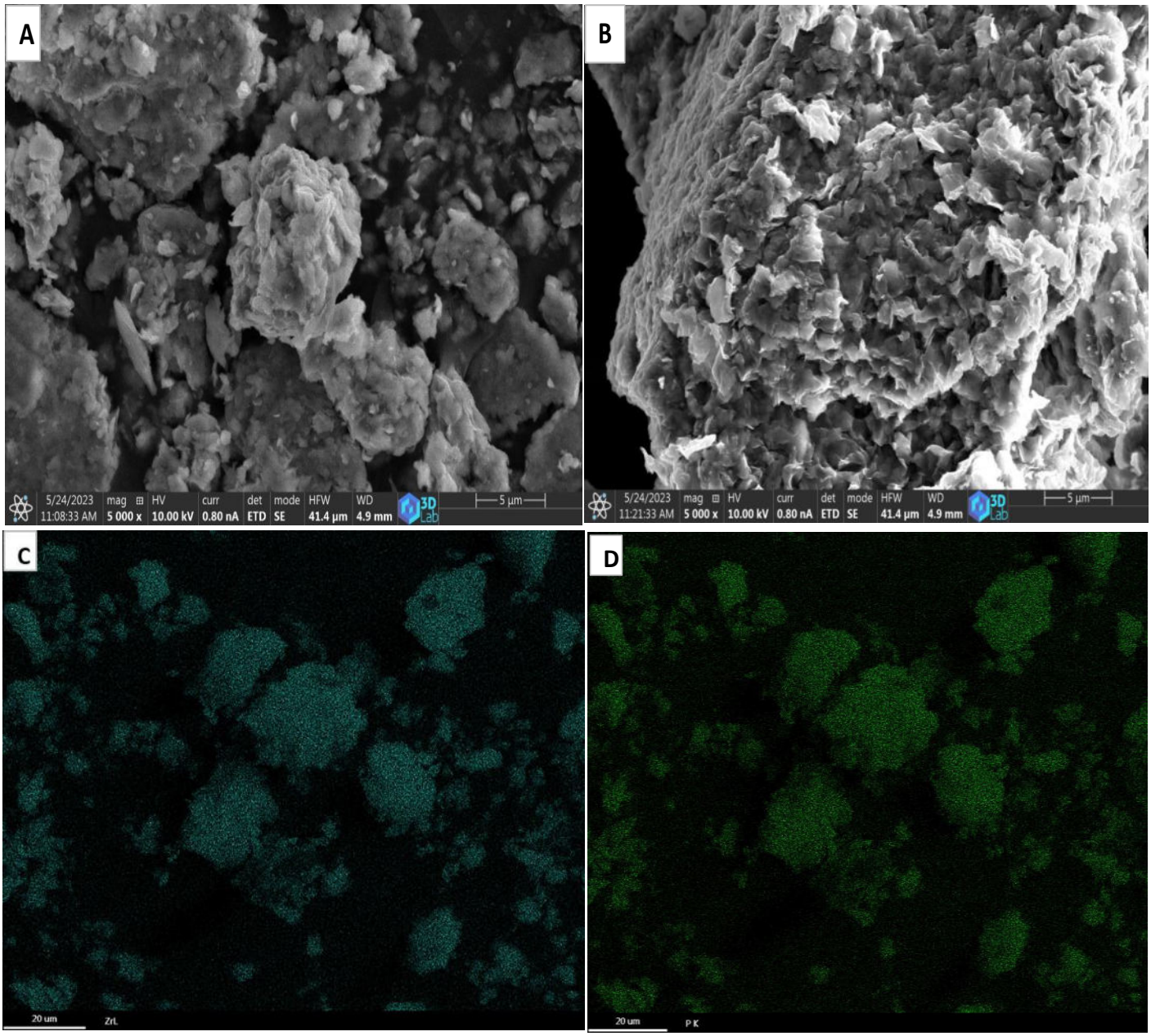

Figure 28: SEM micrographs of Na-Zr-50-5 before **(A)** and after phosphate adsorption **(B)** with EDX elemental mapping of Zr **(C)** and P **(D).**

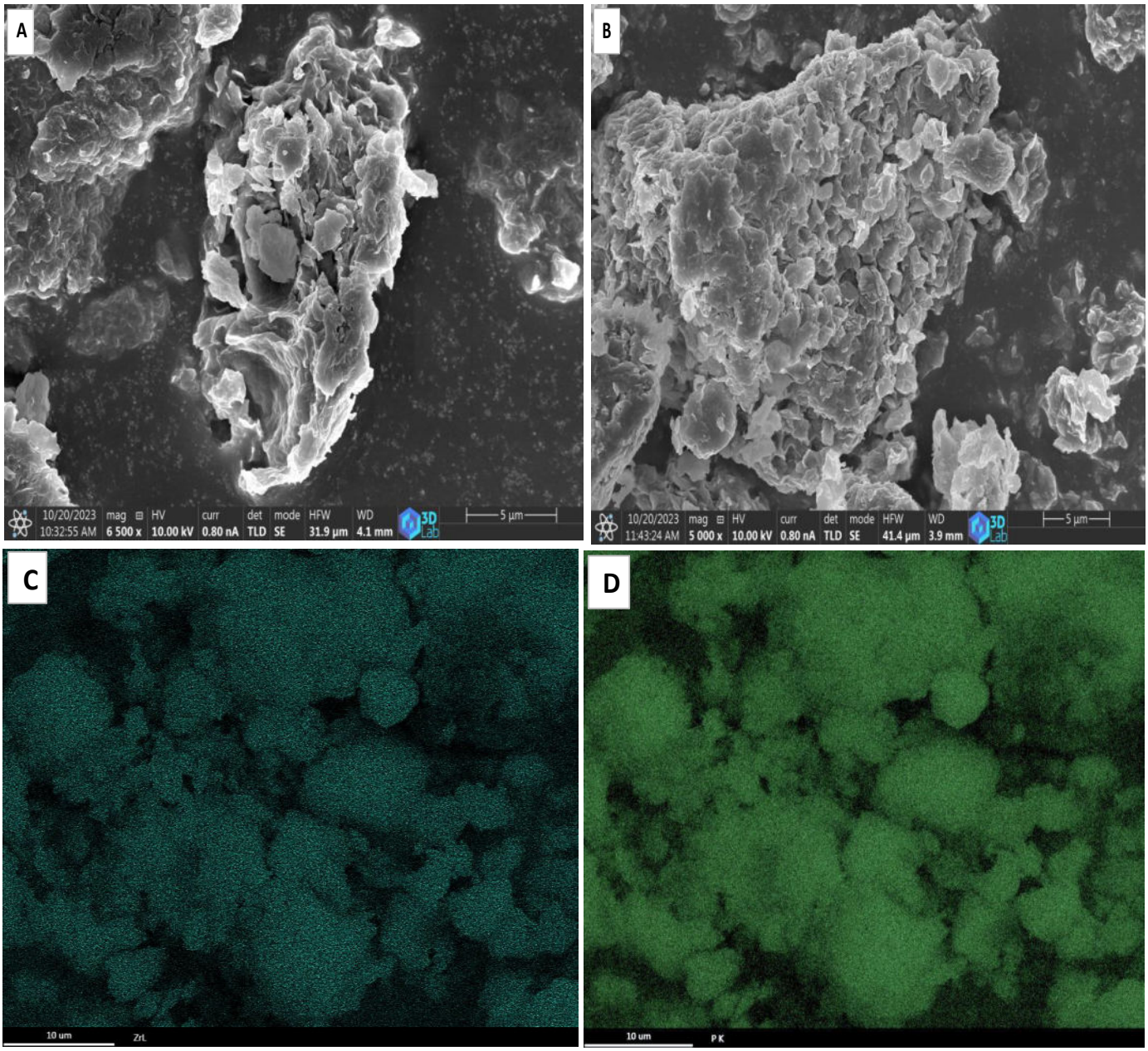

Figure 29: SEM micrographs of Ch-NaZr2.5 before **(A)** and after phosphate adsorption **(B)** with EDX elemental mapping of Zr **(C)** and P **(D).**

6.3 Application of precursor (Na-CM) and zirconium pillared clay (Na-Zr-50-2.5) in *E. coli* adsorption from aqueous solution

6.3.1 Adsorption experiments for *E. coli* using sedimentation technique

For conducting *E. coli* adsorption experiments, the culturing medium was removed from the bacterial suspension solution with the help of a centrifuge and the cells were resuspended in a physiological saline solution. To attain this, 70 mL of the cell suspension was centrifuged for 15 min at 4 °C and 10000 rpm. After that, the supernatant was discarded, and the cell pellet was resuspended in 30 mL of physiological saline solution by vortexing the centrifuge tubes. Again, the solution was centrifuged for 5 min at 4 °C and 10000 rpm and supernatant was discarded. This step was repeated three more times. Finally, the pellet was again resuspended in 30 mL of physiological saline solution. From this bacterial suspension, ten-fold serial dilutions were prepared in the range of 10^{-1} to 10^{-5} in 30 ml physiological saline. The 10^{-5} member of the dilution series was used as the initial cell suspension for the other tests as the bacterial inoculum. For *E. coli* adsorption experiments, 27 mL of sterile physiological saline solution and 3 mL of 10^{-5} diluted cell suspension were mixed in three Erlenmeyer flasks each. The first flask contains no adsorbent material (named as reference). In the second and third flask, 30 mg of sterilized Na-CM and Na-Zr-50-2.5 was added and named Na-CM and Na-Zr-50-2.5. All three flasks were incubated at 37 °C with constant shaking for 1.5 h. After the incubation period, 100 µL of the dispersions from each flask was evenly spread onto LB agar plates in triplicate to determine the initial colony number corresponding to each flask. After that, the suspensions in the flaks were allowed to settle down for 30 minutes. After 30 min, 100 µL of supernatant was taken out and plated onto LB-agar plates. The plates were left for an overnight incubation at 37°C. The next day, the counting of colonies formed was done.

6.3.2 Adsorption experiments for *E. coli* using centrifugation technique

In this case, the method described in section 6.3.1 was modified slightly after the 1.5 h incubation period. At the end of the incubation period, 100 µL of the supernatant from each centrifuge tube (reference, Na-CM, and Na-Zr-50-2.5) was plated onto LB-agar plates. Then, the remaining dispersions were centrifuged at 1000 rpm [100] for 1 min followed by plating using 100 µL of the supernatant from each tube. The plates were then incubated overnight at 37°C, and colonies were counted the next day.

6.3.3 Determination of *E. coli* concentration in residual precipitate phase

To confirm whether the cells that were absent from the supernatant after either sedimentation or centrifugation had adsorbed to the clay material, the precipitate phase (adsorbent material with attached bacterial cells present at the bottom of the tubes) was also examined. The initial steps of this experiment were carried out as described in Section 6.3.1, but after 30 min of settling of the dispersions, 29 mL of supernatant was carefully removed and transferred to another sterile centrifuge tube. After vortexing, 100 µL of this supernatant was plated onto LB plates to determine the number of non-adsorbed bacteria. The centrifuge tubes with the remaining adsorbents and a new portion of sterile saline solution were then placed back in the incubator at 37 °C for an additional 1.5 h shaking (160 rpm). Subsequently, the solution was allowed to settle for 30 minutes. After this incubation time, this second supernatant was sampled and another 100 µL portion of it was plated on LB-agar plates to assess whether the previously adsorbed bacteria detached from the clay adsorbents or not. Following this, 29 mL of the second supernatant was also removed, and the precipitate phase present at the bottom of the centrifuge tubes was resuspended in 1 mL of the remaining saline solution. From each tube, 100 µL of the dispersion was plated onto agar plates to confirm the presence of *E. coli* bacteria and their adsorption to the clay particles.

6.3.4 Results of *E. coli* adsorption test

Table 7 summarizes the concentration of *E. coli* cells before and after the adsorption by using different separation techniques. In the reference sample, a reduction of 5.67% in the cell concentration was observed after sedimentation. However, in Na-CM, a 34.7% reduction was observed and the dispersion of Na-CM in a physiological saline solution was found to be stable even after 30 minutes. This suggests that the dispersed sodium-saturated montmorillonite clay is capable of adsorbing a certain amount of bacteria. In comparison to Na-CM, the Na-Zr-50-2.5 particles showed rapid sedimentation and therefore it was required to shake the sample at 160 rpm to maintain the dispersion during incubation in order to use them as efficient adsorbents for bacterial cells. Na-Zr-50-2.5 sample was able to reduce the bacterial cell concentration up to 62.64% which is almost twice that of unmodified clay (Na-CM).

The separation of cells from suspension after adsorption is very sensitive as it can be affected by external factors such as centrifugation which is the standard method reported in literature used for the separation of adsorbed and non-adsorbed microorganisms [100]. Therefore, to

verify the results of adsorption, we extended our experimental work and included the usage of centrifugation at 1000 rpm for 1 minute. It was found that after applying centrifugation, in the reference sample, only a 2.59% reduction in bacterial cell concentration was achieved which is not a significant amount. This led to the conclusion that centrifugation at 1000 rpm for 1 minute did not significantly separate the *E. coli* bacterial cells from the liquid phase. Therefore, while using an adsorbent material any notable difference in cell concentration between the initial and the post-centrifugated dispersion would indicate the adsorption capacity of the clay particle. However, in the case of Na-CM, only 9.74% of the initial cell concentration was missing from post-centrifugation dispersions. This reveals that sedimentation is a more suitable and effective method for demonstrating the adsorption capacity of the Na-CM particles than 1-minute centrifugation. However, in the Na-Zr-50-2.5 sample, a significant reduction in bacterial cell concentration (60.33%) was observed during centrifugation. In this case, the application of gentle centrifugation (1000 rpm for 1 minute) did not alter the overall observations obtained in the case of sedimentation. This validates that the adsorption capacity of Zr-modified clay is neither affected by sedimentation nor centrifugation.

The possible reason for achieving a higher *E. coli* adsorption capacity in the Zr-pillared clay sample is the stronger electrostatic interaction between PO_4^{3-} and COO^- groups which are present in the bacterial cell wall, and positive groups of pillared clays. The gram-negative bacteria have an outer covering of phospholipids and lipopolysaccharides, which impart a negative charge to the bacteria's surface [132]. The zeta potential values of Na-CM and Na-Zr-50-2.5 in saline solution were found to be -50.4± 2.8 and -5.31± 0.21 mV at pH 5.6. After the intercalation of zirconium ions, the surface of montmorillonite clay becomes more positive, thus facilitating the attachment of negatively charged bacterial cells on its surface. However, despite having a very high negative zeta potential, Na-CM was able to capture a few percentage of *E. coli* cells. The reason could be other non-electrostatic forces such as hydrogen bonding, van der Waals forces and hydrophobic interactions acting between bacteria and clay surface [133].

Table 7: Comparison of the cell concentrations obtained before and after adsorption for adsorbent-free (reference), Na-CM, and Na-Zr-50-2.5 samples using different separation techniques.

	Reference				
	C_i	**C_a**	**C_d**	**difference**	**C_{ads}**
Experiment	**$\times 10^9$ CFU/mL**	**$\times 10^9$ CFU/mL**	**$\times 10^9$ CFU/mL**	**%**	**$\times 10^9$ CFU/mL**
sedimentation	2.35 ± 0.90	2.22 ± 0.19	0.13	5.67	n.a
centrifugation	2.13 ± 0.28	2.07 ± 0.30	0.06	2.59	n.a
sedimentation + resuspension	2.40 ± 0.27	2.48 ± 0.28	-0.08	-3.33	0.04 ± 0.02
	Na-CM				
	C_i	**C_a**	**C_d**	**difference**	**C_{ads}**
Experiment	**$\times 10^9$ CFU/mL**	**$\times 10^9$ CFU/mL**	**$\times 10^9$ CFU/mL**	**%**	**$\times 10^9$ CFU/mL**
sedimentation	2.62 ± 0.35	1.71 ± 0.21	0.91	34.71	n.a
centrifugation	2.16 ± 0.19	1.95 ± 0.13	0.21	9.74	n.a
sedimentation + resuspension	2.25 ± 0.05	1.53 ± 0.11	0.72	33.05	0.65 ± 0.06
	Na-Zr-50-2.5				
	C_i	**C_a**	**C_d**	**difference**	**C_{ads}**
Experiment	**$\times 10^9$ CFU/mL**	**$\times 10^9$ CFU/mL**	**$\times 10^9$ CFU/mL**	**%**	**$\times 10^9$ CFU/mL**
sedimentation	2.27 ± 0.50	0.85 ± 0.28	1.42	62.64	n.a
centrifugation	2.00 ± 0.04	0.79 ± 0.05	1.20	60.33	n.a
sedimentation + resuspension	2.26 ± 0.25	1.07 ± 0.04	1.19	52.65	0.88 ± 0.13

C_i: Initial bacterial cell concentration in the adsorbent-free and adsorbent-containing dispersions after the incubation period (CFU/mL).

C_a: Bacterial cell concentration after adsorption (CFU/mL).

C_d: Difference in the initial and post-adsorption cell concentrations (CFU/mL).

C_{ads}: Cell concentration in the residual precipitate phase during confirmation tests (CFU/mL).

Fig. 30 shows the change in concentrations of bacterial cells after sedimentation and resuspension of the precipitate phase. It depicts that the initial concentration of *E. coli* cells (shown in the orange column) decreases after adding clay adsorbents (green column). The number of cells attached to the clay particles after adsorption is shown by a purple column. In

the reference sample, only the sedimented cells in the pellet are responsible for the decrease of the initial concentration by 0.04×10^9 CFU/mL. Since this quantity is negligible, the cells taken up by Na-CM particles that were sedimented (0.65×10^9 CFU/mL) are directly linked to the adsorption efficiency of the tested particles. For the Na-Zr-50-2.5 sample, it was demonstrated that the adsorption resulted in a decrease of 0.88×10^9 CFU/mL in the initial cell concentration. The sum of the cell concentration of the supernatant after adsorption (green column) and the cell concentration present in the precipitate phase (purple column) should be close to the initial cell concentration (orange column) if there is no other sink of cells. Indeed, the combined values of these two quantities are within 10% of the initial cell concentration for each sample, and this deviation is smaller than the error of the initial cell concentration, ensuring the consistency of our results. Decanting the supernatant from the residual precipitate phase can also offer insights into the adsorption strength of the cells to the adsorbents. Therefore, the decanted phase was also investigated and plated on LB agar plates. On plates, there were not enough cell colonies to count, indicating strong adherence of the cells to the surface of clay particles.

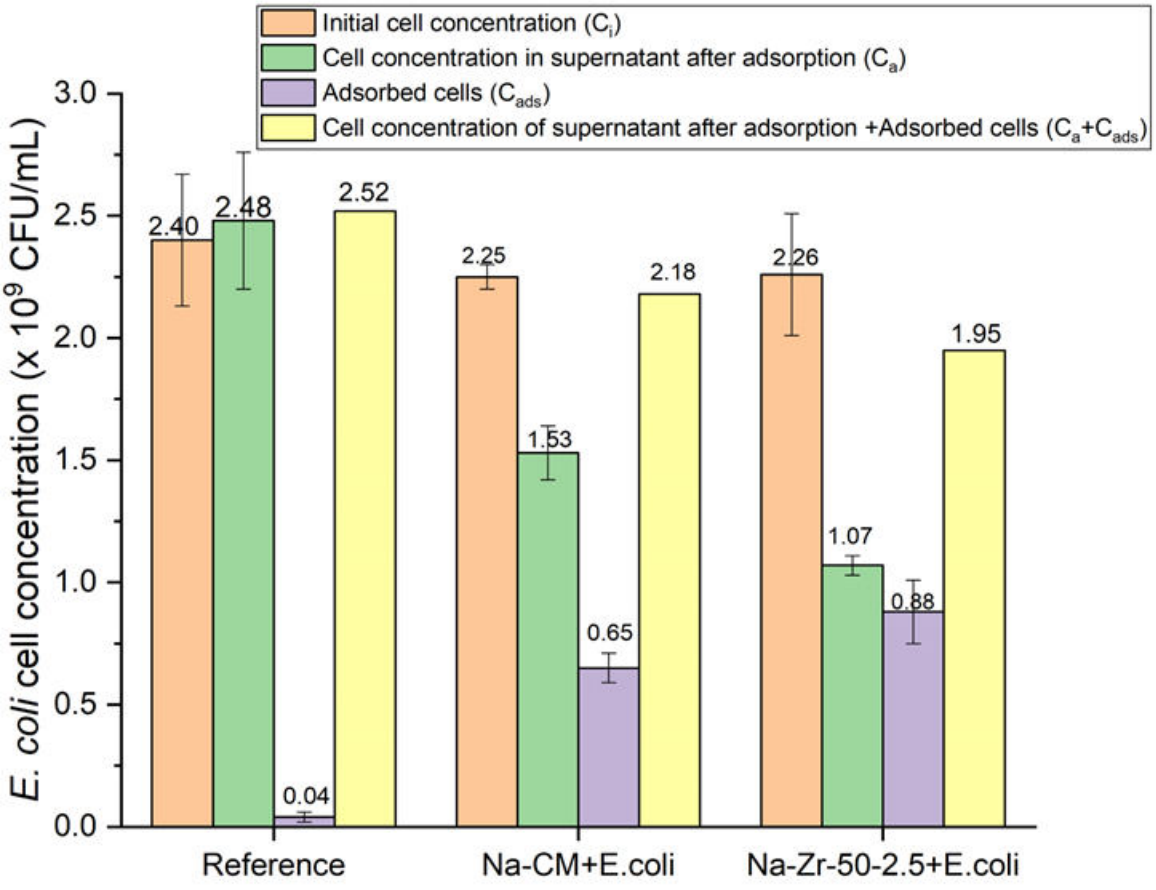

Figure 30: Confirmation of E. coli adsorption tests.

Figure 31-33 shows the photographs of *E. coli* colonies before and after adsorption using different techniques. In **Fig. 31** and **32 (E, F**), it is visible that the number of *E. coli* colonies obtained on LB-agar plates after adsorption are very few which confirms the adsorption of E. coli cells on the Na-Zr-50-2.5 sample. In the sedimentation and resuspension technique, the clay particles were collected from the bottom of centrifuge tubes and plated on LB-agar plates to check the number of adsorbed *E. coli* cells. In **Fig. (33 F, I)** the LB-agar plates show *E. coli* colonies which are missing from the supernatant and are adsorbed to the Na-CM and Na-Zr-50-2.5.

Before adsorption	After adsorption
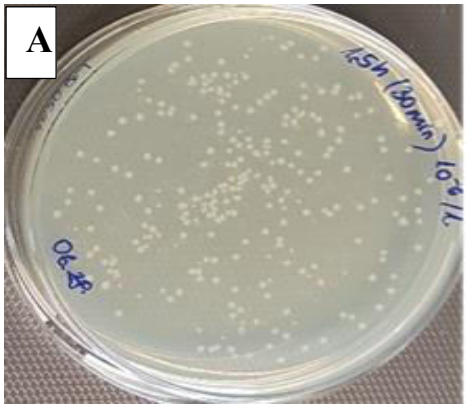	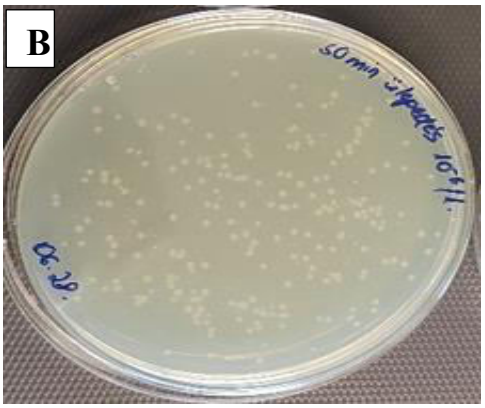
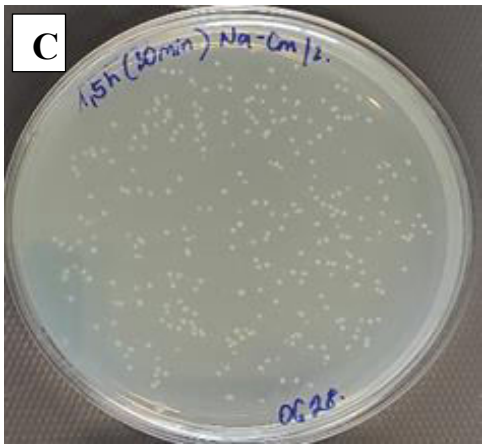	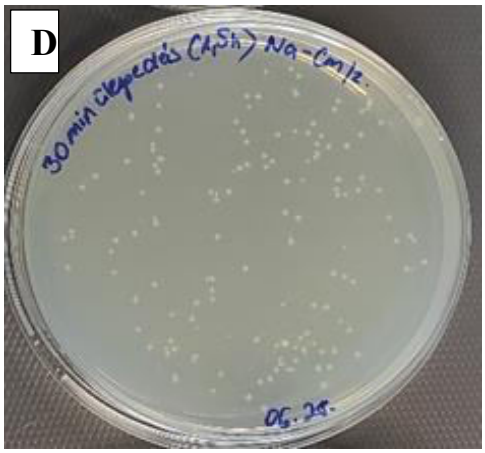
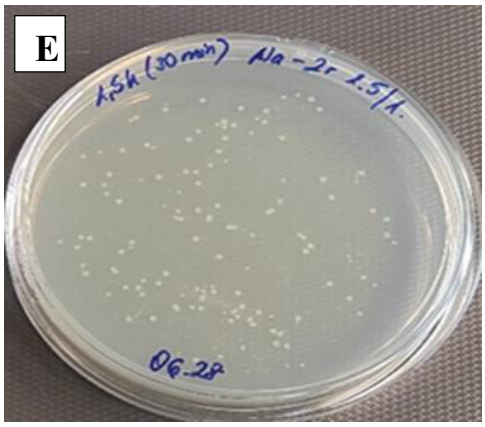	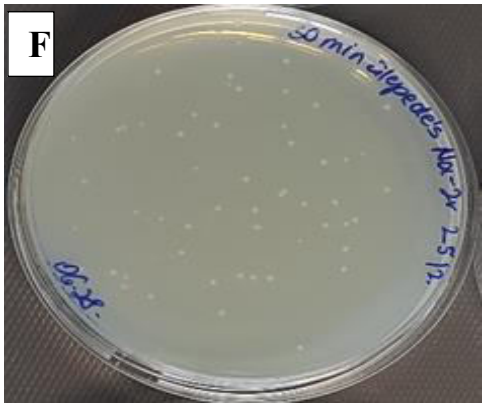

Figure 31: Photographs of E. coli colonies before and after adsorption using sedimentation technique; E. coli reference (**A, B**), Na-CM (**C,D**) and Na-Zr-50-2.5 (**E,F**).

Before adsorption	After adsorption
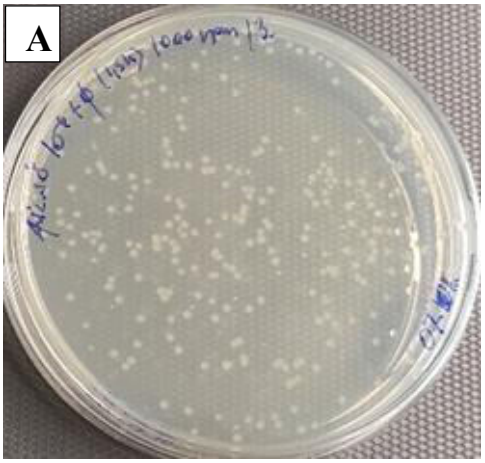	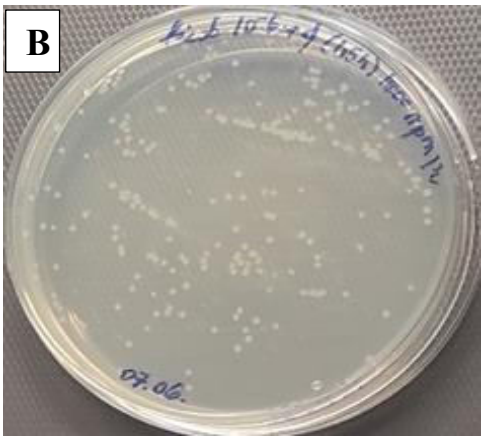
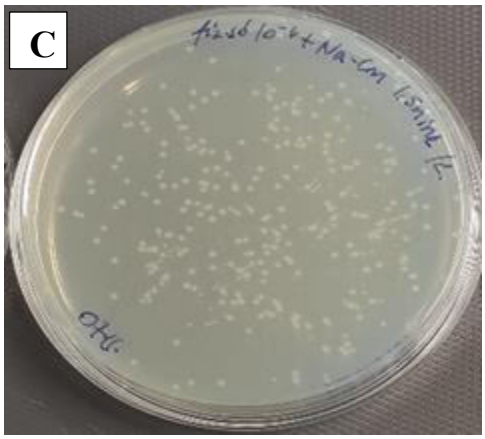	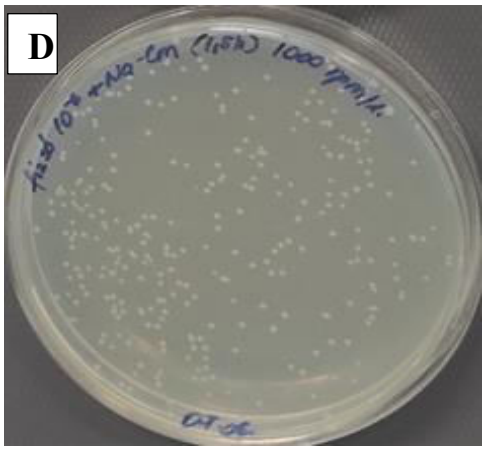
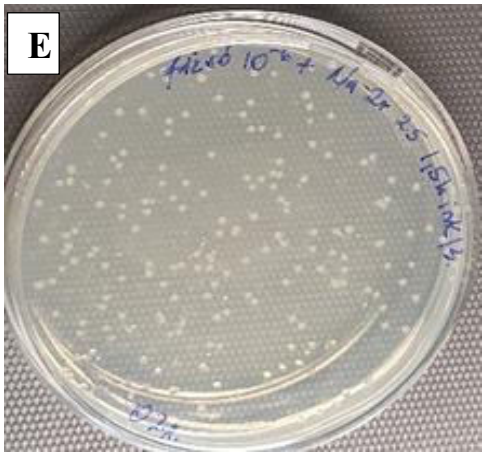	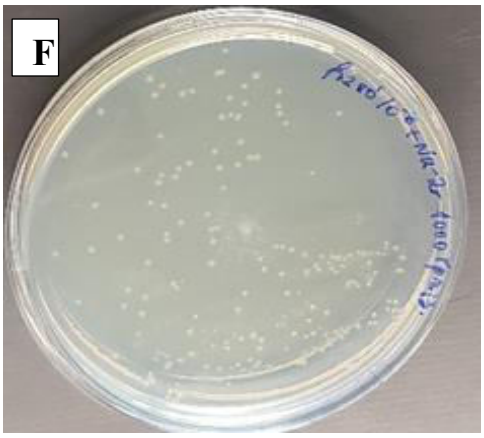

Figure 32: Photographs of E. coli colonies before and after adsorption using centrifugation technique; E. coli reference (A, B), Na-CM (C,D) and Na-Zr-50-2.5 (E,F).

Before adsorption	After adsorption	Adsorbed *E. coli* cells on adsorbent
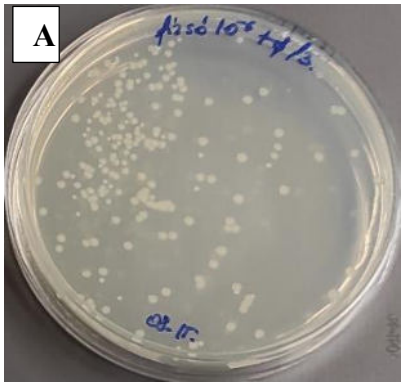	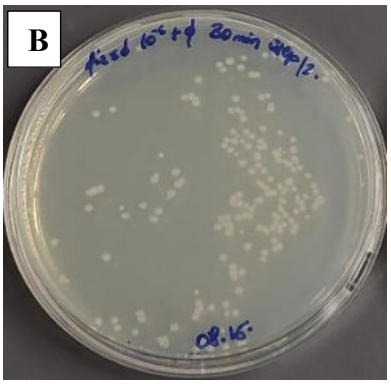	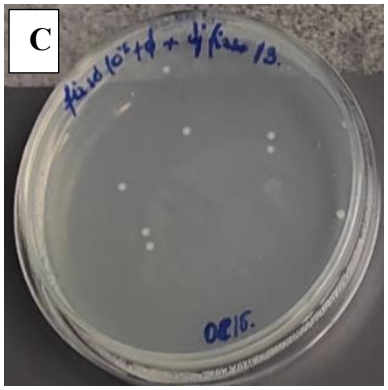
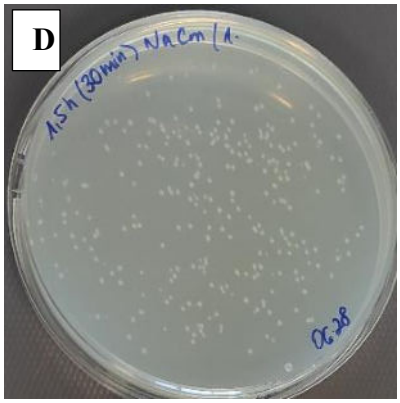	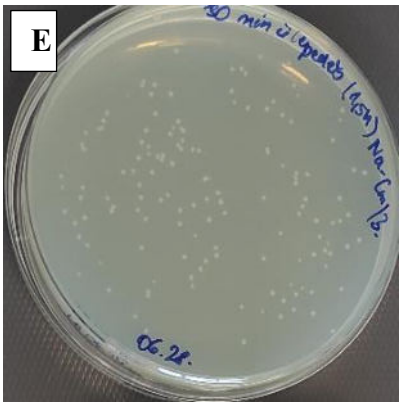	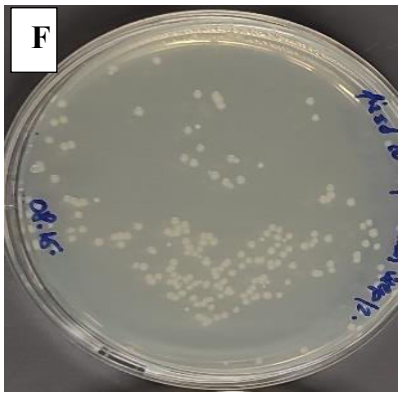
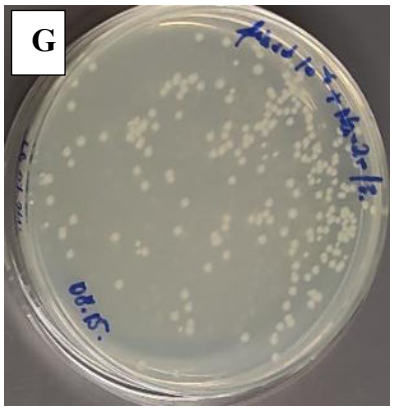	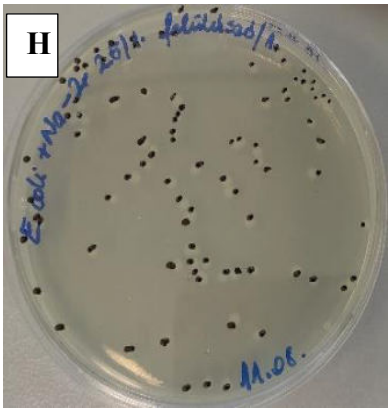	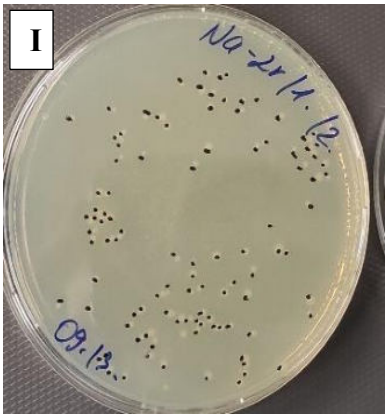

Figure 33: Photographs of E. coli colonies before and after adsorption using sedimentation+ resuspension technique; E. coli reference **(A, B,C),** Na-CM **(D,E,F)** and Na-Zr-50-2.5 **(G,H,I).**

6.3.5 Regeneration of Na-Zr-50-2.5 after *E. coli* adsorption

Regeneration of an adsorbent is an important aspect with regard to its reusability and cost efficiency. Therefore, we decided to conduct *E. coli* adsorption experiments on heat regenerated Na-Zr-50-2.5 sample. In the literature, there are several methods reported which can be used for the regeneration of clay adsorbents such as wet steam (autoclaving), chemical methods and heat treatment [134][102]. However, in this study heat treatment was used; the adsorbent was kept at 120°C for 5h in a drying oven. We used the same method for sterilizing the clay samples as well before performing the adsorption experiments. The *E. coli* removal efficiency of regenerated Na-Zr-50-2.5 adsorbent is summarized in **Table 8**. The original E. coli removal efficiency of this sample was 62.64 % (Table 7) and after the regeneration, it decreased to 55.35%. The difference was only 7.3 % and consequently, it was found that the adsorbent was working effectively even after the regeneration.

Table 8: *E. coli* removal efficiency of regenerated Na-Zr-50-2.5.

	Heat regenerated Na-Zr-50-2.5			
	C_i	**C_a**	**C_d**	**difference**
Experiment	**$\times 10^9$ CFU/mL**	**$\times 10^9$ CFU/mL**	**$\times 10^9$ CFU/mL**	**%**
sedimentation	3.58 ± 0.18	1.60 ± 0.02	1.98	55.35

7. SUMMARY

The goal of this research was to create and optimize the synthesis process of sustainable clay-based adsorbent materials which can be used in the removal of water contaminants. Montmorillonite clay which is used as a base material is found in abundance in nature. This particular type of clay was selected for the study because of its unique chemical structure and physical properties. The structure is made up of aluminosilicate layers and in between these layers (interlayer space), water molecules and small cations are present such as Na^{+}, Ca^{2+} and Mg^{2+}. These ions are mobile and exchangeable in nature. For modification of Mt clay, zirconium and chitosan were used because of their distinctive properties favourable for the adsorption of target molecules. Zr^{4+} possesses a high coordination ability and more selectivity towards phosphates. It can immobilize the phosphates on the clay surface by making inner-sphere complexes. Chitosan is a natural biopolymer with no toxicity and when it is combined with clay more active sites are generated on the clay surface which helps to catch phosphates from water at different ranges of pH.

In this study, interlayer ions of naturally occurring montmorillonite clay were replaced and fixed with Zr^{4+} cations and the process is known as intercalation or pillaring. The study is divided into two parts, the first part consists of the synthesis method used for the development of zirconium pillared clays and chitosan-modified Zr-pillared clays, and the second part mainly focuses on the application of these modified clays in the adsorption of phosphates and *E. coli* from aqueous solution.

To begin with, a comprehensive study was conducted to determine the optimum amount of zirconium uptake into the interlayer space of montmorillonite clay and the effect of sodium pre-treatment on the process of pillaring. Two precursor materials were taken pure raw clay (CM) and sodium ion-saturated montmorillonite clay (Na-CM). From each precursor, three zirconium pillared clays were developed using three different Zr^{4+}/clay ratios (2.5, 5 and 10 mmol/g). The samples were investigated with different techniques such as XRD, FT-IR, TGA, HRTEM and STEM-EDX to confirm the process of intercalation and to get more insight into the zirconium microstructures created during the process of pillaring. After investigation, it was found that pillared clays which were prepared from Na-CM, have shown better intercalation of zirconium ions. Also, samples which were prepared with 2.5 and 5 mmol of zirconium per gram of clay

(Na-Zr-50-2.5 and Na-Zr-50-5) showed an even distribution of ZrO_2 pillars in the interlayer space. The thickness of these pillars was found to be in the range of **1-2 nm,** and they were separated by a distance of **1.5-3 nm**. These two samples were further used in the adsorption of phosphates from water. Among two of them, the **Na-Zr-50-2.5** sample was found to be more effective in the sequestration of phosphates. The Langmuir phosphate adsorption capacity of Na-Zr-50-2.5 and Na-Zr-50-5 was found to be **11.5 ± 0.98** and **9.6 ± 0.93** mg/g respectively at pH 4. A possible reason for this could be that the distribution and arrangement of pillars created in between the silicate layers are influenced by zirconium concentration which further affects the surface charge of pillared clays. Zeta potential measurements revealed that the Na-Zr-50-2.5 sample was able to shift the zeta potential to a more positive value i.e, 11 mV than Na-Zr-50-5 (3 mV) thus favouring the strong interaction between the clay surface and phosphate species. Therefore, zirconium loading of 2.5 mmol per gram of clay is found to be the optimum concentration for achieving maximum adsorption capacity.

In the beginning, the application of clay samples was explored only at acidic pH because in literature it is well documented that phosphate adsorption is favoured at acidic pH because the surface hydroxyl groups of pillared clays get protonated which facilitates the attraction of negatively charged phosphate species. However, to enhance the performance of these materials at higher pH as well further chitosan modification was applied. Positively charged amino groups of chitosan introduced more reactive sites on the surface of clay which are easily accessible to negatively charged phosphate groups. As a result, **Ch-Na-Zr-50-2.5** was perfectly working at pH 4 and pH 7. After chitosan modification, the maximum phosphate adsorption capacity of Ch-NaZr2.5 increased from **11.5 ± 0.98 to 14.5 ± 0.42** and **8.3 ± 0.64 to 11.8 ± 0.35** mg/g at **pH 4 and 7** respectively. The possible major governing mechanism responsible for the adsorption of phosphates was the formation of inner-sphere complexes.

Another application of **Na-Zr-50-2.5** was explored in the removal of *E. coli* from an aqueous solution. As per our knowledge, these zirconium pillared clays have not been used in the removal of biological pathogens so far. In the study, *E. coli* adsorption properties of raw montmorillonite (Na-CM) and Na-Zr-50-2.5 were investigated and compared. To conduct the *E. coli* adsorption experiments, a novel approach was taken for the optimization of the procedure suitable for calculating the adsorption capacity of powder clay materials. Three approaches (sedimentation, centrifugation and residual pellet investigation) were taken to verify the efficiency of clay samples in the removal of *E. coli*. For Na-CM, the sedimentation

technique was found to be more accurate in determining the number of *E. coli* cells adsorbed. The *E. coli* removal percentage of Na-CM was found to be 34.7%. In the case of Na-Zr-50-2.5, the *E. coli* removal percentage achieved from sedimentation and centrifugation techniques was 62.64 and 60.33 % respectively. Both sedimentation and centrifugation techniques produced almost similar results in Na-Zr-50-2.5. To validate these results, the precipitate phase (adsorbent containing attached bacteria) was also examined and plated on agar plates to determine the number of cells attached to the clay particles. The amount of *E. coli* cells attached to the Na-CM and Na-Zr-50-2.5 particles was found to be 0.65 ± 0.06 and 0.88 ± 0.13 CFU/mL**.** The prepared clay-based adsorbent materials have shown satisfying results in the adsorption of phosphates and *E. coli* from an aqueous solution. Application of these newly formed clay materials in wastewater treatment plants can open an alternative pathway which is economically feasible and non-toxic.

8. CLAIMS/NEW SCIENTIFIC FINDINGS

The modified clays were synthesized by intercalating zirconium ions in the interlayer region of montmorillonite clay and the surface of the prepared materials was further modified using chitosan. The powder materials were tested for their applicability as adsorbents in wastewater treatment. These nanoporous clay-based materials were found to be suitable for targeting more than one pollutant from water i.e. phosphates and *E. coli*.

Claim 1: Effect of Na^+-pretreatment and zirconium concentration on the nature of pillars created inside the clay structure.

The Zr-pillared clays were synthesized using two precursor materials; naturally occurring montmorillonite (CM) and sodium-exchanged montmorillonite (Na-CM). I observed that samples which were prepared from Na-CM have shown better pillaring. A possible explanation for this could be when CM was treated with NaCl, sodium ions entered the interlayer space and interlayer water was removed as an effect of heating. This makes the clay structure homogenized and the sodium ions facilitate the subsequent exchange with zirconium ions. Also, the mobility of the interlayer ions depends on the stability of the hydration shell around them. Sodium ions have a less stable hydration shell therefore they have more mobility. In CM, sodium ions are present along with other cations such as calcium and potassium therefore the moving region of Na^+ ions is constrained by the hydration shell of other cations.

I confirmed that Na^+-treatment enhanced the process of pillaring. I established that the optimum concentration for pillaring was found to be 5 mmol/g above this concentration the pillaring was non-uniform. The thickness of the ZrO_2 pillars varied between 1-2 nm and the structures were separated by a distance of 1.5-3 nm in Na-Zr-50-2.5 and Na-Zr-50-5 samples.

Claim 2: Effect of Zr^{4+}/clay ratio and chitosan modification on phosphate adsorption property of Zr-pillared clays

During the phosphate adsorption study, it was observed that the pillared clay having a Zr^{4+}/clay ratio of 2.5 mmol/g (Na-Zr-50-2.5) showed better phosphate adsorption capacity than 5 mmol/g (Na-Zr-50-5). At pH 4, the Langmuir phosphate adsorption capacity was found to be 11.5 ± 0.98 and 9.6 ± 0.93 mg/g respectively. A possible reason for this could be that the distribution

and arrangement of ZrO_2 pillars created in between the silicate layers are influenced by zirconium concentration which further affects the surface charge of pillared clays. Zeta potential measurements revealed that the Na-Zr-50-2.5 sample was able to shift the zeta potential to a more positive value i.e, 11 mV than Na-Zr-50-5 (3 mV) thus favouring the strong interaction between the clay surface and phosphate species.

I confirmed that zirconium loading of 2.5 mmol per gram of clay is found to be the optimum concentration for achieving maximum adsorption capacity. To enhance the performance of Na-Zr-50-2.5 at higher pH as well a further chitosan modification was applied. Positively charged amino groups of chitosan introduced more reactive sites on the surface of clay which are easily accessible to negatively charged phosphate groups. I established that the Ch-NaZr2.5 sample can work effectively in the removal of phosphates from water at both pH.

Claim 3: *E. coli* adsorption capacity of zirconium pillared (Na-Zr-50-2.5) and precursor clay (Na-CM)

Precursor clay (Na-CM) and zirconium pillared clay (Na-Zr-50-2.5) were tested against the removal of *E. coli* bacteria from the saline solution. A novel approach was developed to conduct these experiments which include the usage of different separation techniques for separating powder adsorbent materials from saline solution such as sedimentation and centrifugation. For further validation of the results, the adsorbent materials collected at the bottom of the centrifuge tubes after the adsorption of *E. coli* cells were also investigated separately and the results were in favour of the sedimentation technique. Na-CM was able to reduce the *E. coli* level up to 34.71% and Na-Zr-50-2.5 was able to remove 62.64% which is almost double of precursor material.

I confirmed that Na-Zr-50-2.5 is more effective in the removal of *E. coli* cells from aqueous solution than raw clay due to stronger electrostatic interaction between clay surface and bacterial cells.

9. PUBLICATIONS

PUBLICATIONS CONNECTING TO DISSERTATION

1. **Chauhan, T.,** Udayakumar, M., Shehab, M.A., Kristály, F., Leskó, A.K., Ek, M., Wahlqvist, D., Tóth, P., Hernadi, K. and Németh, Z., 2022. Synthesis, characterization, and challenges faced during the preparation of zirconium pillared clays. *Arabian Journal of Chemistry*, *15*(4), p.103706. **I.F – 6.212 (Q1)**
2. **Chauhan**, **T.,** Németh, Z.,2022. Intercalation of zirconium ions into the montmorillonite clay using stir-age-stir technique.PhD students Almanc, ISSN 2939-7294,vol I
3. **Chauhan,T.,**SzőriDorogházi,E.,Muránszky,G.,Kecskés,K.,Finšgar,M., Szabó,T., Leskó ,M., Németh, Z., Hernadi, K.2024. Application of modified clays in the removal of phosphates and E. coli from aqueous solution. *Environmental Nanotechnology, Monitoring and Management* **(Q1).**

OTHER PUBLICATIONS

1. El Mrabate, B., Szőri-Dorogházi, E., Shehab, M.A., **Chauhan, T**., Muránszky, G., Sikora, E., Filep, Á., Sharma, N., Nánai, L., Hernadi, K. and Németh, Z., 2021. Widespread applicability of bacterial cellulose-ZnO-MWCNT hybrid membranes. *Arabian Journal of Chemistry*, *14*(7), p.103232. (**Q1; IF= 6.212**).
2. M., Shehab, Sharma, N.,Gabor,K., Kristály, F., El Mrabate, B**., Chauhan, T**., Tamás,K., Leskó, A.K.,Katalin,A., Árpád,P.B., Hernadi, K., Németh, Z.,2021.Effect of the synthesis parameters on the formation of TiO2 nanostructures: controllable synthesis and adsorption properties of nanowires and nanotubes. Circular Economy and Environmental Protection, vol. 5, issue 3.
3. Shehab, M.A., Szőri-Dorogházi, E., Szabó, S., Valsesia, A., **Chauhan, T**., Koós, T., Muránszky, G., Szabó, T., Hernadi, K. and Németh, Z., 2023. Virus and bacterial removal ability of TiO2 nanowire-based self-supported hybrid membranes. *Arabian Journal of Chemistry*, *16*(1), p.104388. (**Q1; IF= 6.212**).

Conference presentations

1. Presented oral presentation on the topic: synthesis of Zr-pillared montmorillonite clays'' in INTERNATIONAL IGDIR CONFERENCE ON APPLIED SCIENCE on April 14-15, 2021 / Igdır, Turkey.

2. Presented oral presentation in 8th International Renewable and Sustainable Energy Conference (IRSEC'20) on 25-28, 2020, Morocco.
3. Presented oral presentation in 9th Interdisciplinary Doctoral Conference (IDK2020) on 27-28 November 2020 organised by the Doctoral Student Association of the University of Pécs.
4. Presented oral presentation LATIN AMERICAN CONFERENCE ON NATURAL AND APPLIED SCIENCES held on October 4-6, 2022 / Villahermosa, Tabasco, Mexico Universidad Autonoma de Guadalajara.

10. ACKNOWLEDGEMENT

Completion of my research work and thesis has been possible with the support of many people whom I would like to thank sincerely.

First and foremost, I would like to express my warmest gratitude to my mentor and supervisor **Dr. Zoltán Németh** for giving me the opportunity to work in his research group. His continuous support and motivation helped me to overcome all the challenges faced during my research work. I would like to thank **Prof. Dr. Klára Hernádi** for her continuous guidance and valuable feedback on my scientific articles.

I would also like to express my sincere thanks to **Dr. Ferenc Kristály** for his valuable advice on the process of zirconium pillaring and the XRD measurements. I am also thankful to **Dr. Gábor Muránszky** for helping me with ICP-OES measurements. I also extend my sincere gratitude to **Dr. Mahitha Udayakumar and Dr. Nikita Sharma** for always inspiring and motivating me.

I wish to take this opportunity to acknowledge **Prof. Dr. Béla Viskolcz** and the Antal Kerpely Doctoral School of Materials Science & Technology, for offering me the chance to pursue my doctoral studies at the University of Miskolc. I am thankful to **Ágnes Solczi** for her kind help and guidance in the administrative work.

I would also thank **Tempus Public Foundation** for providing me with financial support through the Stipendium Hungaricum Scholarship programme.

Last but not least, I would like to thank my parents, brother, and friends for their love, support and encouragement throughout my PhD studies.

11. REFERENCES

[1] W. Hole, E. Biology, and P. Systems, "Sources of Nutrient Pollution to Coastal Waters in the United States : Implications for Achieving Coastal Water Quality Goals," *Estuaries*, vol. 25, no. 4, pp. 656–676, 2002.

[2] A. Buranapratheprat, A. Morimoto, P. Phromkot, Y. Mino, and V. Gunbua, "Eutrophication and hypoxia in the upper Gulf of Thailand," *J. Oceanogr.*, vol. 77, no. 6, pp. 831–841, 2021, doi: 10.1007/s10872-021-00609-2.

[3] J. M. Burkholder, D. A. Tomasko, and B. W. Touchette, "Seagrasses and eutrophication," vol. 350, pp. 46–72, 2007, doi: 10.1016/j.jembe.2007.06.024.

[4] R. K. Rosenbaum, "Ecotoxicity. Chapter 8 'Life Cycle Impact Assessment' (Hauschild MZ and Huijbregts MAJ eds)," *LCA Compend. - Complet. World Life Cycle Assessment, Life Cycle Impact Assess.*, pp. 139–162, 2015, doi: 10.1007/978-94-017-9744-3.

[5] Y. Zou, R. Zhang, L. Wang, K. Xue, and J. Chen, "Applied Clay Science Strong adsorption of phosphate from aqueous solution by zirconium-loaded," *Appl. Clay Sci.*, vol. 192, no. January, p. 105638, 2020, doi: 10.1016/j.clay.2020.105638.

[6] E. E. A. R. No, *Nutrient enrichment and eutrophication in Europe's seas*, no. 14. 2019.

[7] R. V Rodrigues, J. S. Patil, and A. C. Anil, "Dinoflagellates cyst assemblage concerning trophic index for eutrophication from major ports along the west coast of India," *Mar. Pollut. Bull.*, vol. 176, no. February, p. 113423, 2022, doi: 10.1016/j.marpolbul.2022.113423.

[8] B. Bera, S. Bhattacharjee, P. Kumar, N. Sengupta, and S. Saha, "Anthropogenic stress on a Ramsar site , India : Study towards rapid transformation of the health of aquatic environment," *Environ. Challenges*, vol. 4, no. April, p. 100158, 2021, doi: 10.1016/j.envc.2021.100158.

[9] A. B. Fulke, J. Panigrahi, S. Eranezhath, J. Karthi, and G. U. Dora, "Environmental variables and its association with faecal coliform at Madh Island beaches of megacity Mumbai , India ☆," *Environ. Pollut.*, vol. 341, no. November 2023, p. 122885, 2024, doi: 10.1016/j.envpol.2023.122885.

[10] B. Ram, "Correlation appraisal of antibiotic resistance with fecal , metal and microplastic contamination in a tropical Indian river , lakes and sewage," *npj Clean Water*, pp. 1–12, doi: 10.1038/s41545-020-0050-1.

[11] Z. Afsheen and A. Khan, "We are IntechOpen , the world ' s leading publisher of Open Access books Built by scientists , for scientists," no. December, 2018, doi: 10.5772/intechopen.80999.

[12] K. S. Hashim *et al.*, "Energy e ffi cient electrocoagulation using ba ffl e-plates electrodes for e ffi cient Escherichia coli removal from wastewater," vol. 33, no. November 2019, pp. 1–7, 2020, doi: 10.1016/j.jwpe.2019.101079.

[13] A. Awasthi, P. Jadhao, and K. Kumari, "Clay nano - adsorbent : structures , applications and mechanism for water treatment," *SN Appl. Sci.*, vol. 1, no. 9, pp. 1–21,

2019, doi: 10.1007/s42452-019-0858-9.

[14] T. Zhang *et al.*, “Removal of heavy metals and dyes by clay-based adsorbents: From natural clays to 1D and 2D nano-composites,” *Chem. Eng. J.*, no. August, p. 127574, 2020, doi: 10.1016/j.cej.2020.127574.

[15] M. K. Uddin, “A review on the adsorption of heavy metals by clay minerals, with special focus on the past decade,” *Chem. Eng. J.*, vol. 308, pp. 438–462, 2017, doi: 10.1016/j.cej.2016.09.029.

[16] H. Yi *et al.*, “Surface wettability of montmorillonite (0 0 1) surface as affected by surface charge and exchangeable cations: A molecular dynamic study,” *Appl. Surf. Sci.*, vol. 459, no. July, pp. 148–154, 2018, doi: 10.1016/j.apsusc.2018.07.216.

[17] K. Y. Park, S. Y. Choi, S. H. Lee, J. H. Kweon, and J. H. Song, “Comparison of formation of disinfection by-products by chlorination and ozonation of wastewater effluents and their toxicity to Daphnia magna,” *Environ. Pollut.*, vol. 215, pp. 314–321, 2016, doi: 10.1016/j.envpol.2016.04.001.

[18] M. Chauhan, V. K. Saini, and S. Suthar, “Removal of pharmaceuticals and personal care products (PPCPs) from water by adsorption on aluminum pillared clay,” *J. Porous Mater.*, vol. 27, no. 2, pp. 383–393, 2020, doi: 10.1007/s10934-019-00817-8.

[19] W. Huang *et al.*, “Effective phosphate adsorption by Zr/Al-pillared montmorillonite: Insight into equilibrium, kinetics and thermodynamics,” *Appl. Clay Sci.*, vol. 104, pp. 252–260, 2015, doi: 10.1016/j.clay.2014.12.002.

[20] M. Chauhan, V. K. Saini, and S. Suthar, “Ti-pillared montmorillonite clay for adsorptive removal of amoxicillin , imipramine , diclofenac-sodium , and paracetamol from water,” *J. Hazard. Mater.*, vol. 399, no. February, p. 122832, 2020, doi: 10.1016/j.jhazmat.2020.122832.

[21] A. Gil *et al.*, “A review of organic-inorganic hybrid clay based adsorbents for contaminants removal: Synthesis, perspectives and applications,” *J. Environ. Chem. Eng.*, vol. 9, no. 5, p. 105808, 2021, doi: 10.1016/j.jece.2021.105808.

[22] X. Tong *et al.*, “Adsorption of 17B-estradiol onto humic-mineral complexes and effects of temperature, pH, and bisphenol A on the adsorption process,” *Environ. Pollut.*, vol. 254, p. 112924, 2019, doi: 10.1016/j.envpol.2019.07.092.

[23] J. Pires and V. K. Saini, “Studies on Selective Adsorption of Biogas Components on Pillared Clays : Approach for Biogas Improvement,” vol. 42, no. 23, pp. 8727–8732, 2008.

[24] M. Abdennouri *et al.*, “Photocatalytic degradation of pesticides by titanium dioxide and titanium pillared purified clays,” *Arab. J. Chem.*, vol. 9, pp. S313–S318, 2016, doi: 10.1016/j.arabjc.2011.04.005.

[25] G. A. O. Tian-yu, Z. Yong-hua, Z. Ze, Z. Qi-jian, L. I. U. Hui-min, and W. Huan, “Acid activation of montmorillonite and its application for production of hydrogen via steam reforming of dimethyl ether,” *J. Fuel Chem. Technol.*, vol. 49, no. 10, pp. 1495–1503, 2021, doi: 10.1016/S1872-5813(21)60103-2.

[26] S. Z. Li and P. X. Wu, “Characterization of sodium dodecyl sulfate modified iron pillared montmorillonite and its application for the removal of aqueous Cu(II) and Co(II),” *J. Hazard. Mater.*, vol. 173, no. 1–3, pp. 62–70, 2010, doi:

10.1016/j.jhazmat.2009.08.047.

[27] H. Xiang, B. Tuo, J. Tian, K. Hu, J. Wang, and J. Cheng, “Preparation and photocatalytic properties of Bi-doped TiO 2 / montmorillonite composite,” *Opt. Mater. (Amst).*, vol. 117, no. February, p. 111137, 2021, doi: 10.1016/j.optmat.2021.111137.

[28] R. M. Barrer and D. M. Macleod, “Activation of montmorillonite by ion exchange and sorption complexes of tetra-alkyl ammonium montmorillonites,” *Trans. Faraday Soc.*, no. 51, pp. 1290–1300., 1955.

[29] R. E. Brindley, G.W.; Sempels, “Hydroxy-Aluminium Beidellites,” *Clay Miner.*, vol. 12, pp. 229–237, 1977.

[30] S. Yamanaka, “High Surface Area Solids Obtained by Reaction of Montmorillonite with Zirconyl Chloride,” *Clays Clay Miner.*, vol. 27, no. 2, pp. 119–124, 1979, doi: 10.1346/ccmn.1979.0270207.

[31] P. C. E. F. Vansant, “Pillared Clays : Preparation , Characterization and Applications,” vol. 1, 1998.

[32] M. A. Vicente, A. Gil, and F. Bergaya, *Pillared clays and clay minerals*, 2nd ed., vol. 5. Elsevier Ltd., 2013.

[33] G. J. J. Bartley, “Catalysis Today,2 (1988) 233-241 Elsevier,” vol. 2, pp. 233–241, 1988.

[34] L. P. Meier, R. Nueesch, and F. T. Madsen, “Organic pillared clays,” *J. Colloid Interface Sci.*, vol. 238, no. 1, pp. 24–32, 2001, doi: 10.1006/jcis.2001.7498.

[35] Y. S. Han, S. Yamanaka, and J. H. Choy, “Acidic and Hydrophobic Microporous Clays Pillared with Mixed Metal Oxide Nano-Sols,” *J. Solid State Chem.*, vol. 144, no. 1, pp. 45–52, 1999, doi: 10.1006/jssc.1998.8115.

[36] M. Önal and Y. Sarikaya, “Preparation and characterization of acid-activated bentonite powders,” *Powder Technol.*, vol. 172, no. 1, pp. 14–18, 2007, doi: 10.1016/j.powtec.2006.10.034.

[37] P. Komadel and J. Madejová, “Chapter 7.1 Acid Activation of Clay Minerals,” *Dev. Clay Sci.*, vol. 1, no. C, pp. 263–287, 2006, doi: 10.1016/S1572-4352(05)01008-1.

[38] M. X. Zhu, K. Y. Ding, S. H. Xu, and X. Jiang, “Adsorption of phosphate on hydroxyaluminum- and hydroxyiron-montmorillonite complexes,” *J. Hazard. Mater.*, vol. 165, no. 1–3, pp. 645–651, 2009, doi: 10.1016/j.jhazmat.2008.10.035.

[39] Y. Wang, F. Ji, W. Wang, S. Yuan, and Z. Hu, “Removal of roxarsone from aqueous solution by Fe / La-modified montmorillonite,” vol. 3994, no. November, 2015, doi: 10.1080/19443994.2015.1108875.

[40] F. Bergaya, A. Aouad, and T. Mandalia, “Chapter 7.5 Pillared Clays and Clay Minerals,” *Dev. Clay Sci.*, vol. 1, no. C, pp. 393–421, 2006, doi: 10.1016/S1572-4352(05)01012-3.

[41] A. Andrea, M. Eugenia, R. Jalil, J. Villarroel-rocha, K. Sapag, and M. Teresita, “Applied Clay Science Fe- and SiFe-pillared clays from a mineralogical waste as adsorbents of ciprofloxacin from water,” *Appl. Clay Sci.*, vol. 220, no. January, p. 106458, 2022, doi: 10.1016/j.clay.2022.106458.

[42] S. Balci and E. Gökçay, “Effects of drying methods and calcination temperatures on the physical properties of iron intercalated clays,” vol. 76, pp. 46–51, 2002.

[43] F. Zermane, O. Bouras, M. Baudu, and J. P. Basly, “Cooperative coadsorption of 4-nitrophenol and basic yellow 28 dye onto an iron organo-inorgano pillared montmorillonite clay,” *J. Colloid Interface Sci.*, vol. 350, no. 1, pp. 315–319, 2010, doi: 10.1016/j.jcis.2010.06.040.

[44] O. Bouras, T. Chami, M. Houari, H. Khalaf, J. C. Bollinger, and M. Baudu, “Removal of sulfacid brilliant pink from an aqueous stream by adsorption onto surfactant-modified ti-pillared montmorillonite,” *Environ. Technol. (United Kingdom)*, vol. 23, no. 4, pp. 405–411, 2002, doi: 10.1080/09593332508618397.

[45] C. Zhou, D. Tong, and W. Yu, *Smectite nanomaterials: Preparation, properties, and functional applications*. Elsevier Inc., 2019.

[46] A. Elmchaouri and R. Mahboub, “Effects of preadsorption of organic amine on Al-PILCs structures,” *Colloids Surfaces A Physicochem. Eng. Asp.*, vol. 259, no. 1–3, pp. 135–141, 2005, doi: 10.1016/j.colsurfa.2005.02.014.

[47] N. Maes and E. F. Vansant, “Study of Fe2O3-pillared clays synthesized using the trinuclear Fe(III)-acetato complex as pillaring precursor,” *Microporous Mater.*, vol. 4, no. 1, pp. 43–51, 1995, doi: 10.1016/0927-6513(94)00080-F.

[48] R. Yu *et al.*, “Removal of Cd2+ from aqueous solution with carbon modified aluminum-pillared montmorillonite,” *Catal. Today*, vol. 139, no. 1–2, pp. 135–139, 2008, doi: 10.1016/j.cattod.2008.08.015.

[49] H. Y. Zhu, Z. H. Zhu, and G. Q. Lu, “Controlled doping of transition metal cations in alumina pillared clays,” *J. Phys. Chem. B*, vol. 104, no. 24, pp. 5674–5680, 2000, doi: 10.1021/jp994385n.

[50] M. Addy, B. Losey, R. Mohseni, E. Zlotnikov, and A. Vasiliev, “Adsorption of heavy metal ions on mesoporous silica-modified montmorillonite containing a grafted chelate ligand,” *Appl. Clay Sci.*, vol. 59–60, pp. 115–120, 2012, doi: 10.1016/j.clay.2012.02.012.

[51] L. Brown, K. Seaton, R. Mohseni, and A. Vasiliev, “Immobilization of heavy metals on pillared montmorillonite with a grafted chelate ligand,” *J. Hazard. Mater.*, vol. 261, pp. 181–187, 2013, doi: 10.1016/j.jhazmat.2013.07.024.

[52] M. Cabuk, Y. Alan, and H. I. Unal, “Enhanced electrokinetic properties and antimicrobial activities of biodegradable chitosan/organo-bentonite composites,” *Carbohydr. Polym.*, vol. 161, pp. 71–81, 2017, doi: 10.1016/j.carbpol.2016.12.067.

[53] C. Song, H. Yu, M. Zhang, Y. Yang, and G. Zhang, “Physicochemical properties and antioxidant activity of chitosan from the blowfly Chrysomya megacephala larvae,” *Int. J. Biol. Macromol.*, vol. 60, pp. 347–354, 2013, doi: 10.1016/j.ijbiomac.2013.05.039.

[54] A. Rajeswari, A. Amalraj, and A. Pius, “Removal of phosphate using chitosan-polymer composites,” *J. Environ. Chem. Eng.*, vol. 3, no. 4, pp. 2331–2341, 2015, doi: 10.1016/j.jece.2015.08.022.

[55] W. Tan, Y. Zhang, Y. shan Szeto, and L. Liao, “A novel method to prepare chitosan/montmorillonite nanocomposites in the presence of hydroxy-aluminum oligomeric cations,” *Compos. Sci. Technol.*, vol. 68, no. 14, pp. 2917–2921, 2008, doi:

10.1016/j.compscitech.2007.10.007.

[56] X. Zheng *et al.*, “Chitosan modified Ti-PILC supported PdOx catalysts for coupling reactions of aryl halides with terminal alkynes,” *Int. J. Biol. Macromol.*, vol. 158, pp. 67–74, 2020, doi: 10.1016/j.ijbiomac.2020.04.203.

[57] Y. Chen *et al.*, “Positron annihilation study of chitosan and its derived carbon/pillared montmorillonite clay stabilized Pd species nanocomposites,” *Polym. Test.*, vol. 114, no. July, 2022, doi: 10.1016/j.polymertesting.2022.107689.

[58] C. Pesquera, I. Benito, E. Herrero, C. Poncio, and S. Casuscelli, “Pillared clays : catalytic evaluation in heavy oil cracking using a microactivity test,” vol. 181, pp. 71–76, 1999.

[59] J. T. Kloprogge and R. L. Frost, “A review of the synthesis and characterisation of pillared clays and related porous materials for cracking of vegetable oils to produce biofuels,” pp. 967–981, 2005, doi: 10.1007/s00254-005-1226-1.

[60] J. Moma, “RSC Advances Synthesis and application of pillared clay heterogeneous catalysts for wastewater treatment : a review,” pp. 5197–5211, 2018, doi: 10.1039/C7RA12924F.

[61] F. Tomul, F. Turgut, and H. Canbay, “Applied Surface Science Determination of adsorptive and catalytic properties of copper , silver and iron contain titanium-pillared bentonite for the removal bisphenol A from aqueous solution,” *Appl. Surf. Sci.*, vol. 360, pp. 579–593, 2016, doi: 10.1016/j.apsusc.2015.10.228.

[62] J. Guo and M. Al-dahhan, “Catalytic Wet Oxidation of Phenol by Hydrogen Peroxide over Pillared Clay Catalyst,” pp. 2450–2460, 2003.

[63] N. R. Sanabria, P. Ávila, M. Yates, S. B. Rasmussen, R. Molina, and S. Moreno, “Applied Clay Science Mechanical and textural properties of extruded materials manufactured with AlFe and AlCeFe pillared bentonites,” *Appl. Clay Sci.*, vol. 47, no. 3–4, pp. 283–289, 2010, doi: 10.1016/j.clay.2009.11.029.

[64] M. Eloussaief, A. Sdiri, and M. Benzina, “Modelling the adsorption of mercury onto natural and aluminium pillared clays,” pp. 469–479, 2013, doi: 10.1007/s11356-012-0874-4.

[65] D. L. Guerra, C. Airoldi, V. P. Lemos, and R. S. Angélica, “Adsorptive, thermodynamic and kinetic performances of Al/Ti and Al/Zr-pillared clays from the Brazilian Amazon region for zinc cation removal,” *J. Hazard. Mater.*, vol. 155, no. 1–2, pp. 230–242, 2008, doi: 10.1016/j.jhazmat.2007.11.054.

[66] P. Taylor *et al.*, “Study of colloidal properties of natural and Al-pillared smectite and removal of copper ions from an aqueous solution,” no. December, pp. 37–41, 2014, doi: 10.1080/09593330.2014.961564.

[67] D. M. Manohar, B. F. Noeline, and T. S. Anirudhan, “Adsorption performance of Al-pillared bentonite clay for the removal of cobalt (II) from aqueous phase,” vol. 31, pp. 194–206, 2006, doi: 10.1016/j.clay.2005.08.008.

[68] A. Georgescu, F. Nardou, V. Zichil, and I. D. Nistor, “Applied Clay Science Adsorption of lead (II) ions from aqueous solutions onto Cr-pillared clays,” *Appl. Clay Sci.*, vol. 152, no. October 2017, pp. 44–50, 2018, doi: 10.1016/j.clay.2017.10.031.

[69] P. Na, X. Jia, B. Yuan, Y. Li, J. Na, and L. Wang, “Arsenic adsorption on Ti-pillared montmorillonite,” no. October 2009, pp. 708–714, 2010, doi: 10.1002/jctb.2360.

[70] Y. Li, J. Rong, S. Yi, J. Wei, J. Zhuo, and P. Na, “TiO 2 pillared montmorillonite as a photoactive adsorbent of arsenic under UV irradiation,” *Chem. Eng. J.*, vol. 191, pp. 66–74, 2012, doi: 10.1016/j.cej.2012.02.058.

[71] P. M. Melia, R. Busquets, P. S. Hooda, A. B. Cundy, and S. P. Sohi, “Driving forces and barriers in the removal of phosphorus from water using crop residue, wood and sewage sludge derived biochars,” *Sci. Total Environ.*, vol. 675, pp. 623–631, 2019, doi: 10.1016/j.scitotenv.2019.04.232.

[72] L. Zhang *et al.*, “Low-Cost Efficient Magnetic Adsorbent for Phosphorus Removal from Water,” *ACS Omega*, vol. 5, no. 39, pp. 25326–25333, 2020, doi: 10.1021/acsomega.0c03657.

[73] C. P. Health, “MANUAL ON SEWERAGE AND SEWAGE TREATMENT PART B : OPERATION AND MAINTENANCE,” no. December, 2012.

[74] J. Xiong, Z. He, Q. Mahmood, and D. Liu, “Phosphate removal from solution using steel slag through magnetic separation,” vol. 152, pp. 211–215, 2008, doi: 10.1016/j.jhazmat.2007.06.103.

[75] E. Zong, X. Liu, J. Jiang, S. Fu, and F. Chu, “Applied Surface Science Preparation and characterization of zirconia-loaded lignocellulosic butanol residue as a biosorbent for phosphate removal from aqueous solution,” *Appl. Surf. Sci.*, vol. 387, pp. 419–430, 2016, doi: 10.1016/j.apsusc.2016.06.107.

[76] M. Zamparas, A. Gianni, P. Stathi, Y. Deligiannakis, and I. Zacharias, “Removal of phosphate from natural waters using innovative modified bentonites,” *Appl. Clay Sci.*, vol. 62–63, pp. 101–106, 2012, doi: 10.1016/j.clay.2012.04.020.

[77] P. Kumararaja, S. Suvana, R. Saraswathy, N. Lalitha, and M. Muralidhar, “Mitigation of eutrophication through phosphate removal by aluminium pillared bentonite from aquaculture discharge water,” *Ocean Coast. Manag.*, vol. 182, no. May, p. 104951, 2019, doi: 10.1016/j.ocecoaman.2019.104951.

[78] S. Tian, P. Jiang, P. Ning, and Y. Su, “Enhanced adsorption removal of phosphate from water by mixed lanthanum / aluminum pillared montmorillonite,” vol. 151, pp. 141–148, 2009, doi: 10.1016/j.cej.2009.02.006.

[79] B. Wu, J. Wan, Y. Zhang, B. Pan, and I. M. C. Lo, “Selective Phosphate Removal from Water and Wastewater using Sorption : Process Fundamentals and Removal Mechanisms,” 2020, doi: 10.1021/acs.est.9b05569.

[80] F. Haghseresht, S. Wang, and D. D. Do, “A novel lanthanum-modified bentonite, Phoslock, for phosphate removal from wastewaters,” *Appl. Clay Sci.*, vol. 46, no. 4, pp. 369–375, 2009, doi: 10.1016/j.clay.2009.09.009.

[81] V. G. Deshmane and Y. G. Adewuyi, “Synthesis of thermally stable, high surface area, nanocrystalline mesoporous tetragonal zirconium dioxide (ZrO2): Effects of different process parameters,” *Microporous Mesoporous Mater.*, vol. 148, no. 1, pp. 88–100, 2012, doi: 10.1016/j.micromeso.2011.07.012.

[82] Q. Zhang *et al.*, “Selective removal of phosphate in waters using a novel of cation adsorbent: Zirconium phosphate (ZrP) behavior and mechanism,” *Chem. Eng. J.*, vol.

221, pp. 315–321, 2013, doi: 10.1016/j.cej.2013.02.001.

[83] H. Liu, X. Sun, C. Yin, and C. Hu, “Removal of phosphate by mesoporous ZrO2,” *J. Hazard. Mater.*, vol. 151, no. 2–3, pp. 616–622, 2008, doi: 10.1016/j.jhazmat.2007.06.033.

[84] J. Lin, B. Jiang, and Y. Zhan, “Effect of pre-treatment of bentonite with sodium and calcium ions on phosphate adsorption onto zirconium-modi fi ed bentonite,” *J. Environ. Manage.*, vol. 217, pp. 183–195, 2018, doi: 10.1016/j.jenvman.2018.03.079.

[85] J. Huo, X. Min, and Y. Wang, “Zirconium-modified natural clays for phosphate removal: Effect of clay minerals,” *Environ. Res.*, vol. 194, no. January, p. 110685, 2021, doi: 10.1016/j.envres.2020.110685.

[86] H. T. Banu, P. Karthikeyan, and S. Meenakshi, “Zr4+ ions embedded chitosan-soya bean husk activated bio-char composite beads for the recovery of nitrate and phosphate ions from aqueous solution,” *Int. J. Biol. Macromol.*, vol. 130, pp. 573–583, 2019, doi: 10.1016/j.ijbiomac.2019.02.100.

[87] I. A. Kumar and N. Viswanathan, “Development of multivalent metal ions imprinted chitosan biocomposites for phosphate sorption,” *Int. J. Biol. Macromol.*, vol. 104, pp. 1539–1547, 2017, doi: 10.1016/j.ijbiomac.2017.02.100.

[88] Q. Liu, P. Hu, J. Wang, L. Zhang, and R. Huang, “Phosphate adsorption from aqueous solutions by Zirconium (IV) loaded cross-linked chitosan particles,” *J. Taiwan Inst. Chem. Eng.*, vol. 59, pp. 311–319, 2016, doi: 10.1016/j.jtice.2015.08.012.

[89] V. Kuroki, G. E. Bosco, P. S. Fadini, A. A. Mozeto, A. R. Cestari, and W. A. Carvalho, “Use of a La(III)-modified bentonite for effective phosphate removal from aqueous media,” *J. Hazard. Mater.*, vol. 274, pp. 124–131, 2014, doi: 10.1016/j.jhazmat.2014.03.023.

[90] R. R. Pawar, P. Gupta, Lalhmunsiama, H. C. Bajaj, and S. M. Lee, “Al-intercalated acid activated bentonite beads for the removal of aqueous phosphate,” *Sci. Total Environ.*, vol. 572, pp. 1222–1230, 2016, doi: 10.1016/j.scitotenv.2016.08.040.

[91] L. G. Yan, Y. Y. Xu, H. Q. Yu, X. D. Xin, Q. Wei, and B. Du, “Adsorption of phosphate from aqueous solution by hydroxy-aluminum, hydroxy-iron and hydroxy-iron-aluminum pillared bentonites,” *J. Hazard. Mater.*, vol. 179, no. 1–3, pp. 244–250, 2010, doi: 10.1016/j.jhazmat.2010.02.086.

[92] L. Mdlalose, M. Balogun, K. Setshedi, and L. Chimuka, “Adsorption of phosphates using transition metals- modified bentonite clay,” *Sep. Sci. Technol.*, vol. 00, no. 00, pp. 1–12, 2018, doi: 10.1080/01496395.2018.1547315.

[93] H. A. T. Banu, P. Karthikeyan, S. Vigneshwaran, and S. Meenakshi, “Adsorptive performance of lanthanum encapsulated biopolymer chitosan-kaolin clay hybrid composite for the recovery of nitrate and phosphate from water,” *Int. J. Biol. Macromol.*, vol. 154, pp. 188–197, 2020, doi: 10.1016/j.ijbiomac.2020.03.074.

[94] H. Jiang, P. Chen, S. Luo, X. Tu, Q. Cao, and M. Shu, “Synthesis of novel nanocomposite Fe 3 O 4 /ZrO 2 /chitosan and its application for removal of nitrate and phosphate,” *Appl. Surf. Sci.*, vol. 284, pp. 942–949, 2013, doi: 10.1016/j.apsusc.2013.04.013.

[95] V. I. Syngouna and C. V. Chrysikopoulos, “Interaction between viruses and clays in

static and dynamic batch systems," *Environ. Sci. Technol.*, vol. 44, no. 12, pp. 4539–4544, 2010, doi: 10.1021/es100107a.

[96] J. K. Kang, C. G. Lee, J. A. Park, S. B. Kim, N. C. Choi, and S. J. Park, "Adhesion of bacteria to pyrophyllite clay in aqueous solution," *Environ. Technol. (United Kingdom)*, vol. 34, no. 6, pp. 703–710, 2013, doi: 10.1080/09593330.2012.715677.

[97] X. Rong, Q. Huang, X. He, H. Chen, P. Cai, and W. Liang, "Interaction of Pseudomonas putida with kaolinite and montmorillonite: A combination study by equilibrium adsorption, ITC, SEM and FTIR," *Colloids Surfaces B Biointerfaces*, vol. 64, no. 1, pp. 49–55, 2008, doi: 10.1016/j.colsurfb.2008.01.008.

[98] C. H. Hu and M. S. Xia, "Adsorption and antibacterial effect of copper-exchanged montmorillonite on Escherichia coli K88," *Appl. Clay Sci.*, vol. 31, no. 3–4, pp. 180–184, 2006, doi: 10.1016/j.clay.2005.10.010.

[99] T. Wu, A. G. Xie, S. Z. Tan, and X. Cai, "Antimicrobial effects of quaternary phosphonium salt intercalated clay minerals on Escherichia coli and Staphylococci aureus," *Colloids Surfaces B Biointerfaces*, vol. 86, no. 1, pp. 232–236, 2011, doi: 10.1016/j.colsurfb.2011.04.009.

[100] T. Undabeytia *et al.*, "Removal of waterborne microorganisms by filtration using clay-polymer complexes," *J. Hazard. Mater.*, vol. 279, pp. 190–196, 2014, doi: 10.1016/j.jhazmat.2014.07.006.

[101] P. Herrera, R. C. Burghardt, and T. D. Phillips, "Adsorption of Salmonella enteritidis by cetylpyridinium-exchanged montmorillonite clays," *Vet. Microbiol.*, vol. 74, no. 3, pp. 259–272, 2000, doi: 10.1016/S0378-1135(00)00157-7.

[102] E. I. Unuabonah *et al.*, "Novel metal-doped bacteriostatic hybrid clay composites for point-of-use disinfection of water," *J. Environ. Chem. Eng.*, vol. 5, no. 3, pp. 2128–2141, 2017, doi: 10.1016/j.jece.2017.04.017.

[103] T. Y. Liu, C. L. Chen, Y. C. Lee, T. Y. Chan, Y. L. Wang, and J. J. Lin, "First Observation of Physically Capturing and Maneuvering Bacteria using Magnetic Clays," *ACS Appl. Mater. Interfaces*, vol. 8, no. 1, pp. 411–418, 2016, doi: 10.1021/acsami.5b09192.

[104] S. Gowri, R. Rajiv Gandhi, and M. Sundrarajan, "Structural, optical, antibacterial and antifungal properties of zirconia nanoparticles by biobased protocol," *J. Mater. Sci. Technol.*, vol. 30, no. 8, pp. 782–790, 2014, doi: 10.1016/j.jmst.2014.03.002.

[105] E. I. Naik, H. S. B. Naik, R. Viswanath, B. R. Kirthan, and M. C. Prabhakara, "Effect of zirconium doping on the structural, optical, electrochemical and antibacterial properties of ZnO nanoparticles prepared by sol-gel method," *Chem. Data Collect.*, vol. 29, p. 100505, 2020, doi: 10.1016/j.cdc.2020.100505.

[106] L. Ammann, F. Bergaya, and G. Lagaly, "Determination of the cation exchange capacity of clays with copper complexes revisited," *Clay Miner.*, vol. 40, no. 4, pp. 441–453, 2005, doi: 10.1180/0009855054040182.

[107] M. Dion and W. Parker, "Steam Sterilization Principles," vol. 33, no. 6, pp. 1–8, 2013.

[108] P. Toth, "Nanostructure quantification of turbostratic carbon by HRTEM image analysis: State of the art, biases, sensitivity and best practices," *Carbon N. Y.*, vol. 178, pp. 688–707, 2021, doi: 10.1016/j.carbon.2021.03.043.

[109] L. M. Gand, M. A. Vicente, and A. Gil, “Preparation and characterization of manganese oxide catalysts supported on alumina and zirconia-pillared clays,” vol. 196, pp. 281–292, 2000.

[110] M. R. S. Kou, S. Mendioroz, and M. I. Guijarro, “A thermal study of Zr-pillared montmorillonite,” vol. 323, pp. 145–157, 1998.

[111] R. L. Frost, H. Ruan, J. Theo Kloprogge, and W. P. Gates, “Dehydration and dehydroxylation of nontronites and ferruginous smectite,” *Thermochim. Acta*, vol. 346, no. 1–2, pp. 63–72, 2000, doi: 10.1016/s0040-6031(99)00366-4.

[112] J. Madejová, “FTIR techniques in clay mineral studies,” *Vib. Spectrosc.*, vol. 31, no. 1, pp. 1–10, 2003, doi: 10.1016/S0924-2031(02)00065-6.

[113] B. B. Zviagina, V. A. Drits, and O. V. Dorzhieva, “Distinguishing features and identification criteria for K-dioctahedral 1M micas (Illite-aluminoceladonite and illite-glauconite-celadonite series) from middle-infrared spectroscopy data,” *Minerals*, vol. 10, no. 2, pp. 1–27, 2020, doi: 10.3390/min10020153.

[114] P. Yuan *et al.*, “A combined study by XRD, FTIR, TG and HRTEM on the structure of delaminated Fe-intercalated/pillared clay,” *J. Colloid Interface Sci.*, vol. 324, no. 1–2, pp. 142–149, 2008, doi: 10.1016/j.jcis.2008.04.076.

[115] J. Zhou, P. Wu, Z. Dang, N. Zhu, and P. Li, “Polymeric Fe / Zr pillared montmorillonite for the removal of Cr (VI) from aqueous solutions,” *Chem. Eng. J.*, vol. 162, no. 3, pp. 1035–1044, 2010, doi: 10.1016/j.cej.2010.07.016.

[116] I. Bačić, V. Mandić, L. Ćurković, H. Otmačić-Ćurković, and S. Kurajica, “Thermal and structural studies of sol–gel-derived yttria-doped ZrO2 nanoparticles: Effect of annealing condition,” *J. Therm. Anal. Calorim.*, vol. 127, no. 1, pp. 197–206, 2017, doi: 10.1007/s10973-016-5904-x.

[117] M. S. Onyango, D. Kuchar, M. Kubota, and H. Matsuda, “Adsorptive Removal of Phosphate Ions from Aqueous Solution Using Synthetic Zeolite,” pp. 894–900, 2007.

[118] A. M. Neris, J. M. Ferreira, M. G. Fonseca, and I. M. G. dos Santos, “Undoped tetragonal ZrO2 obtained by the Pechini method: thermal evaluation of tetragonal–monoclinic phase transition and application as catalyst for biodiesel synthesis,” *J. Therm. Anal. Calorim.*, no. 0123456789, 2020, doi: 10.1007/s10973-020-09286-7.

[119] J. Baloyi, T. Ntho, and J. Moma, “Synthesis of highly active and stable Al/Zr pillared clay as catalyst for catalytic wet oxidation of phenol,” *J. Porous Mater.*, vol. 26, no. 2, pp. 583–597, 2019, doi: 10.1007/s10934-018-0667-3.

[120] H. J. Chae, I. S. Nam, S. W. Ham, and S. B. Hong, “Physicochemical characteristics of pillared interlayered clays,” *Catal. Today*, vol. 68, no. 1–3, pp. 31–40, 2001, doi: 10.1016/S0920-5861(01)00320-0.

[121] N. Igawa and Y. Ishii, “Crystal Structure of Metastable Tetragonal Zirconia up to 1473 K,” vol. 71, no. 188984, pp. 1999–2001, 2001.

[122] Y. Gu *et al.*, “Size Modulation of Zirconium-Based Metal Organic Frameworks for Highly Efficient Phosphate Remediation,” *ACS Appl. Mater. Interfaces*, vol. 9, no. 37, pp. 32151–32160, 2017, doi: 10.1021/acsami.7b10024.

[123] M. A. Al-Ghouti and D. A. Da’ana, “Guidelines for the use and interpretation of

adsorption isotherm models: A review," *J. Hazard. Mater.*, vol. 393, no. February, p. 122383, 2020, doi: 10.1016/j.jhazmat.2020.122383.

[124] B. Dziejarski, "Microporous and Mesoporous Materials Application of isotherms models and error functions in activated carbon CO 2 sorption processes," vol. 354, no. February, 2023, doi: 10.1016/j.micromeso.2023.112513.

[125] Tóth, J., Adsorption Theory, Modeling, and Analysis, vol.107, Marcel Dekker, 2002.

[126] Y. S. Ho, J. F. Porter, and G. Mckay, "Divalent Metal Ions Onto Peat : Copper , Nickel and Lead Single Component Systems," *Water, Air, Soil Pollut.*, vol. 141, no. 1–4, pp. 1–33, 2002.

[127] E. Tombácz and M. Szekeres, "Surface charge heterogeneity of kaolinite in aqueous suspension in comparison with montmorillonite," *Appl. Clay Sci.*, vol. 34, no. 1–4, pp. 105–124, 2006, doi: 10.1016/j.clay.2006.05.009.

[128] E. G. Furuya, H. T. Chang, Y. Miura, and K. E. Noll, "A fundamental analysis of the isotherm for the adsorption of phenolic compounds on activated carbon," *Sep. Purif. Technol.*, vol. 11, no. 2, pp. 69–78, 1997, doi: 10.1016/S1383-5866(96)01001-5.

[129] Y. Sun *et al.*, "Journal of Environmental Chemical Engineering Construction of hollow mesoporous zirconia nanospheres with controllable particle size : Synthesis , characterization and adsorption performance," *J. Environ. Chem. Eng.*, vol. 11, no. 5, p. 110546, 2023, doi: 10.1016/j.jece.2023.110546.

[130] X. Xu, Y. Cheng, X. Wu, P. Fan, and R. Song, "La(III)-bentonite/chitosan composite: A new type adsorbent for rapid removal of phosphate from water bodies," *Appl. Clay Sci.*, vol. 190, no. December 2019, p. 105547, 2020, doi: 10.1016/j.clay.2020.105547.

[131] F. Tomul, "Effect of ultrasound on the structural and textural properties of copper-impregnated cerium-modified zirconium-pillared bentonite," *Appl. Surf. Sci.*, vol. 258, no. 5, pp. 1836–1848, 2011, doi: 10.1016/j.apsusc.2011.10.056.

[132] E. I. Unuabonah, C. G. Ugwuja, M. O. Omorogie, A. Adewuyi, and N. A. Oladoja, "Clays for Efficient Disinfection of Bacteria in Water," *Appl. Clay Sci.*, vol. 151, no. April 2017, pp. 211–223, 2018, doi: 10.1016/j.clay.2017.10.005.

[133] Y. Soleimani, M. R. Mohammadi, M. Schaffie, and R. Zabihi, "An experimental study of the effects of bacteria on asphaltene adsorption and wettability alteration of dolomite and quartz," no. 0123456789, pp. 1–19, 2023.

[134] A. Kalfa *et al.*, "Applied Clay Science Removal of Escherichia coli and total bacteria from water by granulated micelle-clay complexes : Filter regeneration and modeling of fi ltration kinetics," *Appl. Clay Sci.*, vol. 147, no. June, pp. 63–68, 2017, doi: 10.1016/j.clay.2017.06.023.